The Institute of Paper Chemistry

Appleton, Wisconsin

Doctor's Dissertation

An Investigation of the Permeability to Water of Partially Saturated Beds of Glass Fibers

Joseph D. Parker

June, 1958

AN INVESTIGATION OF THE PERMEABILITY TO WATER OF PARTIALLY SATURATED BEDS OF GLASS FIBERS

A thesis submitted by

Joseph D. Parker

B. Ch. E. 1952, North Carolina State College
M. S. 1954, Lawrence College

in partial fulfillment of the requirements
of The Institute of Paper Chemistry
for the degree of Doctor of Philosophy
from Lawrence College,
Appleton, Wisconsin

June, 1958

TABLE OF CONTENTS

INTRODUCTION

A porous medium which contains two fluid phases, such as water and air, is termed a two-phase system. Such a system, containing two fluid phases, is said to be partially saturated with one of the phases. The degree of saturation is expressed as the fractional part of the total pore space, or porosity, of the medium which is occupied by the phase in question. By definition, complete saturation exists when 100% of the pore space is filled with a single phase. Common examples of two-phase systems are wet soils, sands, and paper webs as they are dewatered over the suction boxes on a fourdrinier machine.

Two-phase flow occurs when either or both of the phases in a two-phase system are set in motion. The rate of flow of each individual phase is characterized by a specific unsaturated permeability equivalent to the reciprocal flow resistance of that phase in the system. When the specific permeability is expressed as the percentage of the total permeability at complete saturation, it is referred to as the relative permeability.

The role of two-phase flow in the manufacture of paper is a prominent one. It occurs in practically all of the washing, draining, pressing, and drying operations of the papermaking process. It manifests itself as one of the principal economic factors in the operation of paper machines and as an important quality control factor in the formation and drying of the paper web. An understanding of the two-phase flow process, then, is important to the paper industry, and the systems of specific practical interest are fibrous media containing water and air as the fluid phases.

In actual systems, the possible combinations of solid medium, fluid phases, and conditions of flow are virtually innumerable; and, in the general study of them, it is expedient to classify these systems into technically similar categories. Thus, two-phase flow systems can comprise compressible or incompressible media, consolidated or unconsolidated media, micro- or macroporous media, isotropic or anisotropic media, miscible or immiscible phases, and streamline or turbulent flow. Presumably, the basic mechanism of two-phase flow is the same for all the systems in any one category, allowing, of course, for secondary effects which are characteristic of the particular materials employed. Generally speaking, fundamental investigation of two-phase systems has been discouraged by the highly complex geometry involved. This has been particularly true for cellulose media, in which the additional complications of swelling and surface effects are significant. What little study has been directed toward an understanding of two-phase flow was limited to a small segment of the categories above, and the field of fibrous media has remained practically untouched. As a result, the knowledge of two-phase flow is quite specific and much too limited to recommend an intensive fundamental investigation of the highly complex system of cellulosic media. At the present time, there would be greater merit in a study of simple idealized systems.

In lieu of cellulose fibers, then, the comparatively simple systems of glass fibers were used in this study. Glass fibers provide almost ideal media as they are geometrically well defined, uniform in size and shape, hydraulically smooth, nonporous, and they form dimensionally stable macroporous beds. Since air and water are important phases in many industrial

operations, particularly in the manufacture of paper, and they are easily available and are chemically inert to each other and to the glass fiber, these fluids were chosen as the immiscible phases. Thus, the purpose of this thesis was twofold: (1) to contribute to the understanding of the basic mechanism of two-phase flow in general through the study of previously untested media having a different physical structure and (2) to lay the foundation for subsequent fundamental investigations of more practical, but more complex, two-phase fiber systems.

HISTORICAL REVIEW

In order to investigate the problems of two-phase flow systems, it is helpful to first understand the basic principles of single-phase flow in porous media. There are many sources of general information dealing with this subject, but noteworthy are texts by Muskat (1), Carman (2), and Scheidegger (3). In addition to their review on single-phase flow, the books of Carman and Scheidegger contain sections on two-phase flow. In contrast to the great bulk of literature concerned with single-phase flow, the subject of two-phase flow has received little attention. This has been especially true of two-phase flow in fibrous media, of which limited study has been highly specialized and directed toward practical application. Typically, Palmer (4) and Preston, et al. (5) investigated the migration of liquids in textile fabrics and yarns; the phenomenon of capillary rise in paper sheets was examined by Simmonds (6) and Fujita (7); and the occurrence of two-phase flow in connection with the drying of paper sheets has been discussed by Dreshfield (8). In addition to these works, some empirical studies have been made of two-phase flow operations. Nordman (9), Buchanan (10), and Campbell (11) were concerned with the water removal from paper pulp webs at the machine suction boxes and couch rolls, and Nissan (12) studied the role of the felt in water removal on the machine.

The greatest advances in the study of two-phase flow through porous media have been made in the fields of petroleum technology and soil physics, where the materials used were granular in nature, such as sand, soils, and porous rocks. Although there may be significant differences in the two-phase

flow phenomena in granular and fibrous media, a successful attack on the problem can very likely be made in the same way for both of these types of media. Consequently, it was expedient to make a thorough study of the work accomplished in these fields.

CAPILLARY PRESSURE STUDIES

In any investigation of partially saturated porous systems, it is essential to know the distribution of the different phases in the systems. These distributions are generally evaluated from the static capillary pressure-equilibrium saturation relationships of the systems. In evaluating the distributions of the two phases, it is necessary to know which of the phases is the wetting phase. This is the phase that wets the solid medium, i.e., the phase which has an angle of contact with the medium of less than 90°. The other phase is termed the nonwetting phase. Either of these phases may be liquid or gaseous; however, in this discussion, for the sake of convenience, the wetting phase will always be taken as liquid and the nonwetting phase as gaseous. Basic capillary theory shows that the pressure difference across a curved interface between two fluid phases is given by the equation:

$$\underline{P} = \gamma(1/\underline{R}_1 + 1/\underline{R}_2) \qquad (1)$$

where $\underline{R}_1$ and $\underline{R}_2$ are principal radii of curvature of the interfacial meniscus and γ is the interfacial tension. When the meniscus is confined in a circular capillary tube, Equation (1) takes the approximate form:

$$\underline{P}_c = \frac{2\gamma}{\underline{a}} \cos \theta \qquad (2)$$

where $\underline{P}_c$ is termed the capillary pressure, $\underline{a}$ is the radius of the capillary

tube, and θ is the angle of contact. If a porous medium is considered as a system of interconnected capillaries of varying size, a quantity of wetting phase liquid in the medium will distribute itself in the smallest pores in accordance with Equation (2), and all of the liquid interfaces will have the same curvature. When the distribution is complete, the system is said to be in capillary equilibrium. Conversely, if a pressure, P_c, is imposed on a liquid which completely fills the voids of a porous medium, the liquid will be displaced from the medium until it is retained at capillary equilibrium only in pores which are as small or smaller than $a = (2\gamma \cos \theta)/P_c$. By successive displacements of liquid from an initially saturated medium, a curve of capillary pressure, P_c, vs. liquid content, or saturation, s, can be determined. Such a curve is termed a capillary pressure curve. It should be realized here that P_c is the difference in pressure across the liquid-gas interface, the pressure in the gas, i.e., on the concave side of the meniscus, always being the greater. Thus, the same value of P_c can be obtained by imposing either a positive pressure on the gas or a negative pressure on the liquid. An example of a capillary pressure curve for unbeaten sulfite pulp from Christensen and Barkas (13) is shown in Figure 1. Carman (2) and Scheidegger (3) have briefly reviewed several experimental methods of determining capillary pressure curves.

When a fully saturated porous bed is progressively desaturated, three regimes of liquid saturation are distinguished. The first is the saturated state, in which the voids in the bed are completely filled with liquid. The second is the funicular state, in which air has permeated the pore system and the liquid phase exists as a continuous network of interconnected

channels. In the third, or pendular, state of saturation, the continuity of the liquid network has been destroyed, and the liquid is retained in discrete isolated pockets in the medium. Thus, it is not possible for the liquid to flow in the pendular regime. Several writers have given graphic physical descriptions of the different regimes of saturation and the geometrical configuration of the liquid channels in these regimes (3, 14-16).

By means of Equation (2), an effective pore size distribution can be calculated from the capillary pressure curve. In practically all real porous systems, the capillary pressure curves experience a hysteresis effect (see Figure 1). Explanations of this phenomenon are given by Carman (15) and Emmett (17). Although several hypotheses of the hysteresis phenomenon have been proposed, the most plausible one is that based upon the delayed formation of menisci in the pores. In open pores, i.e., pores which are not connected to the surrounding pore spaces by a comparatively small channel or neck, such as ink-bottle pores, the delay in menisci formation occurs in the absorption cycle of the hysteresis loop. For this reason, the desorption branch of the capillary pressure curve has a greater significance for calculating the pore size distribution than the absorption branch.

The physical meaning of pore size distributions calculated from capillary pressure curves has been discussed at length by Carman (15) and severely criticized by Scheidegger (3). It is seen later, however, that the most advanced and successful theories of two-phase flow incorporate the pore size distribution determined from capillary pressure measurements.

For a noncircular capillary, under the assumption of a zero contact

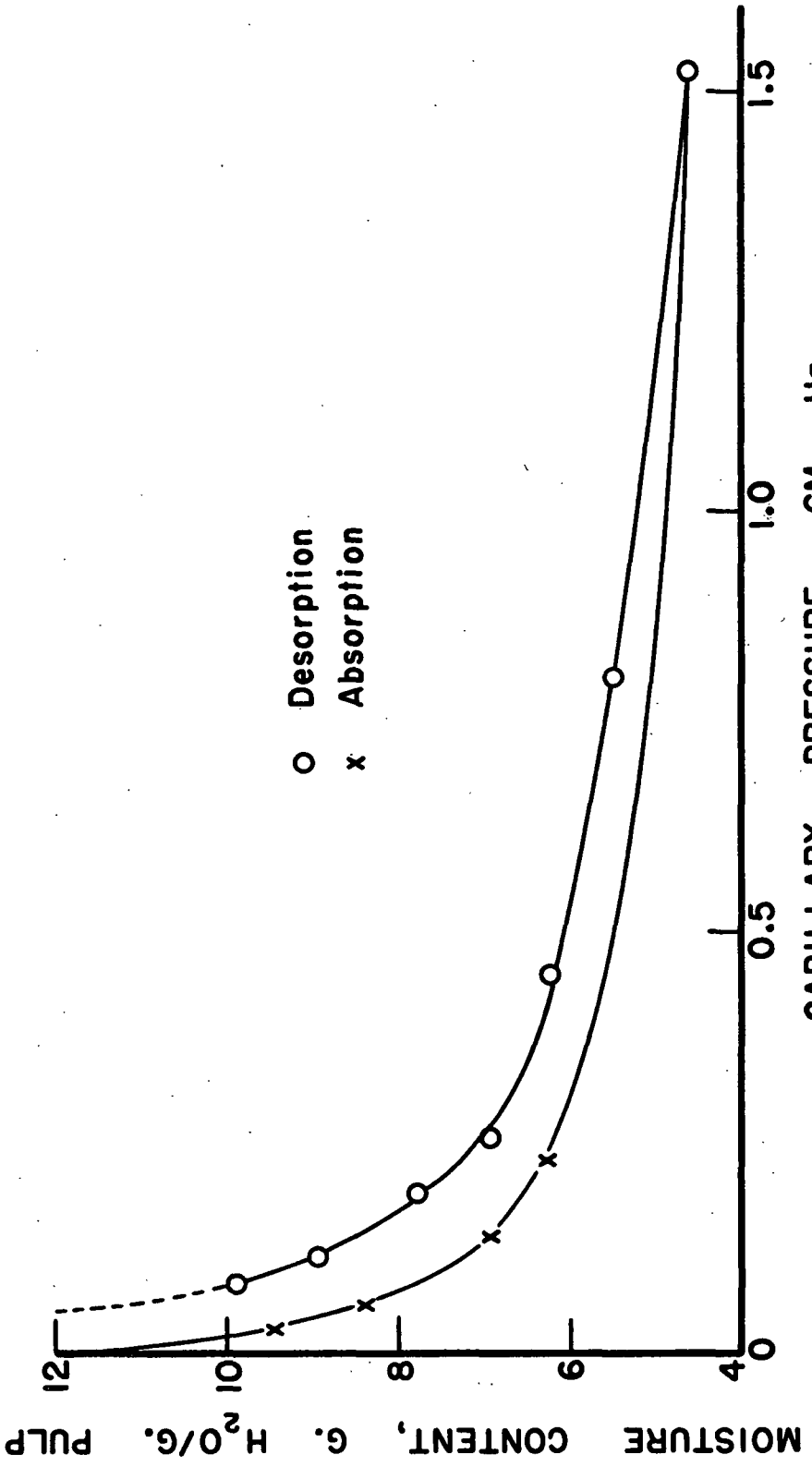

Figure 1. Capillary Pressure Curve of Unbeaten Sulfite Pulp from Christensen and Barkas (13)

angle, the mean hydraulic radius of the capillary can be expressed as

$$\underline{m} = \gamma/\underline{P_c} \text{ or } 1/\underline{m} = 1/\underline{R_1} + 1/\underline{R_2}. \qquad (3)$$

This equation is not rigorous, but it has been shown by Carman (18) to be a good approximation for several regular cross-sectional shapes. Defining $\underline{m}$ as the ratio of volume to surface of a single capillary, Schultze (19), according to Carman (2), obtained an excellent correlation of Equation (3) with capillary rise in noncircular capillaries. It appeared reasonable then to extend this concept to porous media, where $\underline{m}$ is defined as the ratio of the porosity, ϵ, to the surface area per unit volume of the media, $\underline{S_o}$. Carman (2) mentions several data from the literature for capillary rise in sand beds which agree approximately with this theory. Carman goes on to say that for normal granular media, which obey the Kozeny-Carman equation, it is easy to select an initial value of $\underline{P_c}$ which corresponds to a rapid displacement of liquid from the media and also agrees well with the value, $\gamma/\underline{m}$. The criterion for this agreement, of course, is that the pores of the media be uniform in size. In the following discussion of two-phase flow, it is seen that this concept is a very important one in the Kozeny theories of relative permeability. However, it does not necessarily follow that the equivalence of $\epsilon/\underline{S_o}$ and $\gamma/\underline{P_c}$ holds for the myriad of pore shapes and sizes which occur in natural porous media, saturated and unsaturated, simply because these values are approximately equivalent for a variety of geometrical pore shapes. It is possible that such an assumption may lead to gross errors in the evaluation of relative permeability.

EXPERIMENTAL DETERMINATION OF RELATIVE PERMEABILITY

In the past, the term diffusion has been applied indiscriminately to

describe the general transfer of liquids in partially saturated media. It is realized now that many different flow mechanisms were embraced by this terminology. Marshall and Friedman (20) list five possible mechanisms, depending on the structure of the medium. In attempting to quantitatively define the relative permeability, however, it is necessary to know the specific predominating mechanism in operation. A great portion of the work devoted to two-phase flow has been concerned with porous media of relatively large pore sizes, i.e., greater than a few hundred Ångström units such as sands and rocks. In such macroporous systems, over the greater part of the saturation range (roughly from 5 to 100%), the predominant and often exclusive mechanism is that of capillary flow (14, 21-23). In this mechanism, the liquid moves by channel flow through the continuous interconnected (funicular) channels of liquid that exist in the medium.

When capillary flow is in effect, the liquid permeability of an unsaturated system is defined by D'Arcy's law; that is, the permeability is independent of the driving force and flow velocity. Several investigators (23-27) mentioned by Scheidegger (3) have shown this to be true; however, Scheidegger points out that such experiments have only shown the validity of D'Arcy's law approximately. Scheidegger discusses several possible effects, viz., turbulence and molecular effects, such as adsorption, slippage, and diffusion which impose limitations on D'Arcy's law. However, in the majority of cases, these effects are of only second order importance and can be neglected for most practical purposes. It should be noted here that the relative permeability to liquid cannot be considered rigorously as a function of saturation only because of the hysteresis phenomena.

Scheidegger (3) discusses seven different methods which have been used to measure relative permeability. In the measurement of relative permeability, both phases may be flowing simultaneously or either of them may be stationary. So long as the flow is streamline, however, the relative permeability of one phase is little affected by the motion of the other (2). The outstanding characteristic of two-phase flow is that the presence of a second fluid phase greatly diminishes the permeability to the first phase and also to the mixture. Qualitatively, the primary reasons for this are that each phase reduces the cross-sectional area available for flow and the tortuosity of the channel system occupied by the other (2, 3).

Typical relative permeability curves of granular media are those from Wyckoff and Botset (24) for sands shown in Figure 2. Other relative permeability measurements have been presented by Leverett (28) and Childs and George (23) for sands, and Hassler, et al., (25), Gates and Lietz (29), and Brownscombe, et al., (30) for consolidated media. Wyckoff and Botset suggested that the curve they obtained, which was the same for four sands of varying coarseness and was not affected by changes in the viscosity or surface tension of the fluid phases, could be regarded as general for all unconsolidated media and any combination of wetting and nonwetting phases. Though some experimental data agree with Wyckoff and Botset's results, it has been demonstrated conclusively that systems of different pore size distribution can give different relative permeability curves. The well-known concept that as a pore increases in size, it contributes proportionately more to flow than to porosity, is illustrated by the results of Brownscombe, et al., (30). Figure 3 is a graph reproduced from

Brownscombe, et al., showing the effect of progressive plugging of a sandstone core with infusorial earth. As the plugging increased from curve 1 to curve 4, the over-all porosity and the size of the capillaries became smaller. This resulted in a flattening out of the relative permeability curves. If this argument could be projected to high porosity media, such as fiber beds, one would expect the curves for such media to tend toward the less flat curves such as curve 1 in Figure 3. Further, Brownscombe, et al., demonstrated that relative permeability curves could take shapes having inflections in them. They ascribe these irregularities in the curves to the uneven distribution of capillary pore sizes in the samples. It is generally implied in the literature that uniform and regular shaped particles provide for a uniform and relatively simple pore structure of the porous medium constructed from them.

THEORETICAL STUDIES

In attempting to quantitatively define relative permeability in terms of the fundamental two-phase system variables, the same general approaches have been made that were successful in describing single-phase flow. Because of the general success with which the Kozeny equation has been applied to single-phase flow, studies employing the Kozeny approach to two-phase flow have been extensive. It is convenient for this reason to divide the discussion into Kozeny and non-Kozeny approaches. Unless otherwise stated, the term, relative permeability, refers to the liquid wetting phase relative permeability.

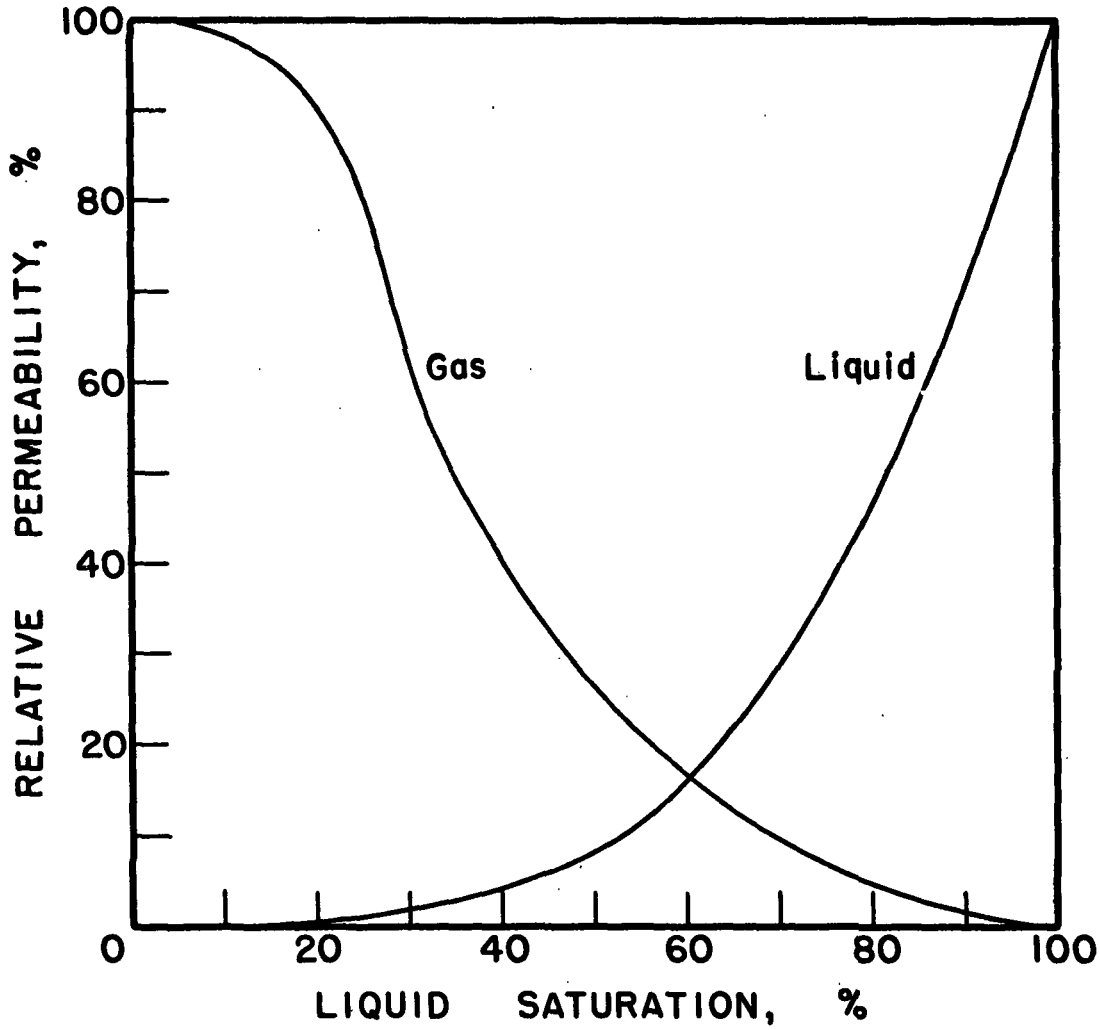

Figure 2. Relative Permeability Curves for Sands from Wyckoff and Botset (24).

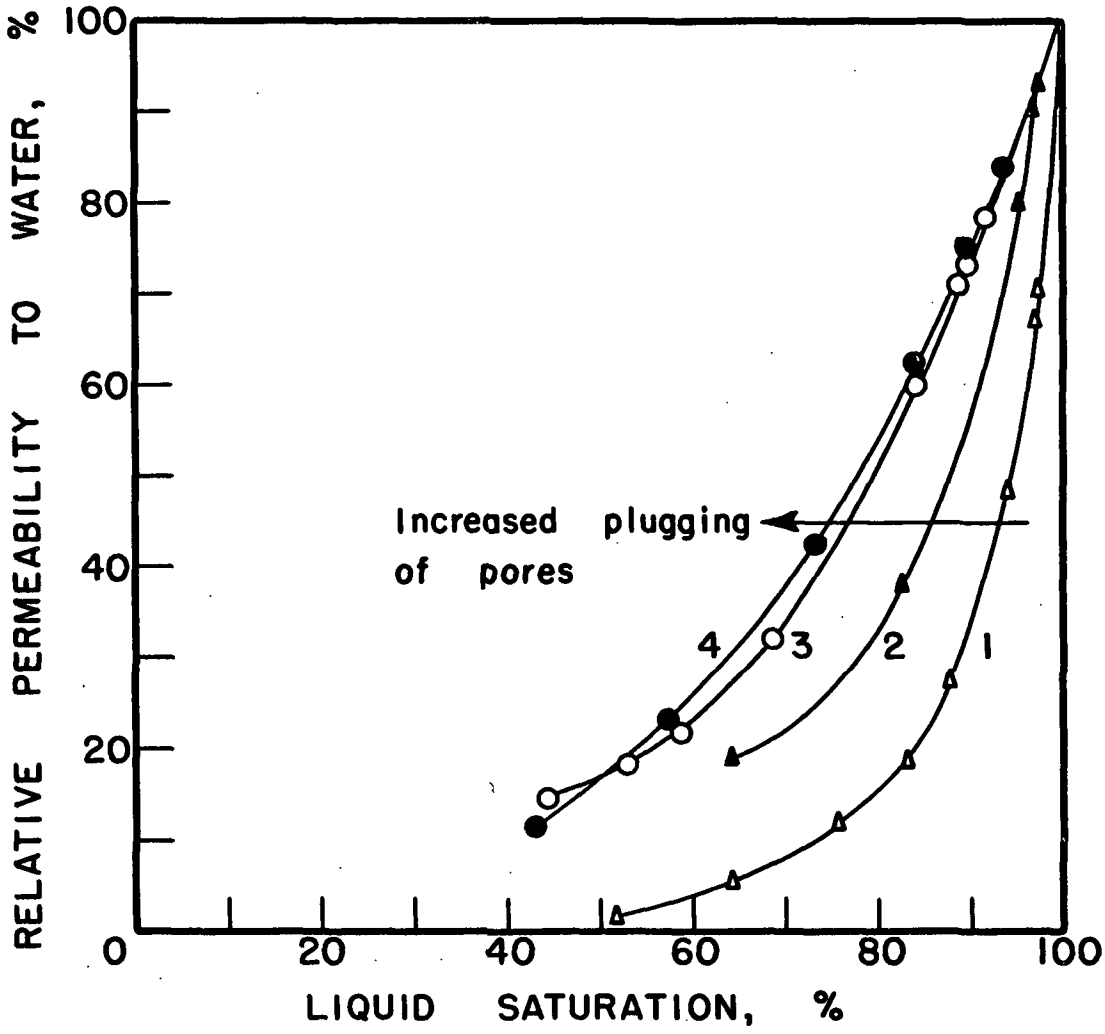

Figure 3. Effect of Plugging on Relative Permeability of a Sandstone Core from Brownscombe, et al., (30)

NON-KOZENY APPROACHES

According to Scheidegger (3), the first possibility in defining relative permeability is to establish heuristic correlations. Scheidegger gives an inclusive survey of the studies of this sort, and some of the notable works are presented here. Brownell and Katz (31) assumed flow through porous media to be analogous to pipe flow. They developed correlations between friction factor and Reynold's number for single-phase flow and extended this correlation to two-phase flow by introducing functions of saturation in the correlations. The one major advantage of this approach is that it applies to turbulent as well as to streamline flow. It is intuitively evident that the relative permeability is related to the pore size distribution. Baver (32) suggested the characterization of porous media in terms of their "noncapillary porosity"; and Smith, et al. (33) elaborated this idea by dividing the range of pore sizes into three discrete units, according to the capillary pressure at which they drained. The greatest success in this direction was attained by Childs and George (23), who developed an equation by which the relative permeability could be evaluated from the effective pore size distribution. Their equation was:

$$\underline{K}_c = \underline{M} \sum_{\underline{r}=0}^{\underline{r}=\rho} \sum_{\underline{r}=0}^{\underline{r}=\sigma} \sigma^2 \, f(\rho)\Delta\underline{r} \;\; f(\sigma)\Delta\underline{r}, \qquad (4)$$

where ρ and σ are discrete values of the pore radius, $\underline{r}, \sigma$ being the smaller of the two, and $f(\rho)\Delta\underline{r}$ and $f(\sigma)\Delta\underline{r}$ are functions of these radii which can be evaluated from the capillary pressure, or effective pore size distribution, curve. The term $\underline{M}$, is an empirical constant of proportionality.

A second possibility of defining relative permeability is in the use of capillary models. Martinelli, et al., (34), analyzed two-phase flow in a single capillary tube theoretically and experimentally. Comparing the data from this analysis with those from two-phase flow in porous media, they concluded that two-phase flow in a single capillary tube is a special case of that in porous systems. Other capillary model theories, in which the porous media are represented by bundles of capillaries, have been advanced by Purcell (35), Gates and Lietz (29), and Fatt and Dykstra (36). The equation of liquid relative permeability developed in these studies is:

$$K_r = \int_0^s (1/P_c)^{2(1+b)} ds \Big/ \int_0^1 (1/P_c)^{2(1+b)} ds \qquad (5)$$

where s is the degree of liquid saturation and b is an empirical constant which takes a value that depends on the type of medium used (3).

Other approaches to this problem have included those based on the assumption that capillary flow is analogous to heat and/or electricity flow (32, 37, 38). These approaches do not lend themselves to fundamental analyses of the two-phase flow mechanism, but were developed primarily for the sake of practical expediency. The method of dynamical similarity was applied to capillary flow systems by Miller and Miller (39). Based on the premise that the microscopic behavior of liquid in a partially saturated porous medium is governed by the laws of surface tension and viscous flow, Miller and Miller developed fully reduced equations describing the macroscopic flow in unsaturated systems.

Scheidegger (3) notes that two promising methods of analysis of single-phase flow, namely, the drag theory developed by Emersleben (40) and Iberall

(41) and the statistical theory of Taub (42) and Scheidegger (43), have not been extended to two-phase flow.

KOZENY APPROACHES

The general impression gained from both the Carman and Scheidegger reviews (2, 3) on two-phase flow is that the Kozeny method of analysis has been the most successful yet in defining the relative permeability. The widespread use of the Kozeny and Kozeny-Carman equations to characterize single-phase flow makes it unnecessary to discuss their development and utility here. Such information is found in many sources (2, 3, 44). The limitations of the Kozeny approach are also comprehensively discussed in many places (2, 3, 23, 43, 44). Two important limitations are (1) the assumption that the Kozeny constant, k, is not markedly influenced by changes in the pore geometry and (2) the implication of uniform pore size. As seen below, in extending the Kozeny equation to two-phase flow, these limitations necessitate basic alterations in the equation developed for single-phase flow.

Evaluation of the Kozeny Constant for Two-Phase Systems

The Kozeny constant, k, is written as the product of two parameters, a shape factor, k_o, and a tortuosity term, $T = \frac{L_e}{L}$, where L_e is the actual average length of the path followed by the liquid in a porous medium of thickness L. Thus,

$$k = k_o\left(\frac{L_e}{L}\right)^2 = k_o T^2. \qquad (6)$$

The evaluation of the Kozeny constant and its components, k_o and T, for

single-phase systems has been considered in detail for many different media (2, 45-50). Scheidegger (3) raises mild objections to the use of these empirical factors, but the usefulness of this concept cannot be denied. It is generally believed that the value of k_o is reasonably constant over a wide range of pore shapes and sizes and hence for most porous systems (2, 45, 49, 50). Carman (51) proposes that k_o lies somewhere between 2.0 and 3.0 for most porous systems and a value of 2.5 has the greatest general utility. This value of 2.5 received support from the work of Wyllie and Rose (52). Wyllie and Spangler (48) suggest that a value of 2.7 for k_o is more generally applicable, while Sullivan and Hertel (45) used a value of 3.0. For the analysis of two-phase flow, since k_o apparently varies so little with observed changes in pore size and shape, it was generally assumed that k_o for the liquid system was constant for all saturations. However, it is definitely realized that extremes in porosity and pore shape and size can cause large deviations in the value of k_o (2, 40, 53). Consequently, the validity of the assumption that k_o is constant for all saturations is questionable.

Assuming a constant value for k_o, it was suggested that an independent evaluation of the Kozeny constant could be achieved through a separate measurement of the tortuosity (45, 46, 52). Sullivan and Hertel (45) proposed a theoretical method of evaluating T, but the technique of defining T from electrical resistivity measurements has been of the greatest interest. Consider a nonconducting porous solid filled with a conducting salt solution. The ratio of the electrical resistance of a unit cube of the saturated medium to that of a unit cube of the solution alone is designated the

formation factor, F, by Wyllie and Spangler (48) and the reciprocal of the conductivity ratio, J, by Carman (2). Wyllie and Rose (52) and Thornton (54) suggest that

$$F = \frac{L_e}{L}\frac{1}{\epsilon} = \frac{T}{\epsilon}. \qquad (7)$$

Cornell and Katz (55), on the other hand, contend that

$$F = \frac{T^2}{\epsilon}. \qquad (8)$$

However, Carman (2) presents evidence in favor of Wyllie and Spangler's Equation (7).

As mentioned previously, a major effect of introducing a second fluid phase into a previously saturated porous medium is to increase the tortuosity of the first phase. In any analytical treatment of two-phase flow, therefore, it is important to account for the increased tortuosity. Rose and Bruce (56) and Rapoport and Leas (57) derived relative permeability equations under the assumption that the Kozeny constant was the same at all saturations, but Thornton recognized that the Kozeny constant is not independent of saturation. Thus, the application of electrical resistivity measurements to partially saturated systems is readily apparent. By analogy with Equation (7), the formation factor of a medium having a saturation, s, is

$$F_c = \frac{T_c}{\epsilon\, s} \qquad (9)$$

where T_c is the tortuosity of the liquid channels at saturation, s. The ratio, F_c/F, is termed the resistivity index, I, pertaining to the saturation, s (48). Thus,

$$I = \frac{F_c}{F} = \frac{T_c}{T}\frac{1}{s}. \qquad (10)$$

Wyllie and Spangler (48) have shown that the relationship between I and s for many consolidated media and unconsolidated sand is

$$I = s^{-n}. \tag{11}$$

As shown in Figure 4, reproduced from Wyllie and Spangler, the exponent, n, takes values from 1.40 to 2.55 for consolidated media and approximately 2.0 for unconsolidated sand. To this writer's knowledge, no such data as presented in Figure 4 exist for fibrous media.

In the use of electrical resistivity measurements for evaluating the Kozeny tortuosity, the question naturally arises as to the equivalence of the electrical and hydraulic tortuosities. This question is discussed in detail by Wyllie and Spangler (48), Wyllie and Gregory (46), and Carman (2). Evidence is presented in the former two references which indirectly support this equivalence. However, there is no conclusive evidence to either substantiate or discredit this equivalence.

Development of Kozeny Equations for Two-Phase Flow

Wyllie and Spangler noted that Rose and Bruce (56) and Rose (58) were probably the first to apply the Kozeny approach to the problem of two-phase flow. They assumed that the Kozeny constant was the same for all saturations and that the surface area per unit of pore volume at $s = 1.0$ is given by

$$S_p = \frac{P_D}{\gamma}, \tag{12}$$

and at any saturation, s, is given by

$$S_p = \frac{P_c}{\gamma}, \tag{13}$$

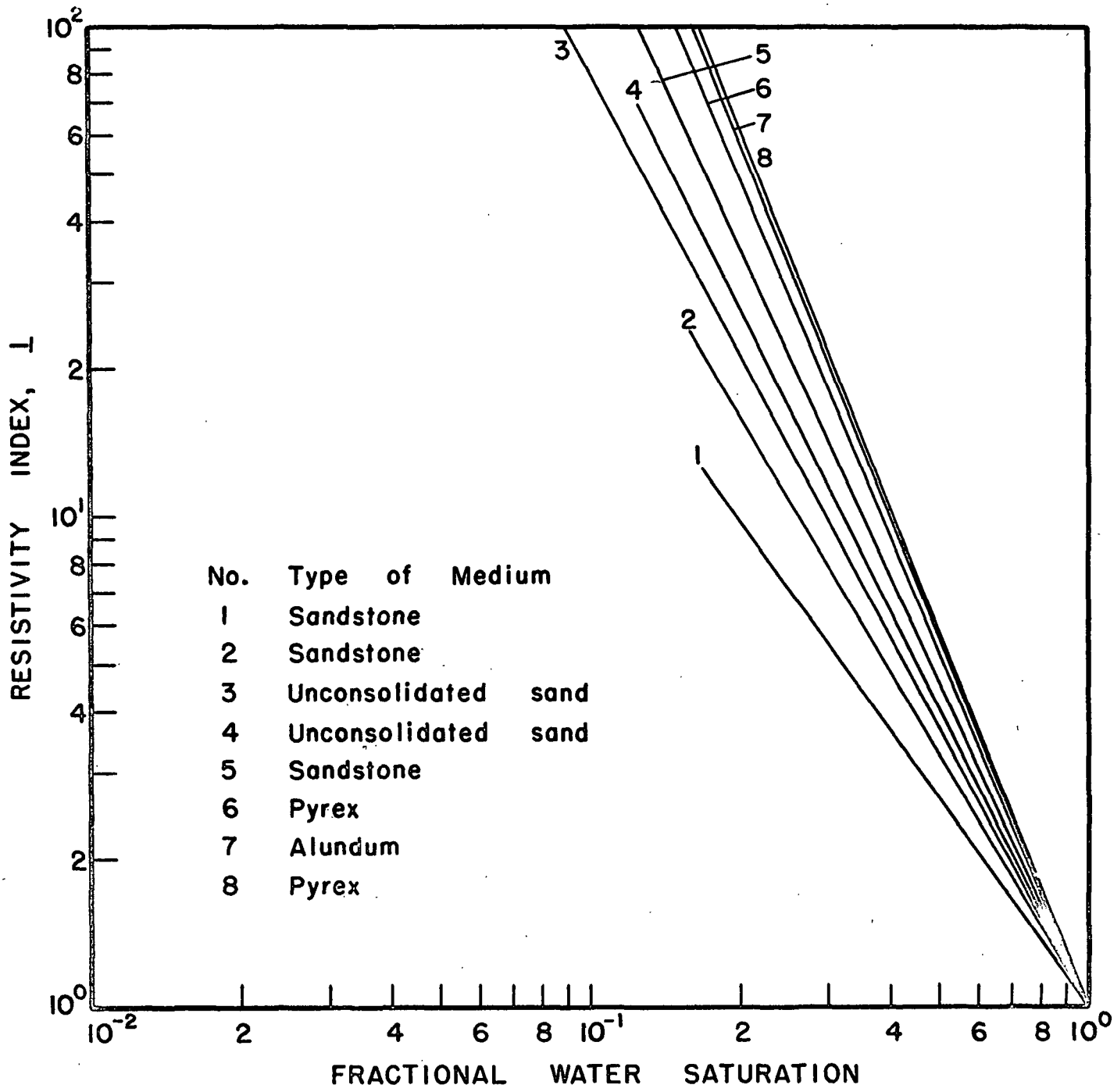

Figure 4. Electrical Resistivity Index Curves from Wyllie and Spangler (48).

as proposed by Carman (18). They obtained the expression,

$$K_r = s\left(\frac{P_D}{P_c}\right)^2, \tag{14}$$

where P_D is the displacement pressure of the saturated system and P_c is the capillary pressure at saturation, s. Thornton's modification of introducing a tortuosity factor (54) resulted in the expression,

$$K_r = \frac{1}{I^2 s}\left(\frac{P_D}{P_c}\right)^2. \tag{15}$$

The chief objection to Equations (14) and (15) is that, in the use of Equations (12) and (13), they apply only to media having uniform pore sizes, i.e., that $P_c = P_D$ at all saturations (48). The capillary pressure curve for such a case would be simply a vertical line at the displacement pressure value. In real porous solids, this condition may be closely approached, as some media do display nearly vertical displacement curves. This near verticality of the capillary pressure curves of unconsolidated sands of Leverett (28) was probably requisite for the agreement between Leverett's experimental data and Equation (15) noted by Wyllie and Spangler (48). For media having a wide range of pore sizes, however, Equation (15) would not be adequate.

Rose and Wyllie (59) propose the equation,

$$K_r = 1/I^2, \tag{16}$$

and Wyllie and Spangler discuss the expression,

$$K_r = 1/I^2 s. \tag{17}$$

Equations (16) and (17) are both subject to the same limitation as Equations (14) and (15), i.e., they apply only to media having pores of uniform size.

Kozeny theories of two-phase flow in which the distribution of pore sizes was considered were offered by Rapoport and Leas (57) and Wyllie and Spangler (48). Rapoport and Leas obtained the expression,

$$\underline{K_r} = \left(\frac{\underline{s} - \underline{s_r}}{1 - \underline{s_r}}\right)\left(\frac{\underline{S_E}}{\underline{S_L}}\right)^2 \qquad (18)$$

where $\underline{s_r}$ is the residual saturation (asymptotic value of $\underline{s}$ which the capillary pressure curve approaches), $\underline{S_L}$ is the surface area of all the liquid per unit volume of medium, and $\underline{S_E}$ is the surface area of the flowing liquid on the same basis. In deriving this equation, Rapoport and Leas assumed that the volume of liquid which is removed from flow is linearly proportional to the volume of gas (nonwetting) phase in the system. Further, they made two assumptions which have proved to be controversial. These are:

(1) There is no slippage at the liquid-gas interfaces in the voids of the system, and

(2) The Kozeny constant is the same at all saturations.

By means of thermodynamic reasoning, Rapoport and Leas evaluated $\underline{S_E}$ and $\underline{S_L}$ from capillary pressure curves using the following derived expressions:

$$\underline{S_E} = -\frac{\epsilon}{\gamma}\int_1^{s_r} \underline{P_c}\, \underline{ds} \qquad (19)$$

$$\underline{S_L} = -\frac{\epsilon}{\gamma}\int_{\underline{s}}^{s_r} \underline{P_c}\, \underline{ds} + 2\underline{I_p} \qquad (20)$$

where $\underline{I_p}$ is the interfacial area between the two phases. If $\underline{S_E}$ represents the surface that separates the flowing liquid from the immobile matrix of

solid medium and stationary fluid, it very likely varies with saturation. Thus, it is difficult to understand Equation (19), which is constant for all saturations. Contrary to Rapoport and Leas' claims, Payne (60) and Wyllie and Gregory (46) assert that Equation (19) can be used to calculate the approximate total surface area of the porous solid. As a consequence of their derivations, Rapoport and Leas were only able to assign theoretical limiting values to the relative permeability.

Wyllie and Spangler's application of the Kozeny approach to two-phase flow resulted in the following equation of relative permeability:

$$\underline{K}_r = \frac{1}{\underline{I}^2 \underline{s}^2} \frac{\int_0^{\underline{s}} \underline{ds}/\underline{P}_c^{\,2}}{\int_0^1 \underline{ds}/\underline{P}_c^{\,2}} = \frac{\underline{T}^2}{\underline{T}_c^{\,2}} \frac{\int_0^{\underline{s}} \underline{ds}/\underline{P}_c^{\,2}}{\int_0^1 \underline{ds}/\underline{P}_c^{\,2}} \qquad (21)$$

In this equation, the effects of both the variation in tortuosity and the pore size distribution have been considered. Wyllie and Spangler show that their theory is in fairly good agreement with the experimental data of Gates and Lietz (29) for consolidated media. Thus, Wyllie and Spangler's expression appears to be the most advanced and generally applicable of all the equations developed for relative permeability. In contrast to the reasoning of Rapoport and Leas, Wyllie and Spangler apparently assume that all the liquid in the porous media is flowing at all saturations greater than residual. That is, the pendular state of saturation is reached simultaneously by all the liquid in the media at the residual saturation. In real systems, the true state of the flowing liquid probably lies somewhere between the two extremes assumed by Rapoport and Leas and Wyllie and Spangler.

In all of the above Kozeny approaches, the shape factor, $\underline{k}_o$, was assumed to be independent of the saturation. Various indirect experimental evidence was presented to support this assumption (2, 46, 48). However, the work that has been mentioned was concerned with granular systems only. It does not necessarily hold that $\underline{k}_o$ is independent of saturation in fibrous systems as well. Furthermore, the assumed equivalence of $\gamma/\underline{P}_c$ and $\epsilon/\underline{S}_o$ in the two-phase systems, which apparently is a good approximation for granular media, is not necessarily true for fibrous media.

DEVELOPMENT OF A MODIFIED KOZENY-CARMAN EQUATION FOR TWO-PHASE FLOW

In general, beds of fibrous substances have much higher porosities than those of granular materials. It is also probable that the geometrical configuration of the pores in fibrous media are markedly different from those in granular media. And the differences in structure of these two types of media may be exaggerated when two fluid phases are present. Thus, the Kozeny expressions, which are strongly dependent on the porosity and pore configurations, developed and tested successfully for two-phase flow through granular media, are not necessarily as equally valid for fibrous media. However, the Kozeny approach remains the most promising method of analyzing two-phase flow in fibrous systems; but a more general form of the Kozeny-Carman equation applicable to two-phase flow in all types of media is required. The aim of the following theoretical treatment is to define a relative permeability to the liquid wetting phase in a partially saturated unconsolidated porous bed in which a gas, e.g., air, at atmospheric pressure is the nonwetting phase. The mechanism of liquid movement is, of course, capillary flow.

As noted in the survey of the literature, Rapoport and Leas (57) assumed that a specific amount of the liquid in an unsaturated flow system was immobilized and did not participate in the flow. Wyllie and Spangler (48), on the other hand, assumed that all of the liquid in the system was flowing. The actual case probably lies somewhere between these two assumptions; however, for a working hypothesis, the experimental work appears to support Wyllie and Spangler. In any case, the difference between these two assumptions is small, and since that of Rapoport and Leas leads to a rather

involved mathematical expression, Wyllie and Spangler's reasoning will be adopted in this work. As the following derivation is based on the Kozeny equation, the final expression is naturally subject to viscous flow only and the other limitations associated with the Kozeny approach.

It has been fairly well established that the mechanism of liquid flow in partially saturated granular media, i.e., capillary flow, is described by D'Arcy's equation. It is proposed that D'Arcy's equation is applicable to capillary flow in all types of macroporous media, including the glass fiber beds of this work. Thus, D'Arcy's general equation for unsaturated systems is

$$\frac{q}{A} = \frac{K_c}{\mu}\frac{dP_f}{dL}, \qquad (22)$$

where K_c is the specific permeability of the over-all medium to the liquid, and dP_f is the differential of fluid pressure in the liquid which corresponds to the driving force necessary to overcome the frictional drag resistance of the flowing liquid. In systems of thin beds and low pressure drops across the beds, a good approximation is to assume that the liquid permeability is constant across the bed. This is rigorously true only for incompressible beds in which the porosity is uniform throughout the thickness of the bed. In such cases, Equation (22) becomes

$$\frac{q}{A} = \frac{K_c \Delta P_f}{\mu L}. \qquad (23)$$

To extend the Kozeny-Carman analysis to these two-phase flow systems, the same basic approach was used as that for single-phase flow. It is understood, of course, that the effect of the Kozeny-Carman analysis is to

define the permeability in terms of the system variables which can be independently evaluated. Thus, for single-phase flow in unconsolidated porous media, the usual form of the Kozeny-Carman equation is

$$\frac{q}{A} = \frac{\epsilon^3}{k_o T^2 \mu S_o^2} \frac{P_f}{L}. \qquad (24)$$

In extending this equation to describe the flow of liquid in an incompressible unconsolidated porous medium at saturation, s, the following modifications were introduced:

(1) The total porosity of the medium, ϵ, was replaced by an "effective porosity" corresponding to the liquid, ϵs. In the partially saturated medium, the nonwetting gas phase was considered, in effect, as a part of the solid medium. The effective void volume, then, was that part of the total porosity which was filled with liquid.

(2) The total external surface area of the particles per unit of bed volume, S_o, was replaced by a surface area term, S_c, which represents the surface of the flowing liquid which is subjected to frictional drag resistance. Rapoport and Leas (57) considered this surface to be the total boundary area of the liquid phase flow matrix, including the areas of contact between the flowing liquid and the solid medium, the gas phase, and the immobilized water. In his discussion of Rapoport and Leas' paper, Dodd (57) objected to the assumption that there is appreciable drag at the gas-liquid interface. In support of Dodd's objection it is argued by those in

the field of surface chemistry (61) that frictional drag of any practical significance at the gas-liquid interfaces could only arise through the formation of condensed surface films on the flowing liquid. In the present work, the formation of such condensed films is deemed highly unlikely since only pure demineralized water was used as the liquid phase, and the solid medium consisted of very clean glass fiber. Since it was postulated in this treatment that no liquid was immobilized in the partially saturated medium, the frictional drag on this element was not considered. Thus, the surface area of drag was only the area of contact between the total liquid (as presumably all the liquid is flowing) and the solid medium. Following the same reasoning used in the development of the Kozeny equation for single-phase flow, two-phase flow was assumed to be analogous to channel flow. Thus, the ratio of the effective liquid porosity, ϵs, to the frictional drag surface area (i.e., the liquid-solid contact area) per unit volume of the medium, S_c, was substituted for the mean hydraulic radius in Poiseuille's equation for open channel flow.

(3) Instead of the tortuosity, T, which applies to the fully saturated medium, an unsaturated tortuosity, T_c, was used. Of course, T_c is a function of the saturation and is simply an empirical index of the average devious path followed by the liquid in the two-phase system. The reasons for making this substitution have been discussed previously in the literature survey. Wyllie and Spangler (48) suggested that the variation of T_c with s follows the same

pattern in all homogeneous porous media; specifically, log $\underline{I}$ is linearly proportional to log $\underline{s}$. However, the experimental confirmation of this hypothesis has been based only on a few experiments with granular media. And even in these cases, absolutely conclusive agreement was lacking. It remains to be determined whether the linear variation of log $\underline{I}$ vs. log $\underline{s}$ is universal, or whether the variation of $\underline{T_c}$ with $\underline{s}$ depends on the type of medium used.

(4) A shape factor term, which is variable with the saturation, $\underline{k_{oc}}$, was substituted for $\underline{k_o}$. In view of the observations made by Carman (2), Emersleben (40), and Sullivan (53) on the variation of $\underline{k_o}$ with porosity and pore shape, it would be naive to assume a constant value of $\underline{k_o}$ for all saturations. Carman points out that the value of $\underline{k_o}$ "...can attain fairly small values when the capillary walls approach to form relatively narrow spaces owing to the formation of sharp angles (triangles) or to the narrowing of an annular space because of the elliptical spacing of a central core." As a liquid-saturated medium is progressively desaturated, the funicular channels of liquid become smaller and more angular in cross section. At the very low saturations, near the pendular regime, this narrowness and angularity of the channel cross sections are probably extreme. One would expect, then, on the basis of Carman's statement that the values of $\underline{k_{oc}}$ for the liquid flow would become quite small at the low saturations. However, another aspect of the variation of $\underline{k_o}$ is offered by Carman when he says: "The success of the Kozeny equation for granular beds must be attributed to a pore

space in which the channels are continuously breaking up, dividing, and reconnecting along the path of flow with the result that the average channel shape factor lies in the range where $\underline{k_o} \simeq 2.5$ and is not greatly affected by shape." This effect of channel dividing in the two-phase system, therefore, may tend to keep the effective variation of $\underline{k_{oc}}$ with $\underline{s}$ from becoming extreme.

The fluid pressure term, $\Delta\underline{P_f}$, applies in the two-phase systems just as it does in the single-phase systems, but it is important to understand the relationship between this term and the capillary pressure, $\underline{P_c}$. In vertical flow, which was used in this work, a correction has to be made for the static gravitational head of water across the bed. Thus, if $\Delta\underline{P_f}$ is the frictional pressure drop across the bed, then $\Delta\underline{P_f} = -\Delta\underline{P_c} - \rho_{\underline{L}}\underline{gL}$. The capillary pressure, $\underline{P_c}$, includes the pressure due to the static head of water across the bed as well as the pressure to overcome frictional drag resistance. Of course, the changes in $\underline{P_f}$ and $\underline{P_c}$ are opposite in sign since $\Delta\underline{P_f}$ refers to the change in fluid pressure of the liquid itself, and $\underline{P_c}$ refers to the difference in fluid pressure of the liquid and that of the surrounding atmosphere. Thus, as the fluid pressure of the liquid decreases, the capillary pressure increases.

When the above modifications were made, Equation (24) became, for upward vertical flow at saturation $\underline{s}$,

$$\frac{\underline{q}}{\underline{A}} = \frac{\underline{\epsilon}^3\,\underline{s}^3}{\underline{k_{oc}}\,\underline{T_c}^2\,\mu\underline{S}^2_{\underline{c}}}\,\frac{\Delta\underline{P_f}}{\underline{L}}. \qquad (25)$$

D'Arcy's law for the permeability of liquid at saturation $\underline{s}$ is

$$\frac{\underline{q}}{\underline{A}} = \frac{\underline{K_c}}{\mu}\,\frac{\Delta\underline{P_f}}{\underline{L}}. \qquad (26)$$

Combining Equations (25) and (26), the resulting equation of specific permeability of the medium to liquid at saturation $\underline{s}$ is

$$\underline{K_c} = \frac{\epsilon^3 \underline{s}^3}{\underline{k_{oc}}\ \underline{T_c}^2\ \underline{S_c}^2}. \tag{27}$$

At complete saturation, i.e., $\underline{s} = 1.0$, the liquid permeability is

$$\underline{K} = \frac{\epsilon^3}{\underline{k_o}\ \underline{T}^2\ \underline{S_o}^2}. \tag{28}$$

The relative permeability, then, is the ratio of $\underline{K_c}$ to $\underline{K}$:

$$\underline{K_r} = \frac{\underline{K_c}}{\underline{K}} = \frac{\underline{s}^3\ \underline{k_o}\ \underline{T}^2\ \underline{S_o}^2}{\underline{k_{oc}}\ \underline{T_c}^2\ \underline{S_c}^2}. \tag{29}$$

It is of interest now to modify Equation (29) to a form in which the pore size distribution is included. An effective pore size distribution can be calculated from the capillary pressure curve by defining a mean hydraulic radius of the pores as $\gamma/\underline{P_c}$, assuming a zero contact angle between the liquid and the porous solid. As discussed in the literature review, it has been shown that for certain sands, $\gamma/\underline{P_c}$ is a fair approximation of the average mean hydraulic radius of the sand bed, defined as $1/\underline{S_p} = \epsilon \underline{s}/\underline{S_c}$. Thus, in some theoretical Kozeny treatments of two-phase flow, $1/\underline{S_p}$ was replaced by $\gamma/\underline{P_c}$. A critical examination of this substitution, however, shows that it is only valid for certain pore shapes and is not generally applicable.

The term $\gamma/\underline{P_c}$ is, in effect, an approximate measure of one-half the radius of curvature of the liquid meniscus contained in a small pore and having a zero contact angle. For certain pore shapes, e.g., cylindrical

pores, this term is equivalent to the mean hydraulic radius of the pore, i.e., the volume to surface ratio of the pore. Pierce (62) and Barrett, Joyner, and Halenda (63), assuming cylindrical pores in various granular materials, calculated the surface area from the effective pore size distribution. Their calculated values of total surface area were in fair agreement with experimentally determined B.E.T. areas from nitrogen adsorption tests. However, the pore sizes of the media they used were quite small (< 300 A.). It is readily seen that this is not generally true for all pore shapes and sizes. By way of illustration, a schematic diagram of the cross sections of two hypothetical pores are shown in Figure 5. A liquid filling these pores would have the same meniscus curvature at the mouth of the pore, but the ratio of the volume of liquid to the surface of the pore would be different for these pores. Conceivably, the variation in pore shape in actual porous media could be much more complex than that illustrated in Figure 5.

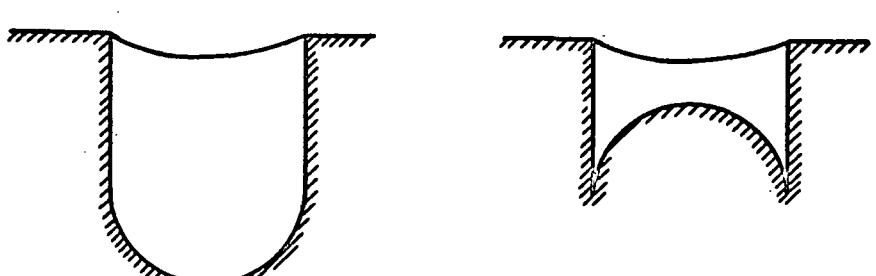

Figure 5. Hypothetical Pore Cross Sections

It is common practice in the field of micromeritics, or small particle technology, to characterize irregular-shaped particles by the ratio of their volume to their external surface area. The surface and volume are expressed as a function of the second and third moments, respectively, of some weight

average linear measure of the particle size, such as obtained from sieving, sedimentation, etc. Speaking of the surface and volume in terms of the particle size makes it necessary to use proportionality or shape factors. Following the notation of Herdan (64), let α_s and α_v be the factors of proportionality between the surface, S, and volume, V, and the second and third moments of the measured particle size, X. Thus, in a distribution of particle sizes:

$$S = \alpha_s \sum X_i^2 N_i, \tag{30}$$

$$V = \alpha_v \sum X_i^3 N_i, \tag{31}$$

and

$$\frac{S}{V} = \frac{\alpha_s \sum X_i^2 N_i}{\alpha_v \sum X_i^3 N_i} \tag{32}$$

where N_i = number of particles of size, X_i. The ratio of the proportionality factors, α_s/α_v, is characteristic of the shape and heterogeneity of the particles. For example, Herdan gives the following values of α_s/α_v: for cubes and spheres, 6.0; for worn particles, 6.4; for sharp particles, 7.0; for angular particles, 7.7; and for crushed quartz, about 11.

The void spaces in a porous medium were likened, geometrically, to small particles, and the same method of characterizing the surface and volume of the void spaces was used. Of course, the void volume of a porous solid and that of a distribution of small particles differ in a major respect. That is, the voids are continuous and interconnected, but the particles are discrete and individual. However, the basic characterization should be the same for both cases. The difference is manifest in the numerical value of the shape factor ratio. It is reasonable to assume that the meniscus curvature of a

liquid contained in a pore bears a definite relationship to the volume and surface of the pore, depending on the pore shape. Thus, the mean hydraulic radius, $\underline{m} = \gamma/\underline{P_c}$, was taken as the measure of the pore size, analogous to the particle size, $\underline{X}$, for solid particles. Therefore, for the pore space in a porous medium, the ratio of frictional drag surface to volume, or $\underline{S_o}/\epsilon$, by analogy with Equation (32) is

$$\frac{\underline{S_o}}{\epsilon} = \frac{\alpha_s}{\alpha_v} \frac{\sum \underline{m_i}^2 \underline{n_i}}{\sum \underline{m_i}^3 \underline{n_i}} \tag{33}$$

For a bed having uniform pores of size, $\underline{m}$, Equation (33) becomes

$$\frac{\underline{S_o}}{\epsilon} = \frac{\alpha_s}{\alpha_v} \frac{\underline{m}^2 \underline{n}}{\underline{m}^3 \underline{n}} = \frac{\underline{C}}{\underline{m}} \tag{34}$$

where $\underline{C} = \alpha_s/\alpha_v$.

Consider now a small element of a homogeneous porous medium having a distribution of pore sizes. Let this element contain all the pores in a very narrow range of pore sizes, $\underline{m_1}$ to $\underline{m_2}$, such that for practical purposes, this element may be considered to contain only pores of uniform size. The porosity of this element is given by $\epsilon\Delta\underline{s}$, where $\Delta\underline{s}$ is the change in saturation of the whole porous medium associated with the change in pore size from $\underline{m_1}$ to $\underline{m_2}$. Similarly, the frictional drag surface area of this element is given by $\Delta\underline{S_c}$. Since the pores of this small element may be filled over a range of saturations of the total medium, there is no single specific value of $\underline{k_{oc}}$ or $\underline{T_c}$ which corresponds to these particular pores. These are average factors, determined for the system as a whole and are independent of any particular pore size. The permeability of this small element, according

to Equation (27) is

$$\underline{K}_{ci} = \frac{\epsilon^3 (\Delta \underline{s})^3}{\underline{k}_{oc} \underline{T}_c^2 (\Delta \underline{S}_c)^2}. \tag{35}$$

Since this small element has pores of uniform size, then by Equation (34),

$$\frac{\epsilon \Delta \underline{s}}{\Delta \underline{S}_c} = \frac{\bar{\underline{m}}}{\underline{C}_c} \tag{36}$$

where $\bar{\underline{m}} = (\underline{m}_1 + \underline{m}_2)/2$ and $\underline{C}_c$ corresponds to $\underline{C}$ at saturation, $\underline{s}$. In this sense, the term, $\underline{C}_c$, is an average value for all the different size pores in the system. Thus, it has the same significance as $\underline{k}_{oc}$ and $\underline{T}_c$.

Substituting Equation (36) into Equation (35),

$$\underline{K}_{c_i} = \frac{\epsilon \Delta \underline{s} (\bar{\underline{m}})^2}{\underline{k}_{o_c} \underline{T}_c^2 \underline{C}_c^2} \tag{37}$$

Wyllie and Spangler (48) have shown that the over-all specific permeability to liquid of the total medium at saturation, $\underline{s}$, is equal to the summation of permeabilities of all the small elements of the medium which are filled at this saturation. Thus,

$$\underline{K}_c = \sum_{\underline{s}=0}^{\underline{s}=\underline{s}} \underline{K}_{c_i} = \frac{\epsilon}{\underline{k}_{oc} \underline{T}_c^2 \underline{C}_c^2} \sum_{\underline{s}=0}^{\underline{s}=\underline{s}} (\bar{\underline{m}})^2 \Delta \underline{s}. \tag{38}$$

and

$$\lim_{\Delta \underline{s} \to 0} \sum_{\underline{s}=0}^{\underline{s}=\underline{s}} (\bar{\underline{m}})^2 \Delta \underline{s} = \int_0^{\underline{s}} \underline{m}^2 \, d\underline{s}. \tag{39}$$

Combination of Equations (38) and (39) yields

$$\underline{K}_c = \frac{\epsilon}{\underline{k}_{oc} \underline{T}_c^2 \underline{C}_c^2} \int_0^{\underline{s}} \underline{m}^2 \, d\underline{s}. \tag{40}$$

At $\underline{s} = 1.0$,

$$\underline{K} = \frac{\epsilon}{\underline{k}_o \underline{T}^2 \underline{C}^2} \int_0^1 \underline{m}^2 \, \underline{ds}. \tag{41}$$

The relative permeability at saturation, $\underline{s}$, is

$$\underline{Kr} = \frac{\underline{k}_o \underline{T}^2 \underline{C}^2}{\underline{k}_{oc} \underline{T}_c^2 \underline{C}_c^2} \frac{\int_0^{\underline{s}} \underline{m}^2 \, \underline{ds}}{\int_0^1 \underline{m}^2 \, \underline{ds}}. \tag{42}$$

This equation would be identical to Wyllie and Spangler's derived equation if $\underline{k}_{oc}$ and $\underline{C}_c$ were assumed to be constant at all saturation.

The distribution of the solid-liquid contact surface, $\underline{S}_c$, with saturation can be determined from both Equations (29) and (36). Thus, from Equation (29),

$$\underline{S}_c = \underline{S}_o \sqrt{\frac{\underline{s}^3 \underline{k}_o \underline{T}^2}{\underline{K}_r \underline{k}_{oc} \underline{T}_c^2}} \tag{43}$$

and from Equation (36),

$$\underline{S}_c = \epsilon \underline{C}_c \int_0^{\underline{s}} \underline{ds}/\underline{m}. \tag{44}$$

The frictional drag surface areas of the glass fibers, which are hydraulically smooth, are probably well defined.

Wyllie and Spangler (48) discuss the physical significance of Equation (38). By their reasoning, Equation (38) implies that flow takes place through discrete channels of pores of the same size without any interference from pores of a different size. Of course, this is not literally true; however, the inaccuracy of this implication can be rationalized by considering

the flow through pores of the same size to occur by way of interconnecting pores of different size. The flow resistance in these different size pores may then be ignored, since this resistance is automatically incorporated in the permeability relationship for each size of pore involved in the flow.

PRESENTATION OF THE PROBLEM

The survey of the literature disclosed that the analysis of two-phase flow has been limited substantially to incompressible granular media and immiscible fluid phases. It is apparently well established that the predominant mechanism of liquid movement in these partially saturated macroporous systems is that of capillary flow. For streamline flow conditions, theoretical expressions of the liquid relative permeability were developed from the Kozeny method of analysis which were moderately successful for these granular systems (48). However, the general applicability of this theory to systems of different physical structure is highly doubtful.

In the macroporous glass fiber-water-air systems of this work, it is reasonable to expect the mechanism of liquid flow to be fundamentally the same as that in granular media. Consequently, the same method of analysis used to characterize two-phase flow in granular media should be valid for the glass fiber beds. However, in the theoretical development of the relative permeability expression, modifications were proposed and introduced to extend the generality of this theory. Thus, the relative permeability is expressed in terms of the pore size distribution and certain empirical factors which are presumably characteristic of the pore structure and, hence, the structure of the solid medium particles. The use of the Kozeny approach naturally imposes certain limitations on the experimental conditions, viz., the beds must have a random pore structure; no pores are sealed off; streamline flow is maintained; and molecular effects are either absent or insignificant. All of these conditions were to be observed in the experimental program. In addition, the glass fiber beds were to be rendered

effectively incompressible by externally compacting them in the experimental runs. Henceforth, these compressed beds will be referred to as incompressible beds. Approximate isothermal conditions were to be maintained during the experimentation to minimize the complications of a variable temperature. Further, the study was to be limited to the flow of water only with the non-wetting air phase stationary in the system. Under these conditions, then, a fundamental and instructive analysis of two-phase flow in fibrous media was feasible.

The specific experimental objectives of this work were to determine (1) static capillary pressure curves of the glass fiber beds from which effective pore size distributions could be determined and (2) steady state liquid relative permeability curves over the range of saturations covered by the capillary pressure measurements. Only the desorption stage of capillary equilibrium was to be investigated, i.e., capillary equilibrium was to be achieved by desaturating the beds in all cases. From these data, the values of the characteristic empirical factors were to be determined and the role of the pore size distribution in the relative permeability evaluated from the theoretical equations. The difference in pore structure between granular and fibrous media should be manifest in the values of the empirical factors. Thus, a comparison of the relative permeability curves and the values of these factors for the granular and fibrous systems should provide pertinent information about the important variables in the two-phase flow system and shed some light on the capillary flow mechanism in systems of diversified structure.

NOMENCLATURE

(In consistent c.g.s. units)

A Cross-sectional area of bed perpendicular to the direction of flow, $cm.^2$

a Pore radius, cm.

b Empirical constant in Equation (5), defining relative permeability, dimensionless

C Factor of proportionality in the relationship, $S_o/\epsilon = C/m$, which applies to the total pore space of a medium, i.e., to the water-filled pores at complete saturation; $C = \alpha_s/\alpha_v$, dimensionless

C_c Factor corresponding to C for partially saturated media, dimensionless

D Length of a chord of a circle used in the calculation of the bed dimensions, cm.

D_b Diameter of bed, cm.

D_p Pore diameter, $D_p = 4m$, cm.

D_t Diameter of flow tube used in the porous plate calibrations, cm.

D_w Weighted average diameter of the fibers from microscopic analysis, cm.

F Formation factor for saturated porous media, determined from electrical resistivity measurements, dimensionless

F_c Formation factor for unsaturated porous media, dimensionless

g Acceleration due to gravity, 980 cm./sec./sec.

h Displacement of a chord of a circle from the subtended arc, used in the calculation of the bed dimensions, cm.

I Resistivity index, $I = F_c/F$, dimensionless

I_p Interfacial area between the wetting and nonwetting phases, $cm.^2$

J Conductivity ratio, $J = 1/F$, dimensionless

K Permeability of a saturated porous medium; D'Arcy's permeability coefficient, $cm.^2$

K_c Wetting phase specific permeability of an unsaturated porous medium, $cm.^2$

K_r Wetting phase relative permeability of an unsaturated porous medium, $K_r = K_c/K$, dimensionless

k Kozeny constant for saturated porous media, $k = k_o T^2$, dimensionless

k_o Channel shape factor in Kozeny constant for saturated porous media, dimensionless

k_{oc} Wetting phase channel shape factor for unsaturated porous media, dimensionless

L Thickness of a fiber bed, cm.

L_e Average tortuous length of the actual flow path of liquid through a saturated bed of thickness L, cm.

L_p Length of gage pegs, cm.

M Empirical constant in Childs and George's derived equation of relative permeability, dimensionless

M_t Differential manometer reading (difference in levels of manometer fluid) at temperature t, cm.

m Mean hydraulic radius of a capillary or pore, $m = \gamma/P_c$, cm.

n Negative slope of log I vs. log s plot, dimensionless

P Fluid pressure, dynes/cm.^{2}

P_c Capillary pressure, or pressure difference across a two-fluid phase curved interface in a capillary or pore, dynes/cm.^{2}

P_D Displacement pressure, equal to the capillary pressure required to displace liquid from a saturated porous medium of uniform pore size, dynes/cm.^{2}

ΔP_f Frictional pressure drop across the bed, dynes/cm.^{2}

ΔP_t Frictional pressure drop across the porous plate at temperature t, dynes/cm.^{2}

q Volumetric rate of fluid flow, cc./sec.

R_1, R_2 Principal radii of curvature of the interfacial meniscus between two fluid phases, cm.

r Pore radius, cm.

S Surface area of solid particles, cm.^{2}

S_c Surface area of flowing wetting phase liquid subjected to drag resistance per unit volume of bed in an unsaturated or two-phase system, $cm.^2/cc.$

S_E Total surface area of flowing wetting phase liquid per unit volume of bed in a two-phase system, $cm.^2/cc.$

S_L Total surface area of all the wetting phase liquid per unit volume of bed in a two-phase system, $cm.^2/cc.$

S_o Surface area of particles per unit volume of the bed, $cm.^2/cc.$

S_p Surface area of particles per unit of pore volume of the bed, $cm.^2/cc.$

S_v Volumetric specific surface of glass fibers, surface area per unit volume of fibers, $cm.^2/cc.$

S_w Surface area of the filtration tube walls covered by the bed per unit volume of the bed, $cm.^2/cc.$

s Liquid wetting phase saturation of a porous medium, equal to the fractional part of the total pore space which is filled with liquid, dimensionless

s_r Residual or pendular saturation of a medium, which is the minimum saturation that can be attained by capillary displacement, dimensionless

T Tortuosity of a saturated porous medium, $T = L_e/L$, dimensionless

T_c Liquid wetting phase tortuosity in a partially saturated porous medium, dimensionless

t Temperature, °C.

V Volume of solid particle, cc.

V_b Volume of glass fiber bed, cc.

V_s Volume of a spherical segment of one base, cc.

W Weight of bonedry fiber in bed, g.

x Linear size of a solid particle, cm.

z Thickness of the compressed glass fiber bed at the edge, cm.

α_s Factor of proportionality between the surface area of solid particles and the second moment of the particle size, dimensionless

α_v Factor of proportionality between the volume of solid particles and the third moment of the particle size, dimensionless

γ Interfacial tension between two fluid phases, dynes/cm.

ϵ Total porosity of a porous bed, void volume per bed volume, dimensionless

θ' Angle of contact, dimensionless

μ Fluid viscosity, dyne - sec./cm.^{2}

$\mu_{\underline{t}}$ Water viscosity at temperature $\underline{t}$, dyne - sec./cm.^{2}

ρ Specific value of pore size in Childs and George's equation of relative permeability, cm.

ρ_L Density of liquid water, g./cc.

$\Delta\rho_{\underline{t}}$ Difference in densities of differential manometer fluid and water at temperature $\underline{t}$, g./cc.

σ Specific value of pore size in Childs and George's equation of relative permeability, cm.

EXPERIMENTAL EQUIPMENT

STATIC CAPILLARY PRESSURE APPARATUS

Two methods have been outstanding in the literature for the determination of capillary pressure curves for macroporous media. These are the mercury intrusion and capillary displacement methods. They are discussed generally by Carman (2) and Scheidegger (3) and more specifically by Pearse, Oliver, and Newitt (14), Barkas, et al. (13, 65), and Grace (66). In the present work, the capillary displacement method was used for two reasons: (1) the apparatus and technique is much simpler for capillary displacement than for mercury intrusion, and (2) since the systems being studied employed water as the liquid wetting phase, results of the capillary displacement method using water as the displaced liquid could be used directly in the analysis of the data. An inherent limitation of this method is that the pore size range which can be covered is restricted at the low pore sizes by the residual saturation. In most macroporous systems, this is only a minor disadvantage. The following features were desired in the experimental apparatus:

(1) The capacity to make a complete and precise determination of the capillary pressure desorption curve using a single fiber bed.

(2) A means to maintain a constant capillary pressure on the system during the approach to capillary equilibrium.

(3) A means to compress the bed to predetermined dimensions during the run.

(4) The capacity to test large beds of the size used for the permeability measurements.

(5) Transparency to permit the detection of air bubbles in the system.

(6) Ease of dismantling and assembly to permit cleaning and calibration of the apparatus.

An apparatus modeled after that of Christensen and Barkas (13) with some major modifications was constructed which incorporated these features. This apparatus is schematically diagrammed in Figure 6 and a photograph of it is shown in Figure 7.

The key piece of equipment in this apparatus was the porous plate on which the fiber bed rests. This plate was constructed from a 90-mm. diameter fine grade fritted glass funnel by welding a ball joint on the funnel stem and sawing the top of the funnel off. When filled with water, this plate provided a means to transmit capillary pressure, or suction, to the water in the bed without allowing air to enter the system. The range of pore sizes in this plate was reported as 4.0-5.5 microns (67), and it could withstand a capillary pressure of 38 cm. Hg. when saturated with water at 23.5°C. Thus, this was the maximum capillary pressure that could be applied to the fiber system. If higher pressures were desired, a plate of smaller pore sizes would have to be used.

This plate was connected through a ball and socket joint, stopcock, right angle tee, and another ball and socket joint to a 50-ml. buret tube as shown. These ball and socket joints permit the apparatus to be easily dismantled and also gives the apparatus flexibility. The buret tube was connected to a vertically adjustable mercury reservoir, which was open to the atmosphere, by a length of 3/16-in. tygon tubing. This buret tube-

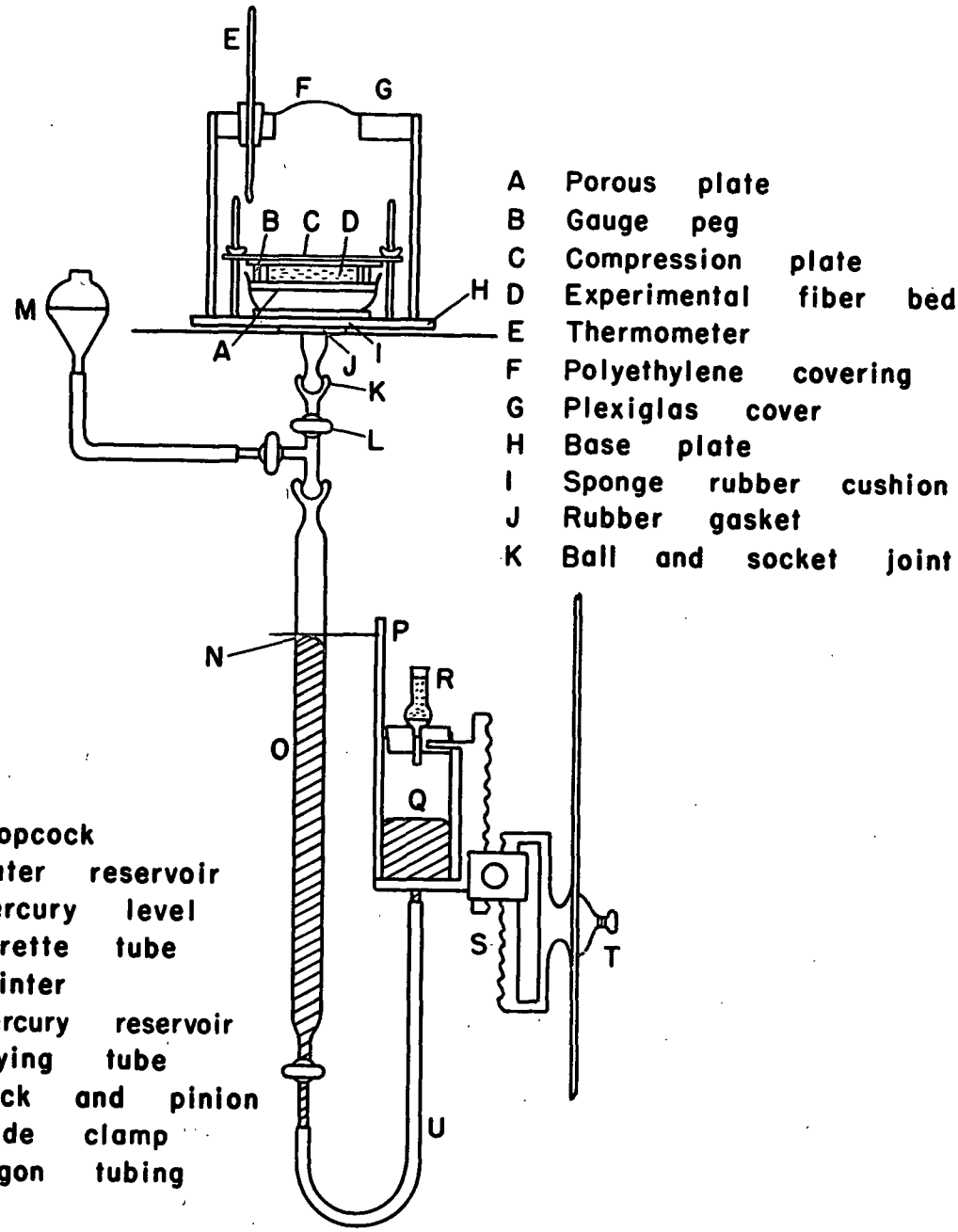

Figure 6. Static Capillary Pressure Apparatus

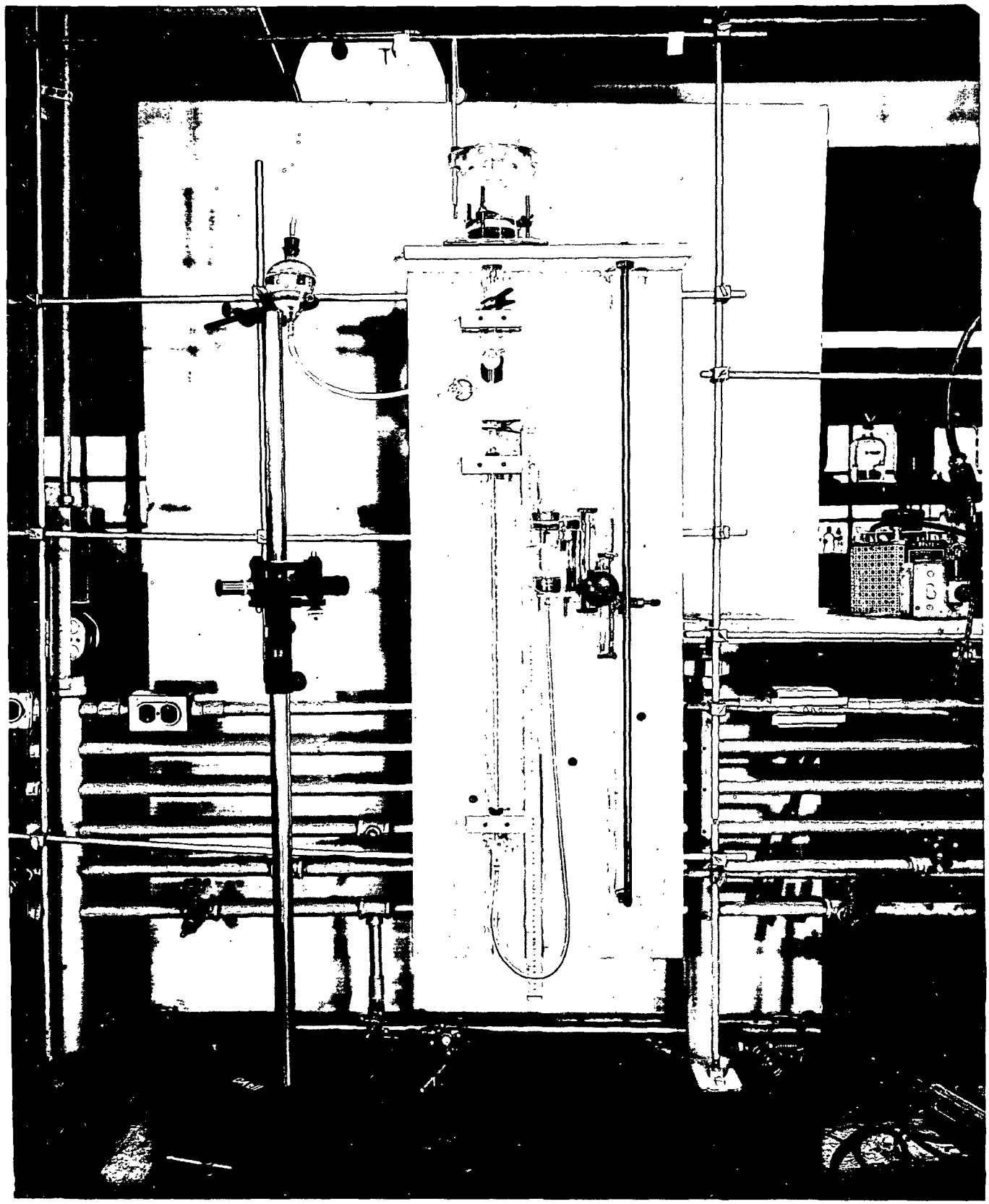

Figure 7. Photograph of Static Capillary Pressure Apparatus

reservoir assembly was, in essence, a mercury manometric arrangement for imposing a capillary pressure on the glass fiber system. The buret tube also served as a means for quantitatively measuring the water expressed from the bed. The mercury reservoir was mounted on a compound rack and pinion that had a maximum displacement of 8 inches. The rack and pinion in turn was mounted on a vertically sliding clamp that could be moved along the entire length of the buret tube. In maintaining a capillary pressure in the run, the sliding clamp served as a fixed coarse adjustment and the rack and pinion offered a manually operable variable fine adjustment. The mercury reservoir was constructed from a cylindrical weighing bottle having an inside cross-sectional area approximately 13.6 times as great as that of the buret tube. By this arrangement, the increase in capillary pressure due to the increasing water head above the buret tube mercury level as the system approached equilibrium was exactly compensated by the decreasing difference between the two mercury levels in the buret tube and the reservoir. A wire pointer fixed to a small stick graduated in centimeters was attached to the mercury reservoir by rubber bands. This pointer served as a visual guide so the mercury reservoir could be moved down in unison with the mercury level in the buret tube. In this way, a constant capillary pressure was maintained on the bed. A water reservoir was connected into the apparatus as shown for the purpose of removing excess water from the system.

In order to maintain a quantitative separation between the water and the mercury in the buret tube, the inside walls of the tube were coated with Desicote*, an organosilicon compound which rendered the glass walls

* For particulars and instructions on the use of this compound, see Beckman Bulletin 262-B, Beckman Instruments, Inc.

nonwettable by water. This treatment minimized the amount of water trapped on the walls of the tube when the tube was refilled with mercury for a repeat run.

The device for compressing the bed on the porous plate is depicted in detail in Figure 8. It consisted of a flat, round solid brass plate, 3-1/4 inches in diameter and 1/8-inch thick, which was laid on top of the bed. On this plate rested a three-cornered brass compression plate equipped with holes at each corner. Three 1/4-inch threaded brass studs were mounted in the 1/4-inch thick brass base plate around the porous plate so they extended through the holes in the compression plate. Compression was effected by screwing down the compression plate with wing nuts on the studs. The thickness of the bed was gaged by three 1/4-inch brass gage pegs set equidistantly around the periphery of the bed to provide a uniform spacing between the round brass plate on top of the bed and the porous plate. Sets of three different length gage pegs were used: .793 cm., .996 cm., and 1.501 cm. The three gage pegs were machined square and agreed in length to within $\pm$.002 in. A sponge rubber doughnut-shaped ring was placed between the porous plate and the base plate to cushion the glass porous plate against the base plate.

The fiber bed, compression device, and porous plate assembly were completely enclosed by a six-inch cylindrical Plexiglas cover. A round hole in the top of the cover was sealed over with a flexible covering of polyethylene sheeting to allow the equalization of air pressure inside the cover with the atmospheric pressure. A thermometer was also sealed in the top of

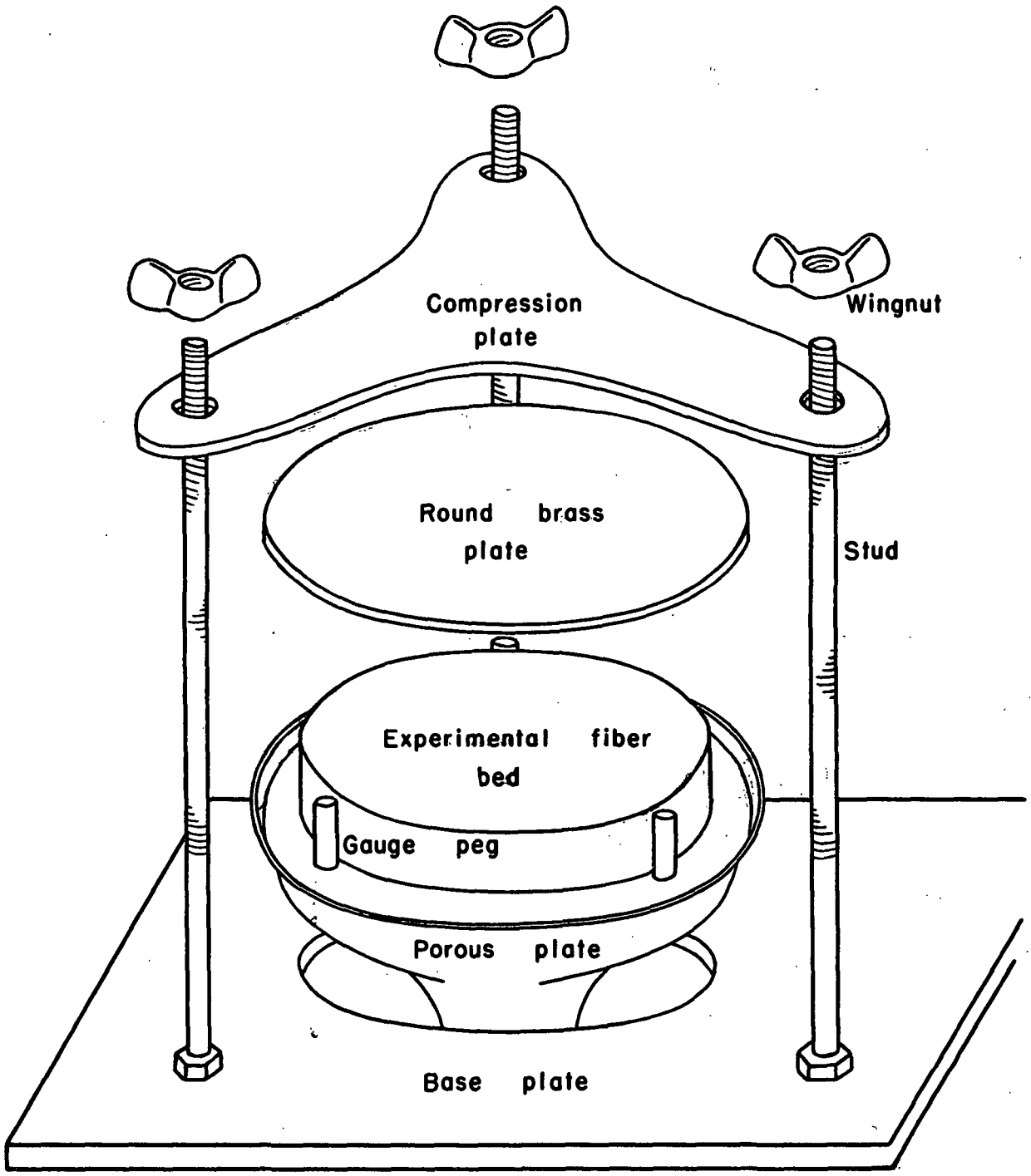

Figure 8. Detail of Compression Device on the Capillary Pressure Apparatus

the cover. The bottom edge of the cover was coated with stopcock grease and pressed against the polished base plate to seal it against the escape of water vapor. A seal around the stem of the porous plate was effected by a snug fitting rubber gasket between the base plate and the mounting board. The whole apparatus was rigidly mounted on a vertically standing plywood panel board.

STEADY STATE PERMEABILITY APPARATUS

The basic plan for determining the water permeability of the glass fiber beds was to measure the steady state water flow rate and pressure drop across thin beds when the beds were at capillary equilibrium and calculate an average over-all permeability from these data by D'Arcy's law. The beds used were thin enough and the pressure drop across the bed small enough so there was only a slight variation in permeability across the bed. The average permeability then would approximate a point value permeability corresponding to the average saturation of the bed. Under these conditions, the flow rates were very small. Thus, the apparatus was constructed with the following features:

(1) A means to maintain a steady-state water-flow rate and pressure drop across the bed at various over-all capillary pressures.

(2) A means to measure very low water-flow rates and pressure drops.

(3) A means to compress the bed to predetermined dimensions during the run.

(4) Ease of dismantling and assembly for cleaning and calibration purposes.

A consideration of these features led to the construction of apparatus depicted schematically in Figure 9 and photographically in Figure 10. This apparatus incorporated the basic plan of that used by Ceaglske and Kiesling (38); however, it was necessary to make some major alterations and additions to their design to adapt it to the materials and conditions of this investigation.

The operational plan of this apparatus was to apply a capillary pressure to the fibrous system independently at each face of the bed. By maintaining a slightly higher capillary pressure at the downstream face, a flow was induced from the upstream to the downstream side. The average capillary pressure in the bed was taken as the mean of the pressures at the upstream and downstream faces. In this work, the water always flowed vertically upward through the bed.

As in the capillary pressure apparatus, the key pieces of equipment in the permeability set-up were the porous plates between which the experimental bed was compressed. Similar to that used in the capillary pressure apparatus, these plates were constructed from 90-mm. fine grade fritted glass funnels. Each plate was equipped with a pressure tap inside the fritted glass plate. Details of this pressure tap construction are shown in Figure 11. A small hole was drilled in the glass wall of the funnel just under the fritted glass plate using a short length of 1/32-inch brass rod in a drill press and a thick paste of coarse carborundum grinding powder. A short nipple of 3/16-inch brass tubing, brazed to a ring of brass sheeting which encircled the funnel and gasketed against the glass funnel with 1/32-inch rubber, was securely sealed over the hole and clamped tight by a bolt

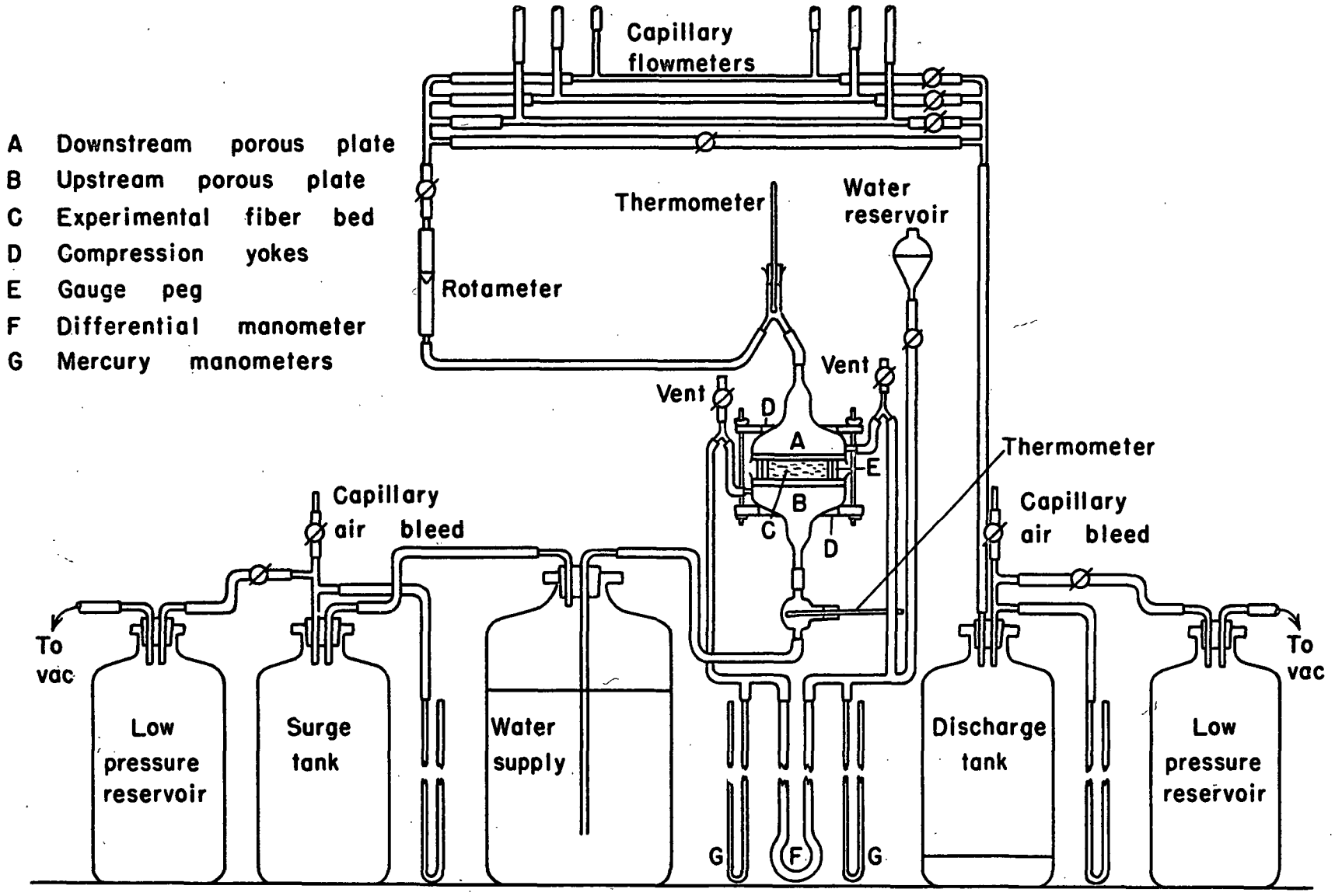

Figure 9. Steady-State Permeability Apparatus

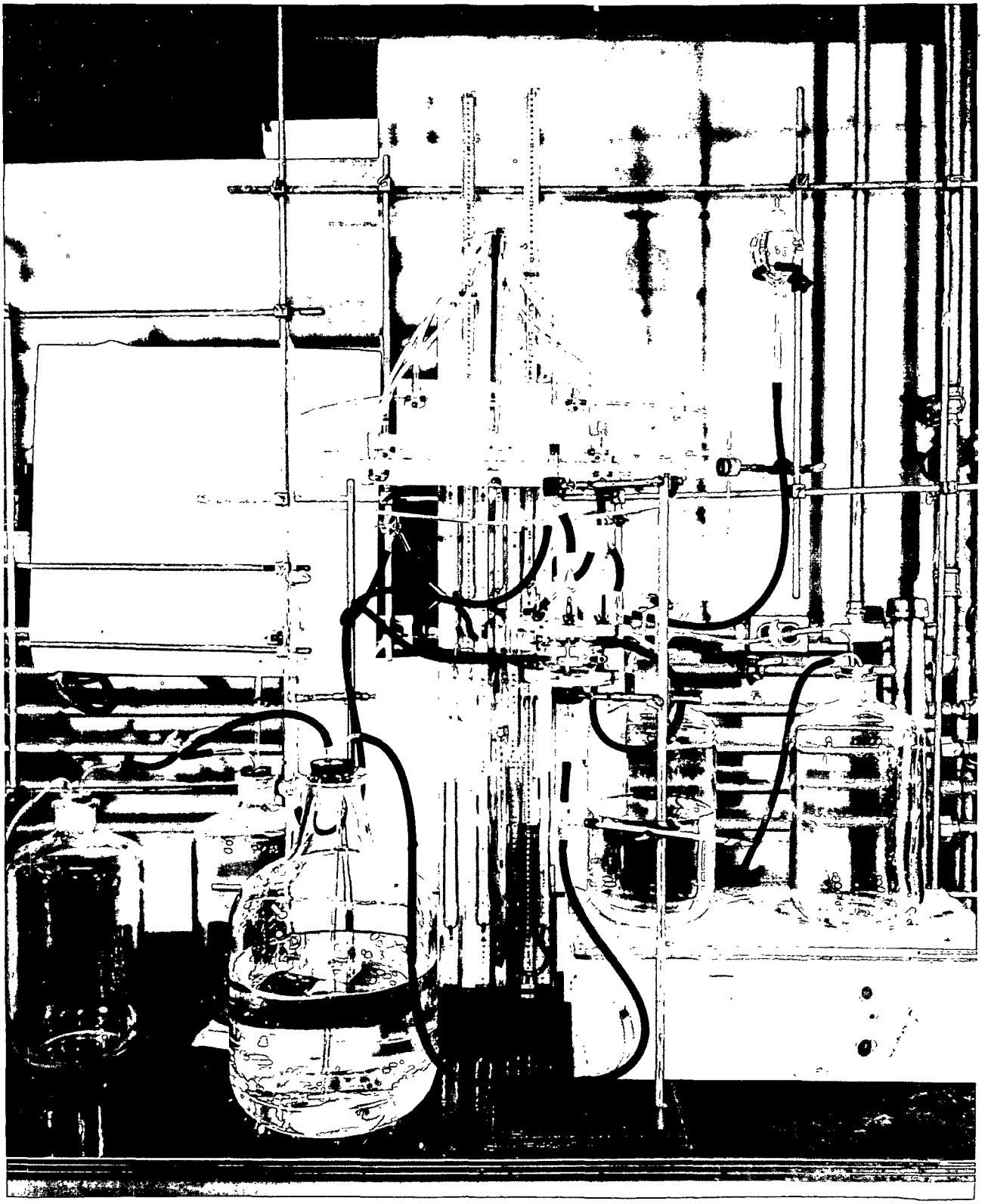

Figure 10. Photograph of Steady-State Relative Permeability Apparatus

A Hole drilled in wall of the porous plate funnel
B Brass clamping ring
C Pressure tap brazed to the clamping ring
D Clamping bolt and wingnut

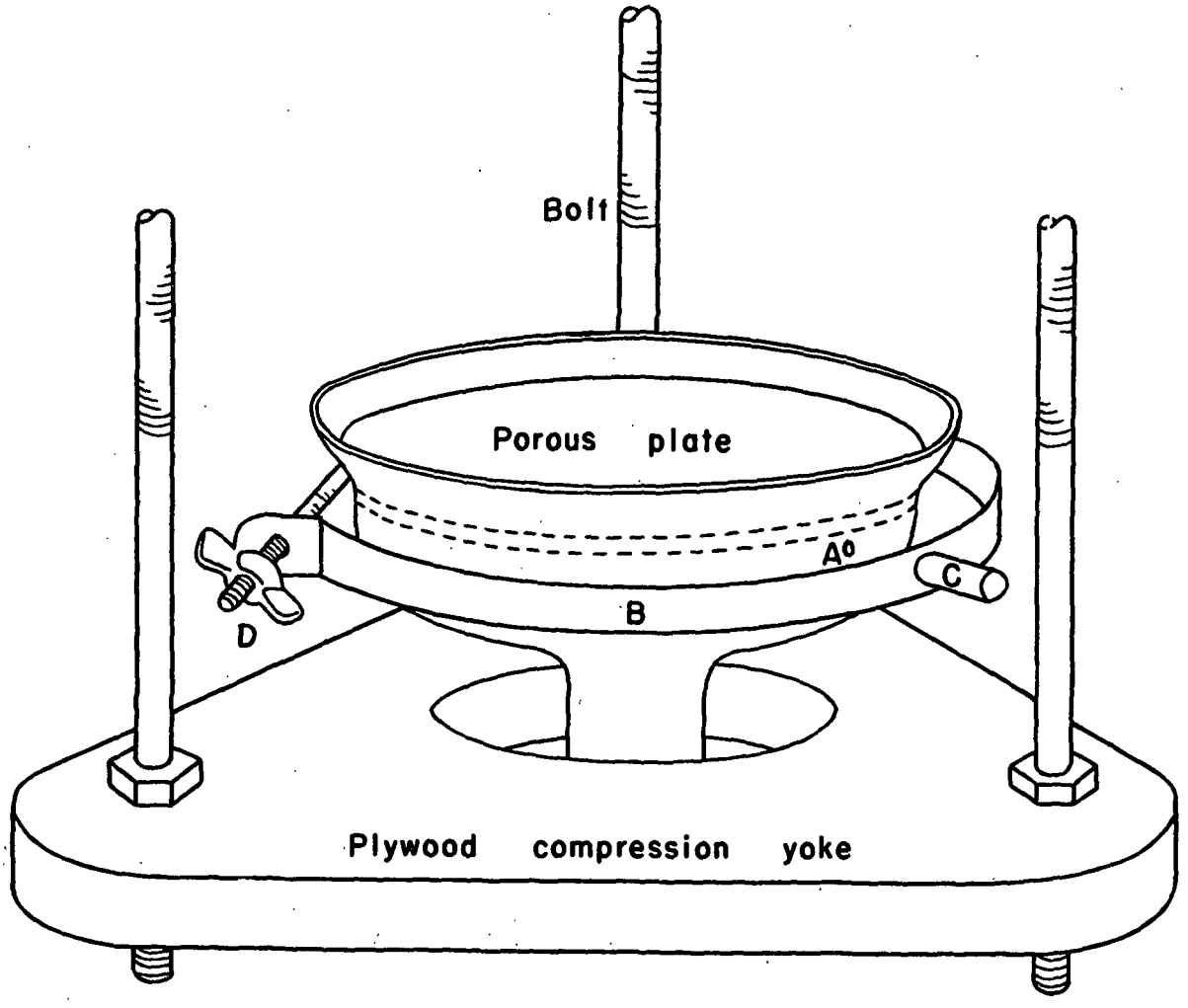

Figure 11. Detail of Pressure Tap Construction and Compression Device on the Porous Plate in the Permeability Apparatus

and wingnut in the ends of the brass clamping ring. By this means, a manometer lead could be attached to the plate for measuring the fluid pressure inside the porous plate. During a run, these plates were clamped in position to a ringstand. In addition to the fine grade plates, medium grade plates were also used for greater accuracy at the high saturations. These medium-grade plates had the same diameter and were constructed similar to the fine grade plates. The range of pore sizes in these plates were listed as 10-15 microns (67).

During the permeability runs, the bed was compressed between the two porous plates by a yoke assembly, one half of which is illustrated in Figure 11. This assembly consisted of two triangular plywood yokes that fitted over the stems of the porous plate funnels. These yokes were clamped together by means of three brass bolts equipped with wingnuts that extended through the corners of the yokes. The thickness of the bed was gaged by the same brass gage pegs used in the capillary pressure apparatus. Prior to a run, the assembled unit of yokes, plates, and bed was enclosed in a double thickness of polyethylene sheeting to reduce any vaporization effects and temperature fluctuations.

A differential manometer was connected across the two porous plates and bed by means of the pressure taps on the plates. Large glass tubing (10 mm. o.d.) was used for this manometer to minimize the capillary effect at the water-manometer fluid interface. It happened, fortuitously, that this size tubing was small enough to be sensitive to slight changes in the pressure drop but was large enough so the pressure drop was stabilized at steady state conditions without undue difficulty. The manometer fluid was

obtained from the Meriam Instrument Company and designated as No. D-8325. The specific gravity of this fluid was specified as 1.75. The variation of its density with temperature over a limited range was determined pycnometrically, and the results are shown in Table I. Apparently, the 1.75

TABLE I

DENSITY OF DIFFERENTIAL MANOMETER FLUID

Temperature, °C.	Pycnometric Density, g./cc.
21.1	1.743
22.2	1.741
23.1	1.740
24.3	1.739
25.2	1.738
26.1	1.737
27.0	1.736

value specified by the manufacturer referred to a temperature of or about 20°C. The temperature-density curve constructed from these data was used in the correction of the pressure drop measurements for temperature variation in the permeability runs. Mercury manometers with one leg open to the atmosphere were connected into both the upstream and downstream differential manometer leads to measure the individual capillary pressures on each side of the bed. A water reservoir was connected into the downstream manometer lead for the purpose of filling the downstream plate and flow lines before making a run. In addition, vents were placed in both the upstream and downstream manometer leads as a means to purge the leads of air bubbles.

Water for the flow system was supplied from a 5-gallon bottle connected by a flexible water-flow line to the upstream porous plate. The purpose of using such a large reservoir was to keep the water level, and hence the capillary pressure on the upstream plate from changing appreciably during a run. The source of vacuum in the upstream system was an aspirator in the city water line connected to the 5-gallon supply bottle through two 9-liter bottles in series. The bottle adjacent to the water supply served as a surge tank and was equipped with a mercury manometer and a capillary air bleed. The other bottle was simply a low pressure reservoir. These bottles were connected with an air-tight rubber hose, and a glass stopcock was placed in the line between them. A pinchclamp was used in the air bleed line.

A flexible water flow line led from the downstream porous plate to a tri-flat rotameter, no. 08F-1/16-20-4* with a steel float, through the capillary flowmeter system and emptied into a 9-liter discharge bottle. The downstream vacuum system was identical to the upstream one, consisting of two 9-liter bottles in series with a water aspirator as the vacuum source. The 9-liter discharge bottle was equipped with a mercury manometer and a capillary air bleed.

The capillary flowmeter system consisted of three different size capillary tubes and a bypass line in parallel. The bores of these capillary tubes were roughly 0.25 mm., 0.50 mm., and 0.75 mm., and their corresponding lengths were 18 cm., 27.5 cm., and 30 cm., respectively. Glass tees were welded to each end of the capillary tubes to serve as manometer taps. Each tube was connected to a separate manometer so that each capillary flowmeter

*See Handbook F & P Tri-Flat Variable Area Flowmeters. Fischer and Porter Company, Hatboro, Pennsylvania, 1954.

was essentially independent of the others. The manometer fluid used in these flowmeter manometers was a solution of carbon tetrachloride and benzene (approximately 23% benzene by weight) having density values which were measured pycnometrically and are listed in Table II. The curve constructed from these data was used to correct the flowmeter calibrations for temperature fluctuations during the permeability runs. Tygon tubing was used for the bypass line, manometer leads, and connections between the capillary tubes and the entrance and exit headers. Glass stopcocks were placed in the flow lines on the downstream side of the flowmeters and in the bypass line. All of the manometers in the apparatus, including the capillary flowmeter, differential, and mercury manometers, had a maximum displacement of 56 cm. The range of flow rates covered by each capillary flowmeter slightly overlapped that of the adjacent sized flowmeter.

TABLE II

DENSITY OF CAPILLARY FLOWMETER MANOMETER FLUID

Temperature, °C.	Pycnometric Density, g./cc.
12.0	1.297
21.0	1.282
24.6	1.278
28.2	1.272

Tygon tubing was used initially for all the flexible connections, including the water-flow lines, manometer leads, and connections in the vacuum system. In time, it was suspected that the tygon tubing caused a

decrease in the surface tension of the water. To verify this, surface tension and viscosity tests were made on water that contacted the tygon and also on water that contacted black rubber tubing, which was a possible substitute for the tygon. A small piece of tygon tubing was placed in each of six 250-ml. bottles filled with freshly deaerated demineralized water. The surface tension and viscosity of these samples were checked periodically to determine if the tygon had an effect. The same experiment was carried out using black rubber tubing. The results of these tests are shown in Table III. The uncorrected Du Nouy tensiometer reading and Ostwald viscometer time at 23.0°C. of the initially pure water were 76.3 dynes/cm. and 240.5 sec., respectively. It is apparent from this test that the surface tension of water is markedly lowered by the tygon. Apparently, the water leaches a surface-active plasticizer out of the tygon, as after the tygon remains in water for a long time, it becomes hard and brittle. The surface tension was only changed slightly, if at all, by the black rubber tubing. Thus, the tygon tubing attached to the porous plates, including the flow lines from the reservoir and to the rotameter and the manometer leads were replaced with black rubber tubing. Since the viscosity of the water was not changed by the tygon, the tygon connections on the flowmeters were retained. The major disadvantage of using black rubber tubing was that it was opaque, and the formation of air bubbles in these lines was not visually apparent. It was observed further that the dissolution of air had no appreciable effect on the surface tension of the water.

Thermometers were inserted in the water-flow lines, both upstream and downstream from the experimental bed. A thermometer was also placed in the

plastic enclosure around the bed to measure the ambient temperature in the vicinity of the bed. The ambient capillary flowmeter and differential manometer temperatures were also measured with thermometers in those positions.

TABLE III

EFFECT OF TYGON AND BLACK RUBBER TUBING ON THE SURFACE TENSION AND VISCOSITY OF WATER

	Uncorrected Du Nouy Tensiometer Reading, dynes/cm.		Ostwald Viscometer Time, sec.	
Time, hr.	Tygon	Black Rubber	Tygon	Black Rubber
0	76.3	76.3	240.5	240.5
4	76.0	76.3	241.7	—
12	75.5	76.2	239.7	239.5
24	70.5	76.1	239.4	239.5
48	63.0	74.6	239.7	239.6
72	60.0	—	239.7	—

APPARATUS FOR FORMING THE GLASS FIBER BEDS

The diameter of the glass fiber beds used in this work was governed by the need to have beds (1) that could be easily handled and transferred, (2) that were large enough so reasonable homogeneity and freedom from wall effects could be easily achieved and so the beds would have an appreciable flow area at low saturations, and (3) that were small enough to be free from undue macroscopic distortion and comply with a reasonable size of apparatus. To meet these needs, the beds were formed in a filtration tube having an inside diameter of 2-1/2 inches. This filtration tube was modeled

after the one constructed and used by Ingmanson (68). A schematic diagram of this tube and the filtration setup is shown in Figure 12. The upper part of the filtration tube consisted of a Plexiglas cylinder of 2-1/2 inches inside diameter which rested on the top of the septum. The top of this cylinder expanded to a 6-inch cylinder as shown. The bottom part of the filtration tube, on which the septum rested, was rigidly mounted on a platform about four feet from the floor. This tube was the same size as the upper filtration tube, 2-1/2 inches i.d. Plexiglas flanges on the two parts of the tube enabled them to be clamped together with brass bolts with the septum between them. This construction permitted the tube to be easily dismantled. Rubber gaskets between the septum and the tube served to make the system air tight. The bottom of the septum was shouldered and the flange on the upper tube was recessed so the septum and filtration tubes were self-centering.

The septum was constructed from brass in two parts, similar to a British sheet mold septum. A diagram of each part is shown in Figure 13. When the septum was assembled, a circular piece of 65-mesh brass screen was fitted into the recessed top of the bottom section of the septum. Over this, a piece of 150-mesh brass screen was molded so that it covered the raised center portion of the bottom section. Thus, as the two sections were bolted together, the 150-mesh screen was drawn taut over the top of the 65-mesh screen. The assembled septum then comprised a circular filtration area of 2-1/2 inches diameter including a 150-mesh screen over a 65-mesh screen and backed up by a brass plate perforated with 1/4-inch holes and having, approximately, a 50% open area. The two sections were gasketed with dental dam.

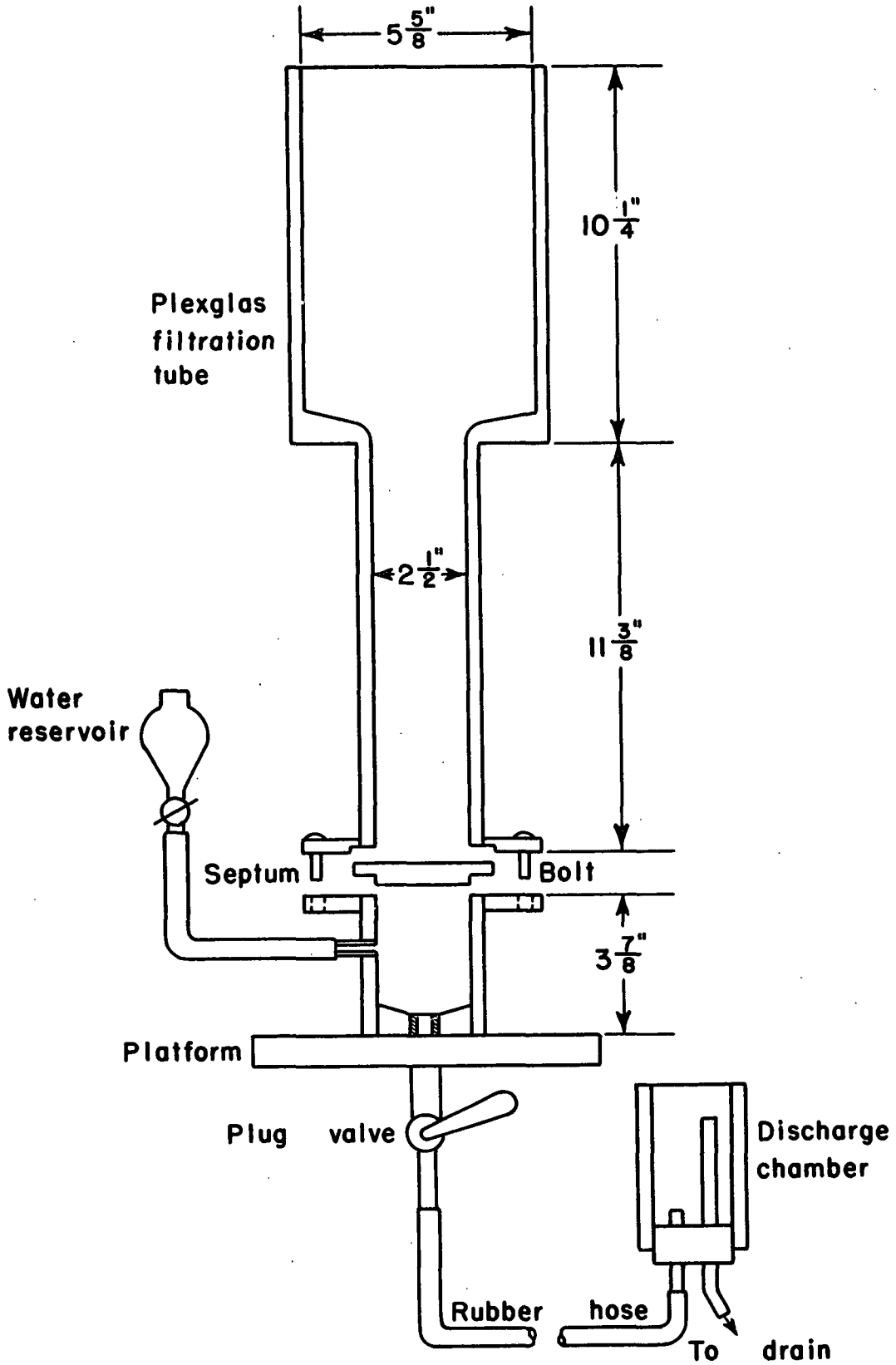

Figure 12. Apparatus for Forming the Glass Fiber Beds

The bottom of the lower filtration tube was sealed by a Plexiglas plug which was drilled and tapped for a 3/4-inch standard pipe. Drainage from the tube took place through a 3/4-inch pipe and plug valve connected into the Plexiglas plug. A vertically adjustable discharge chamber was connected to the plug valve by a long rubber hose. A provision for introducing water under the septum when the apparatus was assembled was made by a small tube leading into the lower filtration tube from a water reservoir. In this manner, all of the air could be excluded from in and around the septum before a filtration was made.

ISOLARIUM

A plastic enclosure was constructed around the equipment for maintaining isothermal ambient conditions during the experimental runs. This enclosure was termed an isolarium, and was made of .003-inch polyethylene sheeting supported on a wooden framework that measured approximately 9 ft. by 5 ft. at table top level and was 8-1/2 ft. high. A one-half ton Westinghouse room air conditioner was mounted in the wall at one end of the isolarium about 3 feet from the floor. The fan and compressor of this unit were powered through separate circuits. The fan operated continuously, while the compressor was connected through a relay to a de Khotinsky thermostat located outside the isolarium. This thermostat operated on a 3°C. temperature differential and only cut the compressor on when the outside room temperature heated up enough to warrant it. The temperature control inside the isolarium was effected by two 660-watt cone heaters mounted directly in the air blast from the conditioning unit. These heaters were

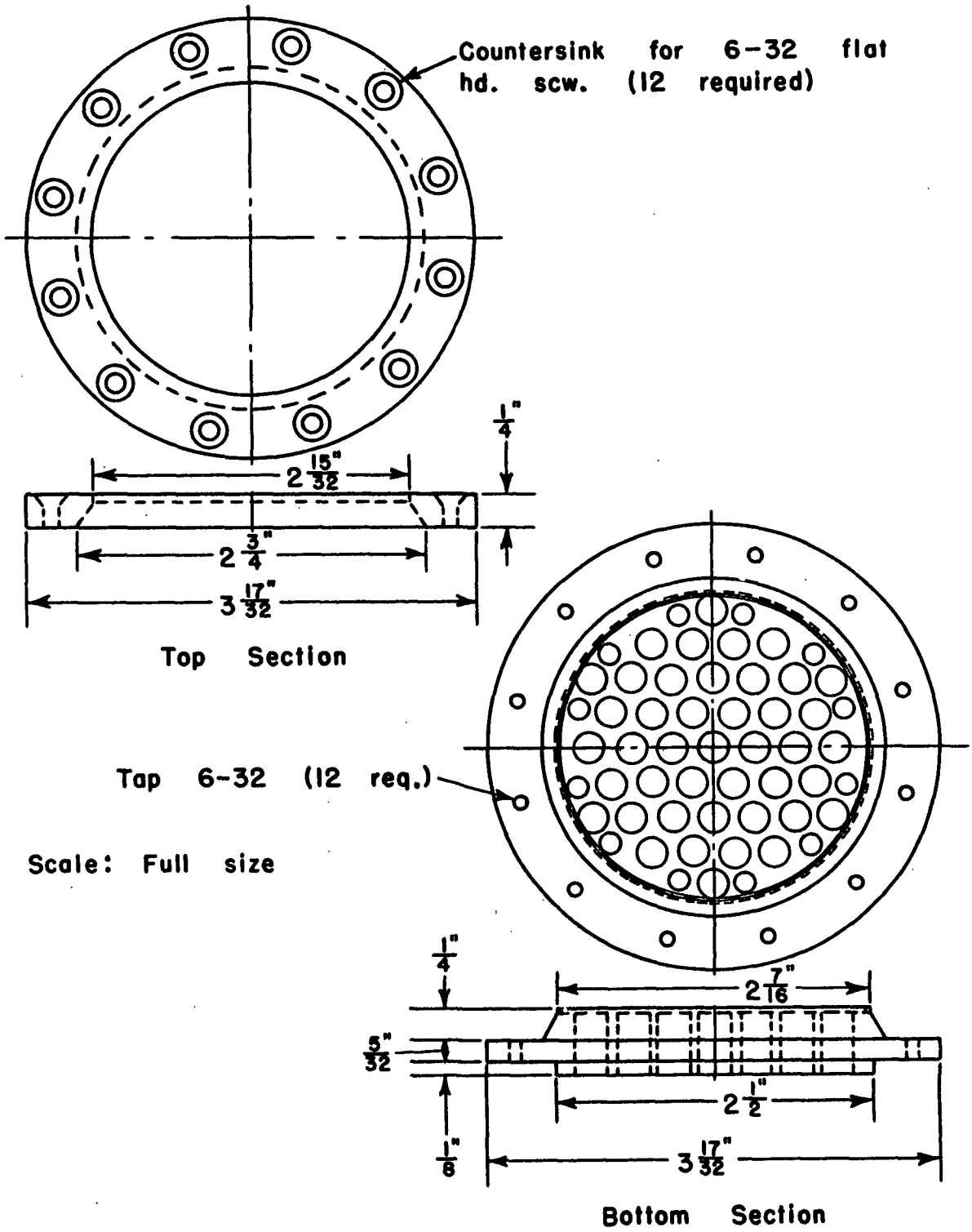

Figure 13. Diagram of Septum Sections

actuated by a Fenwal thermoswitch and relay having an operating temperature differential of 1°F. This switch was located in the air intake port of the conditioning unit and was adjusted to maintain the isolarium temperature at about 24.0°C. A small fan was mounted overhead to improve the circulation.

Under normal operating conditions, the temperature in the isolarium ranged from about 23.0°C. at table top level to 25.0°C. at the top of the enclosure. At any one level in the isolarium, however, the temperature seldom varied more than 1°C. The effects of such a temperature variation on the experimental results were small enough to be readily corrected.

EXPERIMENTAL PROCEDURES

GLASS FIBER PREPARATION

The glass fibers used in this work were obtained from the L. O. F. Glass Fibers Co. in the form of glass wool; i.e., very long fibers. This fiber was exceptionally clean and fairly uniform in size. Two sizes of fibers were used in the experimental program. The diameter range of the smaller size was listed by the manufacturer as 1.2 to 1.4 mu and that of the larger size as 3.0 to 3.5 mu. Henceforth, these fibers will be referred to as 1.2 mu and 3.0 mu fibers, respectively.

It was necessary to reduce the length of these fibers to obtain an adequate dispersion of them in water for the bed formation. To minimize the crushing and splitting of the fibers, they were cut to short lengths using a paper cutter. For the 1.2 mu fibers, ten-gram batches of the dry glass wool were cut into about 1/8-inch wide strips and these strips were cut into about 1/4-inch lengths. A large supply of this shortened fiber was mixed and stored in a double plastic bag from which the fiber was drawn as needed. The preparation of the 3.0 mu fiber consisted of disintegrating ten-gram batches of the glass wool in a standard disintegrator for 100 counts. This disintegrated fiber was filtered on a Buchner funnel and the mat sectioned with the paper cutter into 1/8-inch wide strips and then 1/4-inch lengths. These shortened fibers were then air dried, thoroughly mixed, and stored in a double plastic bag.

Microscopic measurements of these fibers revealed that the fiber diameter covered a much broader range than that specified by the manufacturer.

In Figure 14 are photomicrographs of these fibers taken at a magnification of 475 times. Two separate counts of each fiber were made by the fiber microscopy group at the Institute* using 970X magnification with oil immersion and an eyepiece micrometer having 0.5 micron divisions. In two counts of the 1.2 mu fiber of 342 and 241 fibers, values of the weighted average fiber diameter, $\underline{D}_{\underline{W}}$, of 1.45×10^{-4} cm. and 1.37×10^{-4} cm., respectively, were obtained. The average of these two values is 1.41×10^{-4} cm. Using this value, the volumetric specific surface of the fibers, $\underline{S}_{\underline{V}} = 4/\underline{D}_{\underline{W}}$, was calculated as 28,400 $cm.^2/cc.$ This value of specific surface compares quite favorably with that of 29,700 $cm.^2/cc.$ determined from permeability measurements, which are discussed later. It was observed in the microscopic study of this fiber that it was virtually free of fine debris, i.e., all of the particles had a long cylindrical shape.

The two counts of the 3.0 mu fiber consisted of 260 and 506 fibers, yielding weighted average fiber diameters of 4.77×10^{-4} cm. and 4.32×10^{-4} cm., respectively. The average of these values is 4.54×10^{-4} cm., which gives a specific surface of 8,810 $cm.^2/cc.$ There was considerable debris in this fiber, and it was manifest in the high value of specific surface determined from permeability measurements; viz., 11,400 $cm.^2/cc.$

The solid density of the 1.2-mu fiber was determined from pycnometric displacement of water by the fiber and by glass powder obtained from grinding the fiber in a mortar. By reducing the fiber to a readily dispersed powder, it was much easier to obtain an air-free mixture of the water and

* The Author is indebted to Jack Hankey of this group for these microscopic analyses.

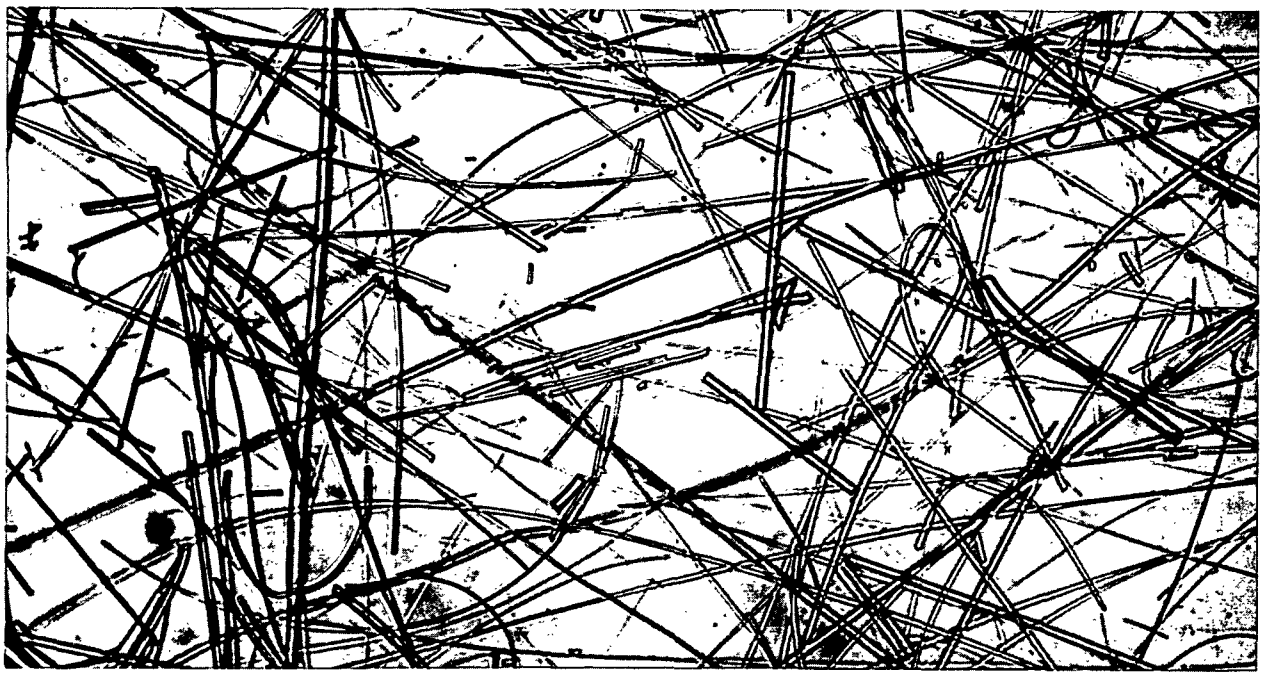

a. 1.2-mu Fiber - 475X Magnification

b. 3.0-mu Fiber - 475X Magnification

Figure 14. Photomicrographs of Glass Fibers

glass in the pycnometer. The pycnometers used were of the side-arm type of 25-ml. capacity. The technique of obtaining an air-free water dispersion of the glass consisted of adding hot water to the pycnometer containing the glass and boiling it under vacuum in a vacuum desiccator. To guard against the loss of fiber from the pycnometer, care was taken not to boil the glass dispersion too vigorously. After boiling, the pycnometer and its contents were cooled under vacuum, and the pycnometer was filled with cold deaerated water. The average density value obtained from nine measurements on the 1.2-mu fiber was 2.539 g./cc. In a personal communication, the manufacturer of the glass fiber reported the solid density to be 2.535 ± .02 g./cc. determined by the settling method (69). Thus, the working value of the 1.2-mu glass fiber density was taken as the mean of these two values, 2.537 g./cc.

The solid density of the 3.0-mu fiber was determined from pycnometric displacement of both water and toluene by the fiber only. The same procedure was used in these measurements as for the 1.2-mu fiber. The average value of five measurements on these fibers was 2.593 g./cc. with all the measurements falling within ± .014 g./cc. of this value. So this value of 2.593 g./cc. was taken as the working value.

GLASS FIBER BED FORMATION

The beds of both size fibers were formed in the same way using the filtration set-up depicted in Figure 12. In both the capillary pressure and permeability runs, reproducibility was the principal criterion of accuracy. It was desired then to keep the variation in porosity as small as possible.

To minimize the porosity variation, it was necessary to minimize the variation in the weight of fibers used to make up the bed. For this reason, a standardized procedure for preparing the fiber beds was developed. From the initial use of this procedure, it was known how much fiber loss was to be expected in the treatment of disintegration and deaeration of the fibers and the formation and compression of the bed. With this information, the weight of dry fiber required initially to produce a final bed of a given porosity could be determined. In preparing a fiber bed, then, the required amount of dry fiber was accurately weighed out and dispersed in two liters of demineralized water with the standard disintegrator. For the 1.2-mu fiber, 1000 counts of disintegration time was necessary to adequately disperse the fibers; but only 100 counts was required for the 3.0-mu fiber. Since the water used in this procedure would eventually be part of the wetting phase water in the two-phase systems, it was necessary that it be relatively pure. Thus, it was drawn from a standard supply that was kept on hand for all the experiments involving wetting phase-pure water. The source of this supply will be discussed later. The fiber dispersion was then transferred quantitatively to a 4-liter suction flask and deaerated to completion using a water aspirator as the vacuum source. For the 1.2-mu fiber, this deaeration required about 18 hours. For the 3.0-mu fiber, it was essentially complete in 8 hours. During this deaeration, it was important to keep the fiber from drying on the wall of the flask, as this would cause an excessive loss.

When the deaeration was complete, the filtration tube and septum were assembled. It was important that the septum be clean and dry, so, prior to assembly, it was brushed clean with soap and water, rinsed in water and acetone, and dried in the 105°C. oven. In the assembled filtration tube, air was purged from under the septum by slowly raising the water level

through the dry septum. The resulting air-free septum and filtration tube assembly allowed a filtration which was uninhibited by air bubbles. The deaerated fiber suspension was then poured into the tube and the tube completely filled with freshly deaerated demineralized water. The volume of the filtration tube was nearly 5 liters and the volumetric consistency of the prefilt fiber suspension ranged from .03 to about .09%. At these consistencies, the fibers had a strong tendency to flocculate, but were easily redispersed by vigorous stirring. In the filtration procedure, the suspension was initially stirred, the plug valve opened full, and the stirring continued during practically the entire filtration. The purpose of this stirring was to prevent the fibers from flocculating immediately before they were drawn into place in the bed. Care was taken to keep the fibers dispersed near the surface of the bed without disturbing the bed itself. The stirrer used was similar to that used with the British sheet mold, composed of a thin brass disk, perforated with several large holes and attached to the end of a long rod, which fitted closely into the small filtration tube. When the filtration was nearly complete, the stirrer was replaced by a compacting tool used to compress the bed during the last stages of the filtration. This tool consisted of a circular brass plate, 1/16-inch thick, perforated with 1/16-inch holes and brazed to the end of a long brass rod similar to the construction of the stirrer. This plate fitted the filtration tube closely, but was free to move easily. With the bed compacted on the septum, the filtration was stopped with the water level about a centimeter above the top surface of the bed. The filtration tube was then dismantled and the bed pushed out of the tube on the septum. Thus,

a preformed cylindrical bed was obtained fully saturated and free to be manipulated on the septum. It was then transferred to the porous plate for either the capillary pressure or the permeability run. At this point, the formation of the bed appeared to be homogeneous and was very regular in shape, that is, a right cylinder.

In the formation of beds for the capillary pressure runs, samples of water were taken at the start and at the end of the filtration from the tap under the septum for the reservoir line. These samples were checked for surface tension, as they were a good measure of the surface tension of the water in the bed.

MEASUREMENT OF BED DIMENSIONS

The total volume of the bed was calculated from the experimentally measured diameter and the gaged thickness of the bed, assuming that the bed was perfectly cylindrical. Since the beds were not confined in a cylindrical tube, the determination of the bed volume was not as accurate as if it were. Some deviation from cylindricality was expected, but the excellent dimensional stability of these glass fiber beds, particularly as they were compressed, made any error on this account small.

An important advantage of not confining the beds is that it provides more free surface area and, hence, greater access of the nonwetting air phase to the interior of the bed. Thus, it is much less probable in these open beds that any large pores are sealed off in the interior of the bed than it is in enclosed systems used by other investigators (24, 25, 30).

In addition, the time to reach capillary equilibrium is considerably reduced.

The measurement of the diameter of the compressed beds in place in the apparatus using calipers was both impractical and inaccurate. A more precise visual technique was developed in which the cathetometer was employed, but this too was difficult and impractical to use on the beds in the apparatus. Separate equipment was set up, therefore, to obtain accurate measurements of the bed diameter. The compression device on the capillary pressure apparatus, including the base plate with studs and the compression plate, were removed to a separate table on which the measurements could be made. A porous brass septum to which the fiber bed was to be transferred from the filtration tube septum was centered on the brass plate. The brass gage pegs were employed in this technique as was the round brass plate which rested on the top of the bed. In this method, then, the fiber bed was compressed in virtually the same way as in the capillary pressure apparatus.

A schematic diagram of this visual method set-up is shown in Figure 15. A straight steel rule, graduated in 1/64 inch was propped on its edge directly behind and very close to the fiber bed. On the opposite side of the bed from this rule, the cathetometer was located about 2-1/2 feet from the bed. The plane of the rule was set normal to the line passing through the center of the cathetometer scope and the center of the bed. This was done quite accurately by fastening a string at a point behind the bed and drawing it taut over the center of the bed and the cathetometer scope. Using this as a reference line, the rule was lined up perpendicular to the

string by sighting on the intersection of the rule and the string from overhead and employing the right angle of a large draftsman's triangle to indicate perpendicularity. With the compressed bed in place and the rule normal to the line of centers, the fixed distances between the plane of the rule and the cathetometer, $\overline{AB}$, and between the center of the bed and the cathetometer, $\overline{OA}$, were recorded. The cathetometer was focused and set so its vertical hair line coincided with the edge of the bed. When examined through the cathetometer scope, the compressed beds had a slight bulge in the center. In comparison to this bulge, the fiber roughness of the bed surface was only of second order magnitude and could safely be ignored. At this setting, then, the vertical hair line projected visually through the bulge such that half of the bulge was excluded from the bed diameter. In all cases, the projection of the bulge beyond the line of contact of the edges of the bed with the compression platens was never greater than 1/32 inch, or less than 1 mm. With the cathetometer set at this point, the focus was changed so the reading on the rule coinciding with the vertical hair line could be read. This procedure was followed for both sides of the bed and the readings of the rule were recorded as N_1 and N_2. The smallest unit of measurement was 1/64 inch. It is easily shown, trigonometrically, that the radius of the bed, $\overline{OC}$, is given by the relation,

$$\overline{OC} = \frac{\overline{OA}(\overline{BN_2}/\overline{AB})}{\sqrt{1 + (\overline{BN_2}/\overline{AB})^2}}, \qquad (45)$$

where the distances in this relation are indicated in Figure 15.

Measurements of the bed diameter were made by this visual method on four beds of the 1.2-mu fiber and two beds of the 3.0-mu fiber. These

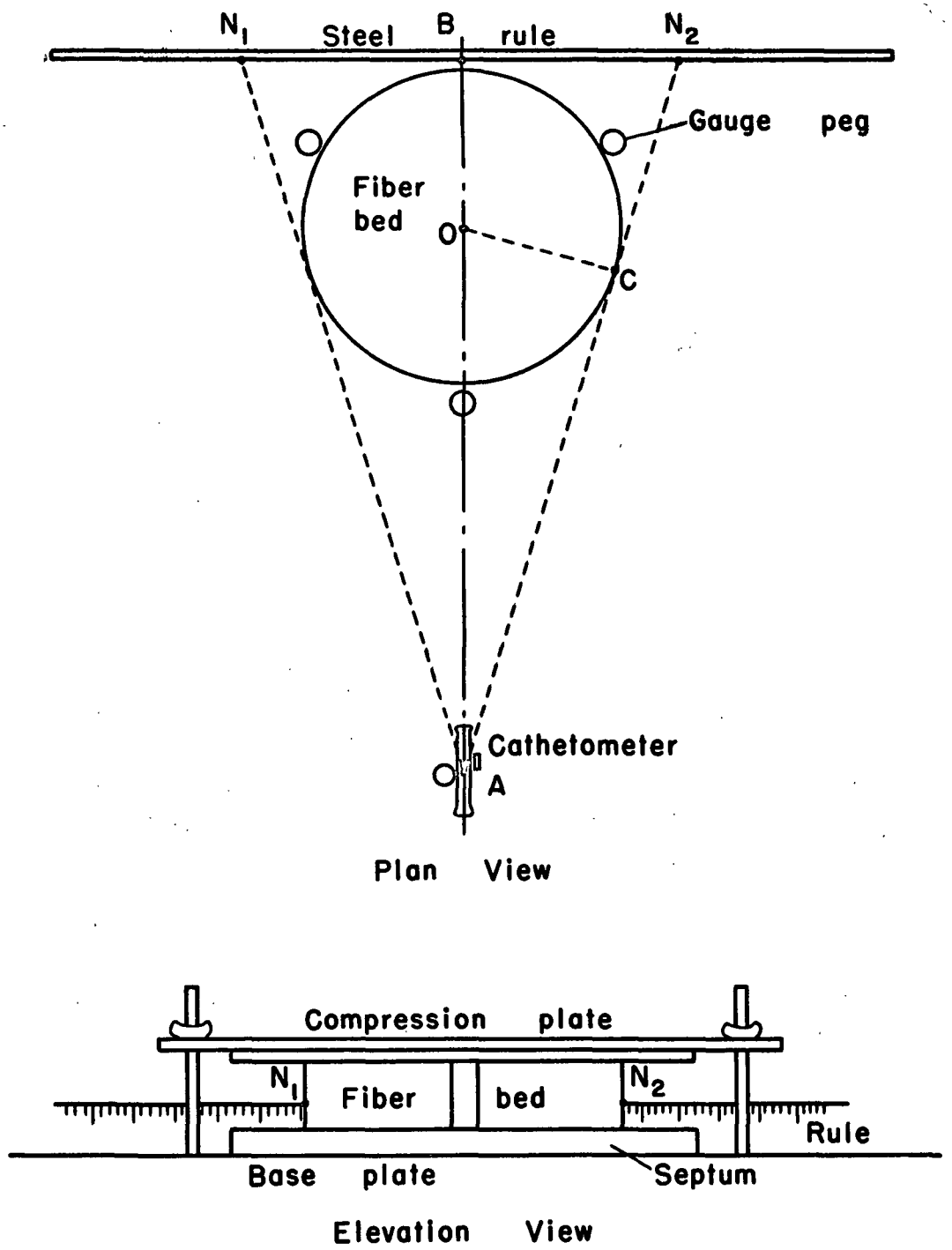

Figure 15. Diagram of the Visual Technique for Measuring the Fiber Bed Diameter

measurements were made when the beds were fully saturated and when they were at different degrees of partial saturation. To desaturate the beds, they were simply allowed to air dry in place. After 24 hours of drying, the beds were essentially bone dry. In addition to the visual measurements, the diameters of the beds at the end of the drying period were measured at different points with calipers. The fixed distances, $\overline{AB}$ and $\overline{OA}$, were measured as 83.6 cm. and 78.9 cm., respectively. The results of the bed diameter measurement are shown in Table IV. It is seen from this table that the shrinkage of the bed is slightly greater for the 3.0-mu fiber than for the 1.2-mu fiber. Since this shrinkage is quite small, about 1%, and occurs primarily within a small change from complete saturation, it should not have an appreciable effect on the calculated permeability results. The permeability measurements were made, for the most part, in the intermediate and low saturation ranges where the bed volume was constant. The working value of the bed diameter was taken as the desaturated diameter, measured by the visual technique; specifically, 6.44 cm. for the 1.2-mu fiber beds and 6.40 cm. for the 3.0-mu fiber beds. These diameters were about 2-1/2 cm. less than the diameter of the porous plates. This allowed room for the 1/4-inch gage pegs to be placed around the bed centered on the plate. From the results in Table IV, the average deviation of this diameter for four separate beds of different thickness of the 1.2-mu fiber was less than .01 cm. Further, the average diameter from triplicate caliper measurements on each bed agreed within 0.2% of this value. Thus, the assumption of cylindricality of the bed appears to be a reasonable one. The measurements of the beds of 3.0-mu fiber were not so extensive as those of the 1.2-mu

fiber; however, these beds should have exhibited approximately the same degree of reproducibility as the 1.2-mm fiber beds. This is indicated by the two measurements made. It is seen that diameter measurements were not made on the 1.5-cm. thick beds. As these beds were not used until the last part of the program, it would have involved a complete repetition of the experimental set-up to make these measurements. Since the change in thickness from 0.80 to 1.00 cm. had no appreciable effect on the measured diameter, it was assumed that the 1.50-cm. thick beds also had essentially the same diameter. The reproducibility of the final capillary pressure and permeability runs using 1.50-cm. thick beds attests to the accuracy of this assumption.

Assuming cylindricality of the fiber beds, then, the calculation of the bed volume would have been a simple and straightforward matter had the porous plates been plane. However, it was found that these plates were curved. To detect the curvature of the plates, a 3/8-inch wide steel bar, machined smooth and flat, and having a length of 7.45 cm., was placed across the center of the plates. It was easily seen then that the porous plate used in the capillary pressure apparatus was concave, that both the fine-grade plates used in the permeability apparatus were convex, and that the upstream medium-grade plate used in the permeability apparatus was concave, while its downstream counterpart was convex. The degree of curvature of the concave plates was determined with the same steel bar. Small pieces of brass shimstock, of known gage, were placed under the center of the bar lying across the plate. The correct displacement of the bar from the lowest point of the plate was determined as the thickness of the shimstock when the

TABLE IV

RESULTS OF THE BED DIAMETER MEASUREMENTS

1.2-mu Fiber

Bed No.	Approximate Bed Thickness, cm.	Visually Measured Diameter, cm. Initially Fully Saturated	After 12 Hours Drying	After 15-18 Hours Drying	After 24 Hours Drying	Average Caliper Measured Diameter, 24 Hours Drying
1	1.00	6.457	6.439	—	6.439	6.436
2	0.80	6.495	--	6.439	6.439	6.469
3	0.80	6.476	--	—	6.446	6.459
4	1.00	6.457	--	—	6.439	6.420
				Average	6.441	6.446

3.0-mu Fiber

1	0.80	6.482	6.410	6.386	—	—
2	0.80	6.482	6.447	—	6.410	6.400
			Average	6.398		6.400

bar was contacting the plate at both ends and the shimstock in the middle. The displacement of the bar from the plate was measured in two perpendicular directions on the plate. It was observed that the plates were not spherical; however, as a reasonable approximation, sphericity of the plates was assumed with the displacement taken as the average of the two measured values. The same procedure was followed for the convex plates, except the displacements were measured at both ends of the bar rather than at the middle. The displacement values determined for the five different plates are given in Table V.

TABLE V

CURVATURE DISPLACEMENTS OF THE POROUS PLATES

Location of Plate	Porosity Grade	Type of Curvature	Measured Displacement, in. 1	2	Average Displacement, in.
Cap. Press. App.	F	Concave	.017	.012	.015
Perm. App., Upstr.	F	Convex	.017	.017	.017
Perm. App., Dnstr.	F	Convex	.017	.015	.016
Perm. App., Upstr.	M	Concave	.013	.014	.014
Perm. App., Dnstr.	M	Convex	.012	.012	.012

From the bed diameter, length of the gage pegs, and degree of curvature of the plates, the volume and average thickness of the fiber beds was calculated for every case. As an example of this procedure, the calculation of volume and average thickness of a 1.2-mu fiber bed in the capillary pressure apparatus is given in Appendix I. A summary of the calculated results of the volumes and average thickness for both the 1.2-mu and 3.0-mu fiber beds for the three different length gage pegs in both the capillary pressure and permeability apparatus is presented in Table VI.

TABLE VI

FIBER BED VOLUMES IN THE CAPILLARY PRESSURE APPARATUS

Length of Gage Pegs, cm.	1.2-mu Fiber Volume of Bed, $cm.^3$	3.0-mu Fiber Volume of Bed, $cm.^3$
0.793	26.81	26.44
0.996	33.45	—
1.501	—	49.15

FIBER BED VOLUMES AND AVERAGE THICKNESS IN THE PERMEABILITY APPARATUS

Fine-Grade Plates

Length of Gage Pegs, cm.	1.2-mu Fiber		3.0-mu Fiber	
	Volume, $cm.^3$	Average Thickness, cm.	Volume, $cm.^3$	Average Thickness
0.793	—	—	25.09	.78
0.996	31.91	.98	31.50	.98
1.501	48.37	1.49	47.89	1.49

Medium-Grade Plates

0.793	—	--	25.62	0.80
0.996	32.56	1.00	32.15	1.00
1.501	49.01	1.51	48.40	1.51

STATIC CAPILLARY PRESSURE MEASUREMENT

The specific object of these experiments was to obtain values of the water saturation of the fiber beds as a function of the capillary pressure in the two-phase system. Briefly, the procedure, employing the apparatus in Figure 6, consisted of subjecting, stepwise, the initially fully saturated bed to individual capillary pressures, progressing from low to high and allowing the bed saturation to come to capillary equilibrium at each value of the capillary pressure. Naturally, as greater capillary pressures were applied to the system, water was drawn out of the bed displacing the mercury downward in the buret tube. The amount of water displaced from the bed for each change in capillary pressure was determined from the change in mercury level in the calibrated buret tube. At the end of a run, the water content of the bed was determined gravimetrically. On the basis of this value, the water content at each value of capillary pressure measured was calculated from the amount of water displaced. In this way, several capillary pressure-equilibrium saturation points were determined by using only a single experimental bed.

An accurate measure of the buret tube volume corresponding to the linear displacement of the mercury level was required in these experiments. A buret tube was chosen for this apparatus because of the volumetric uniformity along its length. Calibrations were made by filling the dismantled tube with water and draining a quantity of water from the tube into a tared container which was then weighed. Cathetometer readings of the water meniscus were taken before and after the water was drained out.

These calibrations were carried out with the buret tube in place on the apparatus mounting board to duplicate the actual run conditions. The calibration results consisted, therefore, of a mass of water corresponding to a linear change in the meniscus level in the buret tube. The calibration was carried out periodically during the program for various changes in meniscus level over the whole length of the tube. Invariably, the result was precisely a value of 0.876 grams water per centimeter change in meniscus level for all sections of the buret tube.

The constancy of this calibration was threatened by small droplets of water clinging to the walls of the tube when the tube was refilled with mercury after a desorption run. The loss of calibration was minimized by Desicoting* the tube. As many as four runs could normally be made before the amount of water trapped on the walls of the tube became appreciable; and to insure accurate measurements, the apparatus was dismantled periodically and the buret tube cleaned and re-Desicoted.

In making a capillary pressure run, the apparatus was prepared prior to the run by the following procedures:

1. The porous plate was cleaned and completely saturated with deaerated water. The cleaning procedure consisted of brushing out any fiber embedded in the plate and passing through the porous plate, set in a suction flask, in succession: acetone, hot chromic acid cleaning solution, cold water, and hot water. The plate was then immersed in the boiling water in a vacuum desiccator and boiled under vacuum for an hour. The immersed plate was then allowed to cool under vacuum.

* See page 49 for information about Desicote.

2. The water reservoir was filled with freshly deaerated demineralized water and the mercury level raised to the top of the buret tube by adjusting the height of the mercury reservoir. The remainder of the system up to the upper ball and socket joint was then filled with water from the water reservoir.

3. The water-saturated porous plate was removed from the desiccator, rinsed, and completely filled with freshly deaerated demineralized water. Being careful not to allow any air bubbles in the system, the filled plate was placed in position in the apparatus. In doing this, water was allowed to drip from the ball joint welded to the plate stem. In this way, the ball and socket joint was assembled with the porous plate completely saturated at zero capillary pressure. A small amount of water was left standing on the plate to insure a water seal between the bed and the plate.

In all of these operations, it was necessary for the water to be as pure as that used for the wetting phase in the bed. In fact, in both the capillary pressure and the permeability runs, large quantities of pure air-free water were required. The water used in these runs was obtained by running tap water through a Penfield mixed bed demineralization column using Penex M-8 resins (Penfield Manufacturing Co., Inc., Meriden, Conn.). Immediately preceding the demineralization column, the tap water was filtered through a Fulflo filter (BR8 model equipped with wound cotton yarn cartridges). The water from the demineralization column was filtered through a small bed of Pyrex glass wool. This water was deaerated by heating to boiling in 5-gallon bottles and boiling under vacuum. When cool, this water

had a surface tension of 71.5 dynes/cm., and for practical purposes, was free of dissolved air. A large supply of it was stored in 5-gallon bottles under vacuum and was used for all fiber preparations, experimental runs, and calibrations in which water of wetting phase purity was required.

To remove the preformed bed from the septum to the plate, the bed was first transferred to a thin brass disk by holding the disk against the top of the bed and inverting the septum. The bed was loosened from the septum by washing with a small amount of water. Placing the disk with the bed on the porous plate, it was a simple matter to slide the disk out from under the bed leaving it on the center of the plate. This method of transfer was sure and easy to perform and did not mar or distort the bed. The three gage pegs were then evenly distributed around the bed, the compression device assembled, and the bed squarely compressed to the thickness of the pegs. During the compression, the bulk of the water, which was expressed from the bed, was removed from the plate with a small pipet. Finally, the Plexiglas cover was sealed to the base plate and the system was allowed to stand for an hour so that the atmosphere around the bed might become saturated.

The excess water around the bed was removed through the plate by lowering the water reservoir and opening the stopcock in the reservoir line. The capillary pressure measurements were then begun at a total capillary pressure of about 1 or 2 cm. Hg. In making measurements, the stopcock at the bottom of the buret tube was shut off and the mercury reservoir lowered until the difference in mercury levels plus the water head above the mercury was

approximately equivalent to the total capillary pressure desired. The pointer was adjusted to mark the mercury level in the buret tube. The buret tube stopcock was opened allowing the capillary pressure to be transmitted to the water in the bed. As the water drained from the bed, the mercury reservoir was manually lowered in unison with the buret tube mercury level by means of the rack and pinion. Actually, the movement of the reservoir was not exactly synchronized with that of the mercury level, but was made stepwise, and the reservoir always trailed the mercury level. However, so long as the final equilibrium value of the capillary pressure was never exceeded, and the deviation from the final pressure was kept small, no appreciable discrepancy was introduced in the equilibrium saturation. When the system reached capillary equilibrium, i.e., when the level of mercury in the buret tube came to rest, cathetometer readings of the mercury levels in the buret tube and the reservoir were recorded. The ambient temperature around the bed was also recorded. This procedure was repeated for each point desired on the capillary pressure desaturation curve until the residual saturation. At the end of the run, the stopcock just below the porous plate was closed, sealing off the fiber bed at its residual saturation. The plastic cover was removed and the compressed bed was quickly released and transferred quantitatively to a tared weighing bottle. Approximately 30 seconds were required to complete this transfer. The moisture content of the bed was determined gravimetrically and a check of the surface tension was made on the water in the porous plate at the end of the run. Usually about 12 to 14 separate equilibrium measurements were made in each run which lasted about 48 hours total time.

The water content of the bed at each capillary pressure was calculated from the gravimetrically determined water content of the bed at the end of the run and the measured amount of water displaced from the bed. Since the porous plate gave up a small amount of water during the run, it was necessary to correct the total water volume change in the buret tube for the water displaced from the porous plate alone. Blank calibration runs were made on the apparatus without an experimental bed in which the same schedule of capillary pressure was applied as in regular runs. A plot of these blank runs in terms of the capillary pressure vs. the volume of water retained by the plate is shown in Figure 16. The amounts of water in this plot are, of course, relative, and the zero value is taken arbitrarily at a capillary pressure of 35.5 cm. Hg. Since the plates were prepared in a standard way, the reproducibility of the calibration was satisfactory. In the calculation of the capillary pressure results, these values of displaced water were subtracted from the total water displaced in the run at each equilibrium point. A sample calculation of a capillary pressure run is shown in Appendix II.

STEADY-STATE PERMEABILITY MEASUREMENT

Values of the permeability to water of the glass-fiber beds at various saturations were determined with the apparatus in Figure 9. From measurements of the steady-state water-flow rate and pressure drop across the experimental beds, the permeability was calculated by D'Arcy's equation. Measurements of the flow rate were made directly with the calibrated capillary flowmeters. But the experimentally measured pressure drop

included the pressure drop across the bed and that across the confining porous plates. Independent measures of the pressure drop across the porous plates alone were determined from calibration experiments and subtracted from the experimental values to give the pressure drop across the bed alone.

Calibrations of the capillary flowmeters were made with the apparatus shown schematically in Figure 17. This set-up consisted of a large supply of water at an elevated position from which the flowmeters were fed. The tygon supply line from this supply reservoir contained a flow-limiting capillary tube which adjusted the flow rate to the desired range. The supply line led to the tri-flat rotameter and capillary flowmeter system just as they were used in the permeability apparatus. The exit header of the flowmeter was attached to a long piece of tygon tubing which ended in a small glass discharge tube. This tube extended through a rubber stopper which fitted into a 25-ml. receiving flask. The discharge tube was held by a vertically sliding clamp on a ringstand. With this vertical adjustment of the flow discharge end, the driving force and, hence, the water-flow rate through the capillary flowmeters could be easily controlled. The discharged water was collected in the small receiving flask in which the rubber stopper fitted tightly. A vent tube was also inserted in the stopper.

To make a calibration run, the capillary flowmeter tubes were cleaned and assembled, and the entire system was filled with water to the exclusion of air. The discharge tube was set at the level to give the approximate desired flow rate through the bypass line, according to the rotameter, which had a flow-rate range that covered the ranges of all three capillary flowmeters. However, the rotameter was not accurate enough to provide the

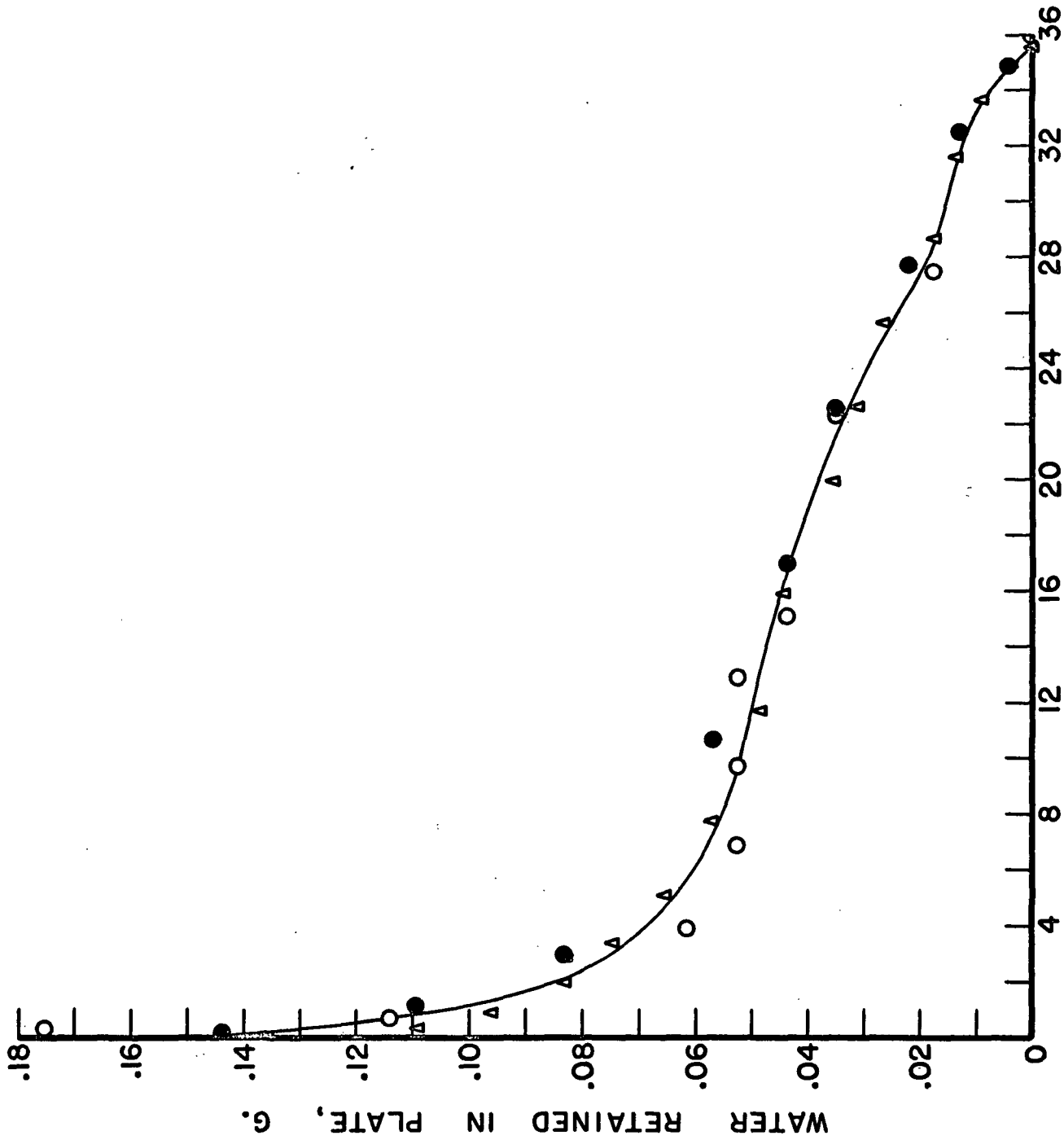

Figure 16. Blank Runs on the Capillary Pressure Apparatus

actual flow-rate measurement. The stopcock on the proper flowmeter line was opened and the bypass line closed so the flow was diverted through the single flowmeter tube. A constant flow rate was maintained until the manometer reading reached its equilibrium position for this flow rate. The receiving flask, which had been previously tared, was positioned and a quantity of water was collected over an accurately timed period at this constant flow rate. To minimize any evaporation from the flask, it was enveloped in a sheet of dental dam during the run. The water collected was determined gravimetrically. Manometer readings were made at the start and at the finish of the run. There was a significant capillary effect in these flowmeter manometers, so it was necessary in all the calibration and permeability runs to approach the final manometer reading from the same direction. Thus, the manometer readings were taken after it had increased. That is, the equilibrium position of manometer fluid meniscus in the downstream leg was always convex to the water when the reading was made. The ambient flowmeter temperature was also recorded.

The calibration results were calculated as grams water flowing per minute at a given manometer reading, i.e., difference in levels of manometer fluid in centimeters. These results were corrected to 25.0°C., which was the average ambient flowmeter temperature, from the observed ambient temperature for two factors, the change in viscosity of the flowing water and the change in density of the manometer fluid. Although the ambient temperature does not necessarily coincide with the water and manometer fluid temperatures, the degree and rate of change of the ambient temperature is so small that it presumably is a good estimate of these temperatures. Thus,

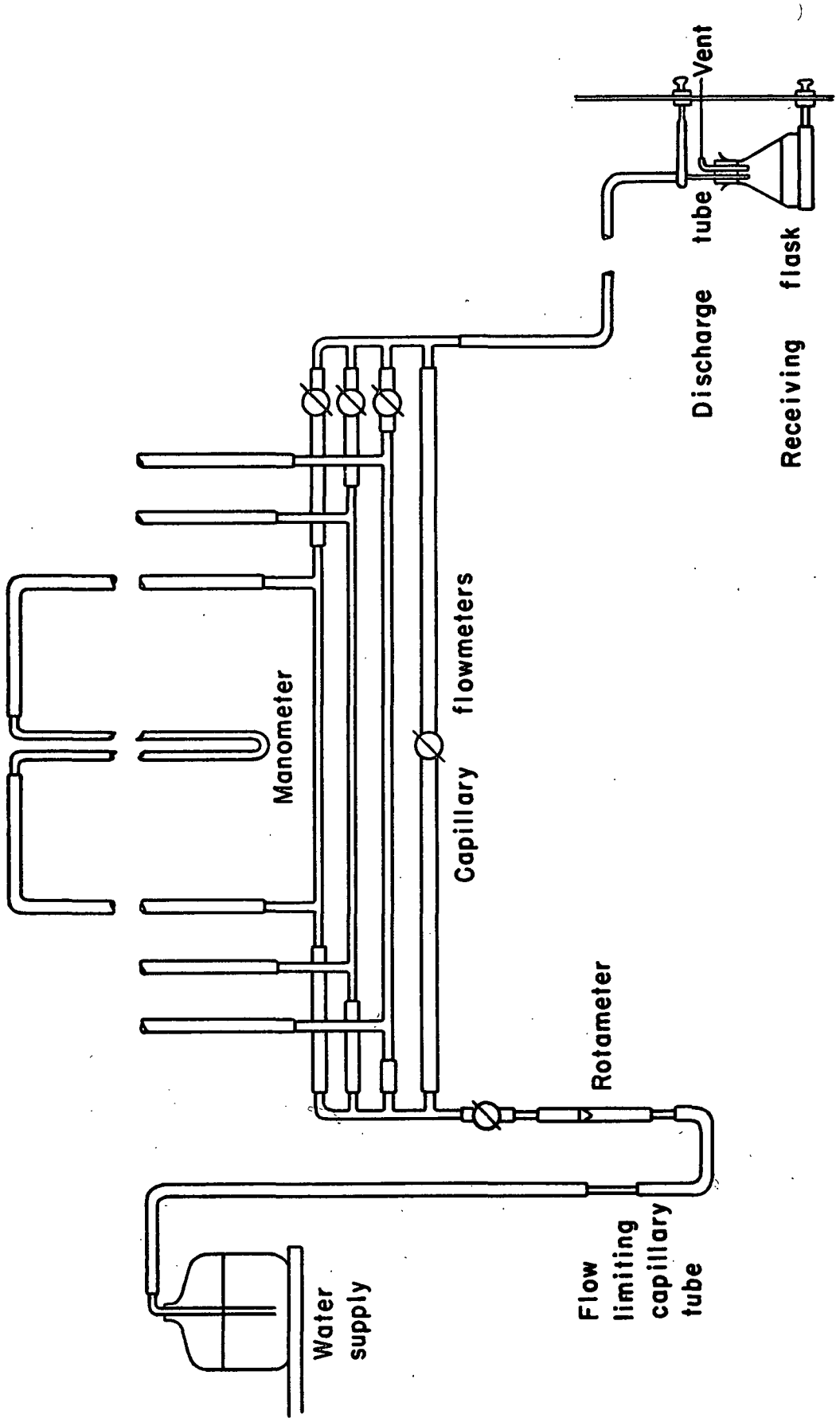

Figure 17. Capillary Flowmeter Calibration Apparatus

if M_t is the manometer reading observed at temperature t, and $\Delta\rho_t$ and μ_t are the difference in densities of the manometer fluid and water and the viscosity of water at temperature, t, respectively, then the manometer reading at a temperature of 25.0°C. for the observed flow rate is given by

$$M_{25} = \left(\frac{\Delta\rho_t}{\Delta\rho_{25}}\right)\left(\frac{\mu_{25}}{\mu_t}\right)M_t, \qquad (46)$$

where the subscript, $_{25}$, denotes a temperature of 25.0°C. Applying this correction to the experimental results, calibration values of M_{25} for each flow rate were obtained. The calibration results are shown in Figures 18, 19, and 20 for the three flowmeters designated as low, intermediate, and high to indicate their relative flow-rate range. The experimental points refer to 25.0°C. The other lines are the calibrations for different temperatures calculated by Equation (46) from the line of best fit for the 25.0°C. data.

Immediately after each calibration and permeability run, the capillary flowmeters were dismantled and cleaned. Without cleaning, the calibration of the flowmeters would gradually change, apparently because of the contamination from the water. The cleaning procedure consisted of drawing through the tubes in succession: acetone, hot chromic acid cleaning solution, cold water, and hot water. The tubes were then stored in polyethylene bags until used again.

Initially, calibrations of the porous plates were made in which the flow took place over the entire area of the plate. It was soon found, however, that the permeability of the plate varied from the center of the

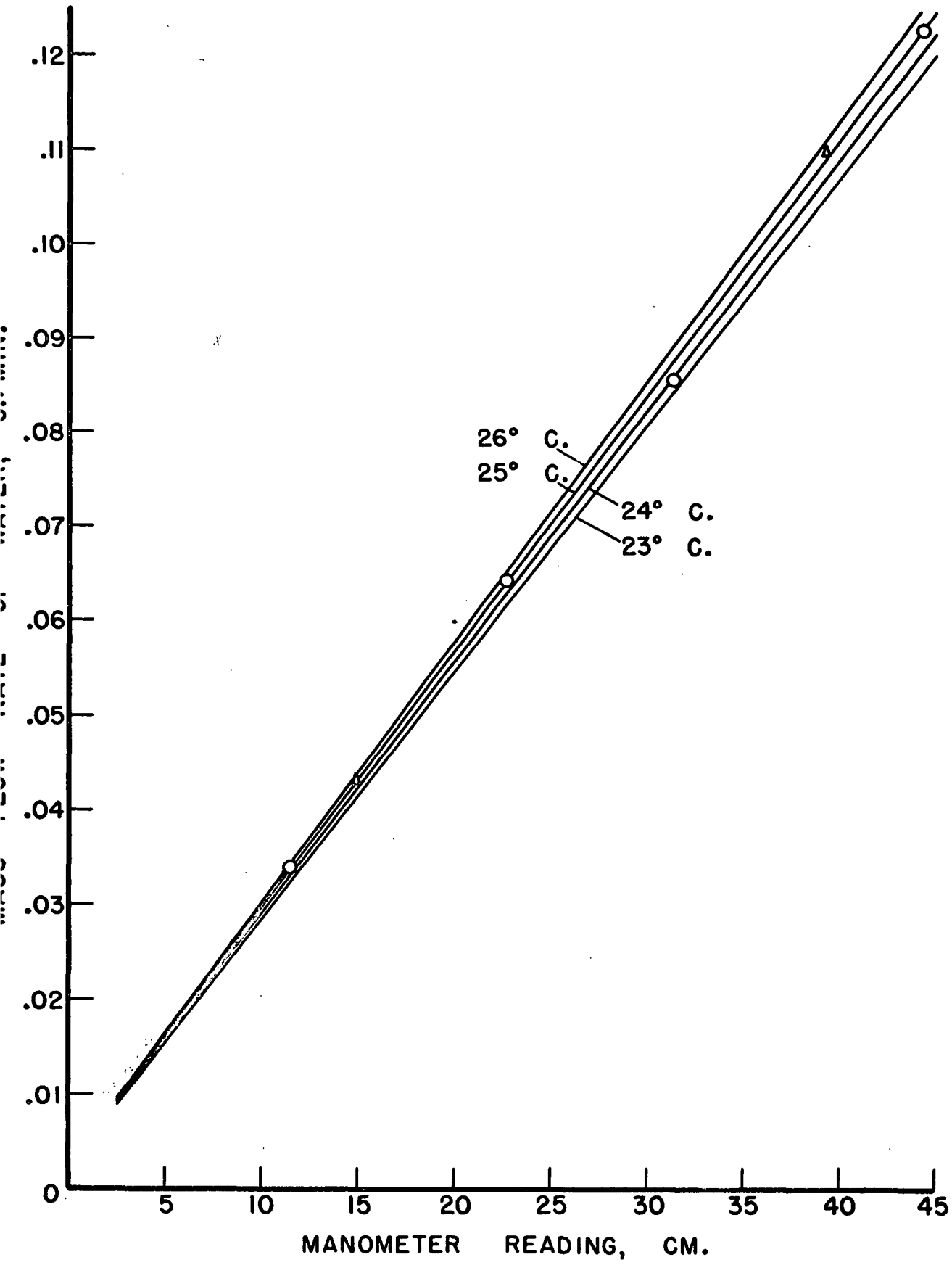

Figure 18. Low Capillary Flowmeter Calibration

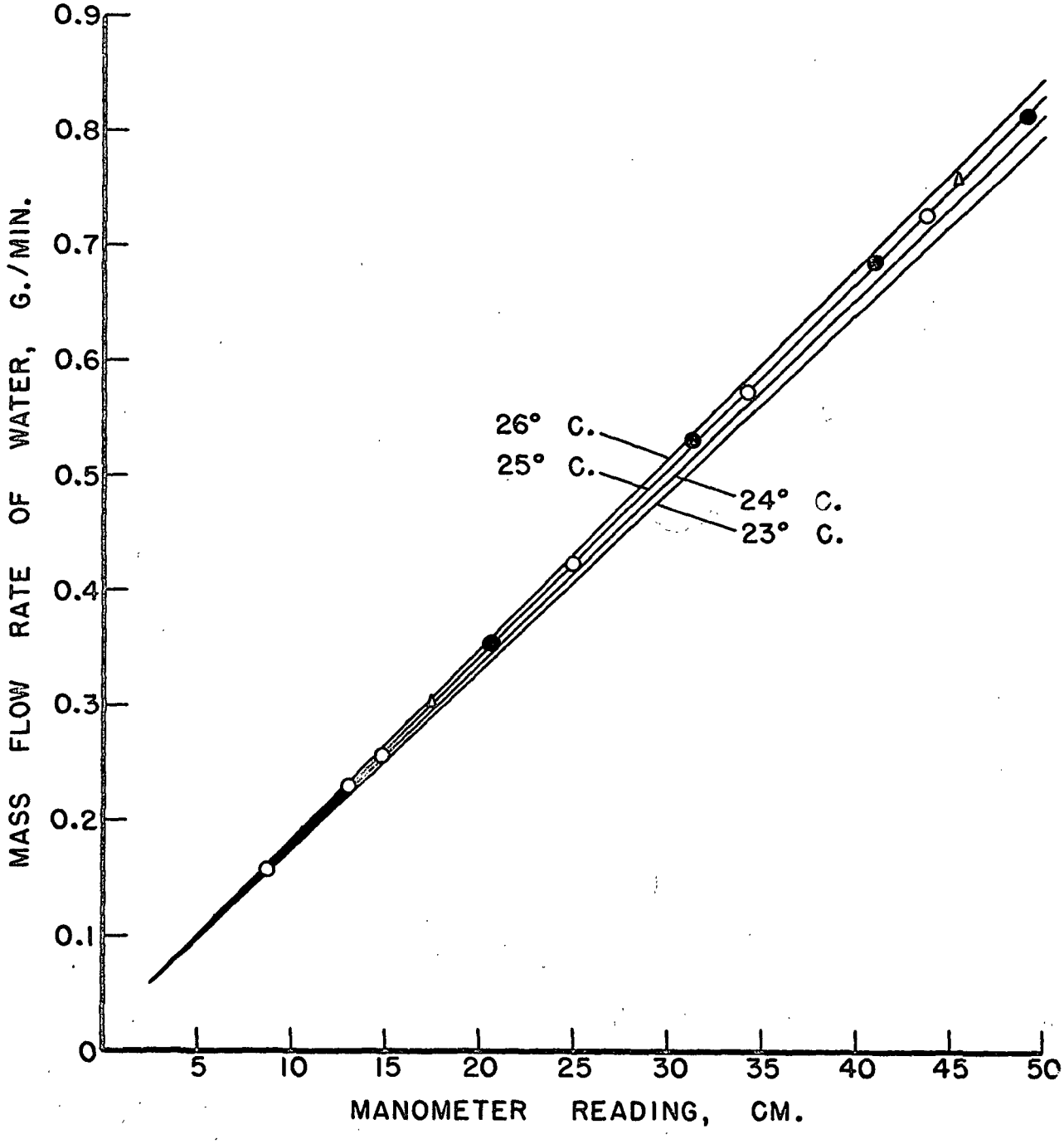

Figure 19. Intermediate Capillary Flowmeter Calibration

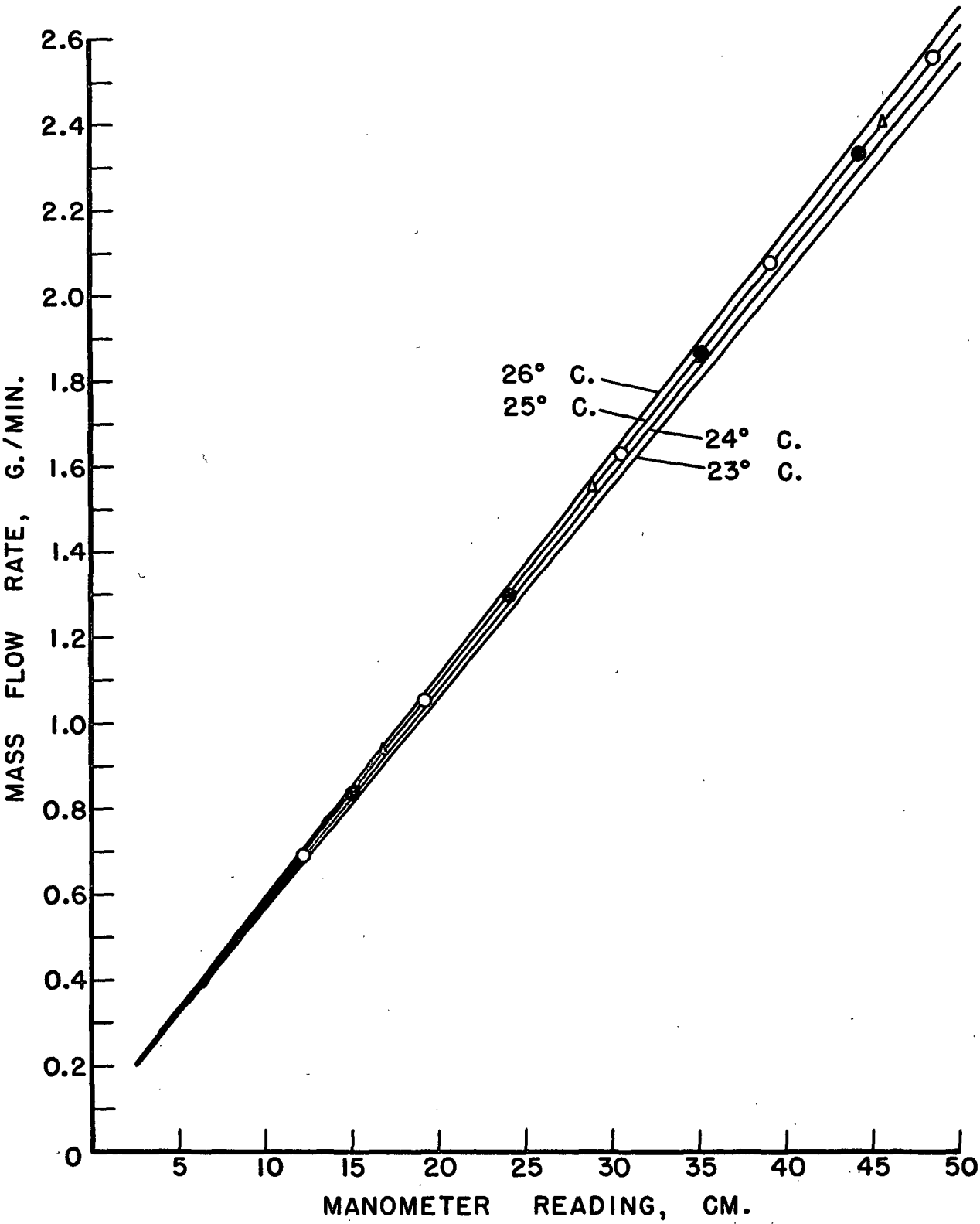

Figure 20. High Capillary Flowmeter Calibration

plate to the outer edge. Since the experimental beds covered only the center portion of the plates, a new calibration procedure was adopted in which the center of the plate only was tested. A pictorial diagram of the calibration set-up is shown in Figure 21. The apparatus consisted of a 2 1/2-inch i.d. Plexiglas flow tube that rested on the plate being calibrated. This was the same size tube used in the filtration apparatus for forming the bed, so the cross-sectional area of the bed was approximated quite closely for the calibration tests. This tube was clamped against the plate by the same yoke arrangement used to clamp the two plates together in the permeability apparatus. A flange was attached to the middle of the flow tube for this purpose. The yoke is not shown in the diagram. A gasket of 1/32-inch rubber, cemented to one end of the flow tube, sealed the tube against the surface of the plate. Holes were drilled in the walls of the tube to accommodate a flow line, a tap for the differential manometer lead, and a thermometer, as shown. The top of the tube was sealed with a rubber stopper. The pressure drop across the plate was measured with the differential manometer and water was supplied from a large reservoir open to the atmosphere. The downstream side of this calibration set-up was the same as that in the permeability apparatus, consisting of the rotameter, capillary flowmeters, and vacuum system. In calibrating the downstream porous plate, the flow was directed through the plate from outside in as illustrated in Figure 21. For the upstream plate, however, the flow lines and manometer leads were reversed so the flow was directed from the inside out. Thus, the conditions of flow in the permeability runs were very nearly duplicated in the calibration procedure.

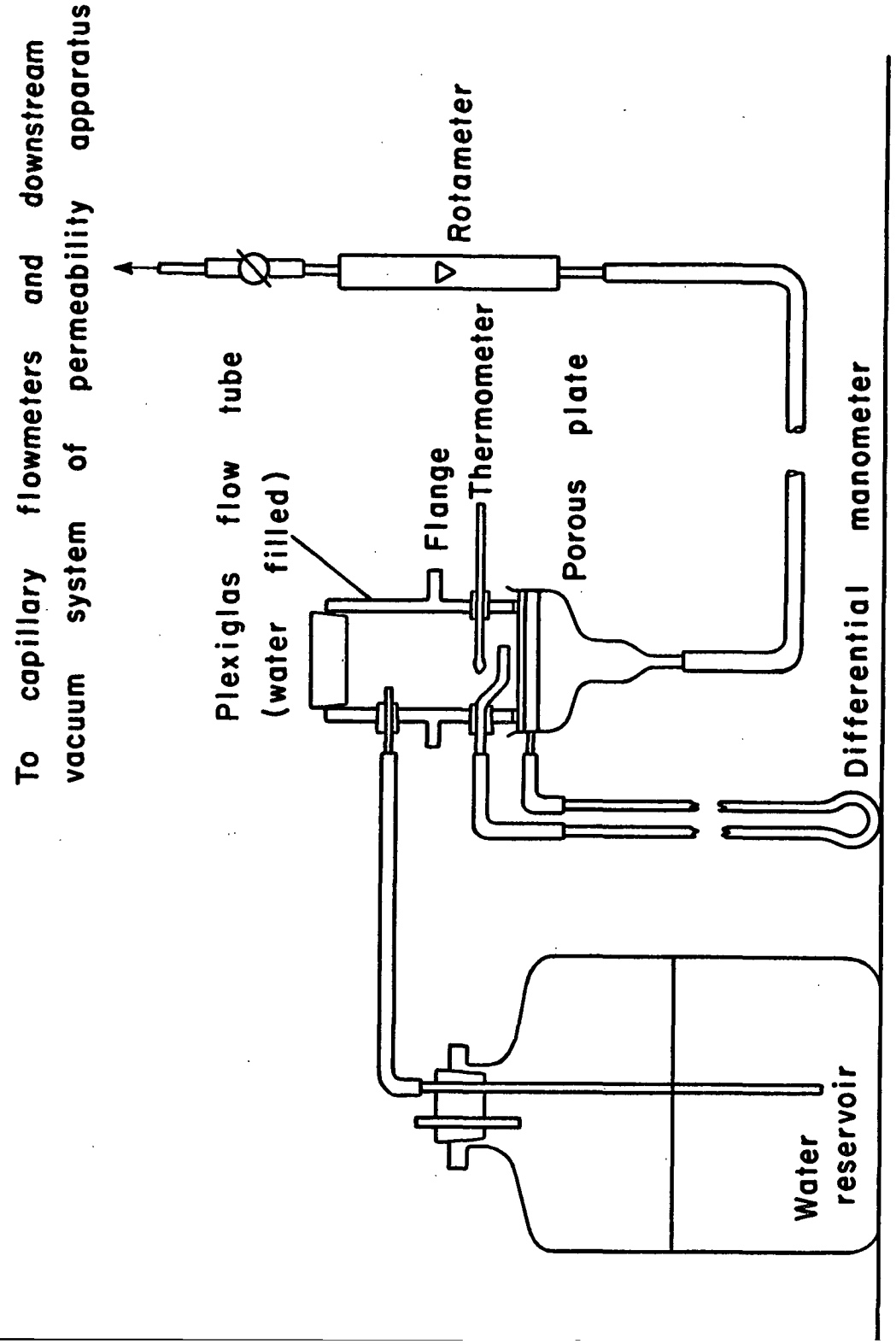

Figure 21. Porous Plate Calibration Apparatus

The porous plates were cleaned and saturated with deaerated water before the calibration and permeability runs by the same procedure used for the plate in the capillary pressure apparatus. To prepare for a calibration run, the saturated plate was filled with water and clamped to the flow tube. The flow tube, flow lines, and manometer leads were filled with water and assembled as in Figure 21. Air was excluded from the flow tube by putting the stopper in the tube last. The height of the porous plate was adjusted several centimeters above the water level in the reservoir so a positive capillary pressure always existed at the surface of the plate. This prevented any water leakage out of the exposed portion of the plate. Flow was regulated through the plate by adjusting the downstream vacuum system. In making a calibration measurement, flow was initially established through the bypass line. The water flow was then switched to the proper flowmeter and the system was allowed to come to steady state at the selected flow rate. At steady state, readings were taken of the capillary flowmeter and differential manometers. The water temperature and ambient temperature around the flowmeters and differential manometer were also recorded. This procedure was repeated for several different flow rates.

The results of the calibrations were obtained in terms of a pressure drop in g./cm.^{2} across the plates for a given flow rate in g./min.* These results were corrected to 23.0°C., the mean water temperature for viscosity, and to the approximate diameter of the experimental beds. Thus, for a given flow rate, where the measured pressure drop was ΔP_t across an area of the plate of diameter D_t, the diameter of the flow tube, and for a water

* For convenience in the calculations, these pressure drops were recorded as grams force/cm.^{2} However, it is realized that strict conformance to the metric system of units would dictate the use of dynes/cm.^{2}

viscosity, μ_t, at a water temperature, t, the pressure drop at 23.0°C. for an area of the plate having a diameter equal to that of the fiber bed, D_b, is

$$\Delta P_{23} = \Delta P_t \left(\frac{\mu_{23}}{\mu_t}\right)\left(\frac{D_t}{D_b}\right)^2, \qquad (47)$$

where the subscript, $_{23}$, denotes a water temperature of 23.0°C. The diameter of the flow tube was 6.35 cm., and the diameter of the experimental beds was taken as 6.44 cm. Of course, the proper area of the plate to which the correction applied was the area of contact between the bed and the plate, and this area was subject to slight variations. Using these values, the calibration results at 23.0°C. were determined for both the fine-grade and medium-grade plates. Plots of these results are shown in Figures 22, 23, 24, and 25. In these graphs, the experimental points refer to 23.0°C. The other lines refer to calibrations at different temperatures calculated by Equation (47) from the line of best fit for the 23.0°C. data.

In observing the bed through the cathetometer scope, it was apparent that the diameters of contact between the bed and the porous plates were very nearly the same as that of the bed itself. In some cases, a slight spreading of the bed on the lower upstream plate made the area of contact a bit greater. In these permeability runs, the diameters of contact were measured after the runs and were usually found to be the same as that of the bed. Corrections were made on the calibration values if the diameters of contact were different from 6.44 cm.

Tests for permeability decay of the porous plates were made by allowing the flow to continue through the plates for about 60 minutes and then

repeating the measurements. In both the fine-grade and medium-grade plates, the permeability decay at flow rates less than 1 g./min. was imperceptible for this period of time. At higher flow rates, however, a slight permeability decay was noticeable. At a flow rate of 1.03 g./min., the permeability of the downstream fine-grade plate decayed 1.48% in 60 minutes, and at 1.85 g./min., it decayed 2.75% in 40 minutes. In this work, though, flow rates greater than 1 g./min. were seldom employed for more than a few minutes. Consequently, the permeability decay of the plates in this work was almost always a negligible factor.

The porous plate calibrations exhibited good precision, but since the experimentally measured pressure drop across the bed was strongly dependent on the permeability of the porous plates, the accuracy of this measurement was checked by using three different thickness beds. In this way, the overall measured permeability of the bed plus plates was varied without changing the presumably constant permeability of the plates. The agreement of the calculated bed permeabilities for the different thicknesses would confirm the validity of the plate calibrations. The purpose of using the medium-grade plates was to improve the accuracy of the pressure drop measurements at high saturations, since the flow resistance of the fine-grade plates at high saturations, i.e., low capillary pressures, was overwhelmingly large compared to that of the experimental beds. The use of medium-grade plates, then, simply reduced this plate flow resistance. However, the useful capillary pressure range of these plates was severely limited.

Preliminary to a permeability run, the following preparations were made:

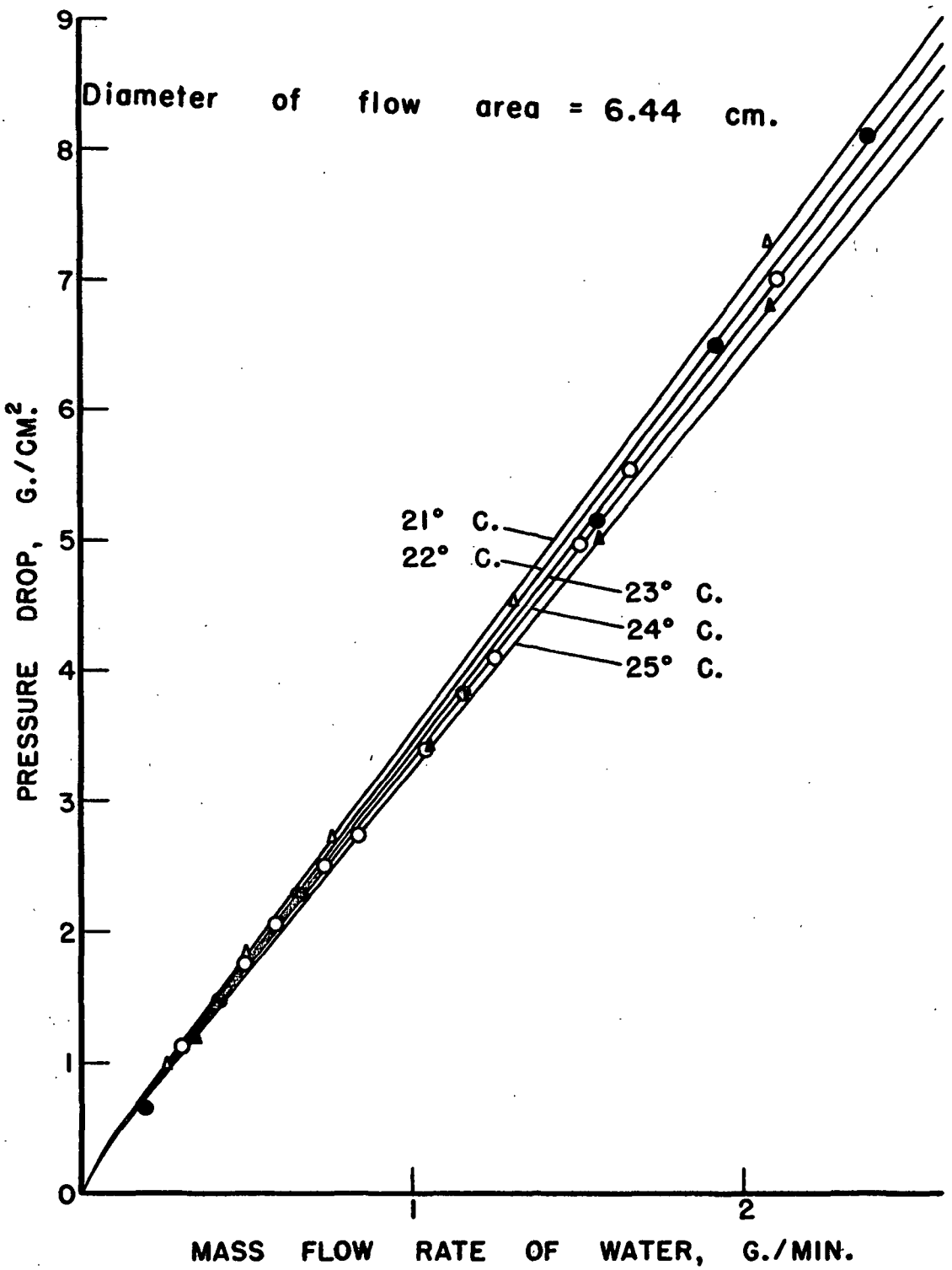

Figure 22. Upstream Fine Grade Porous Plate Calibration

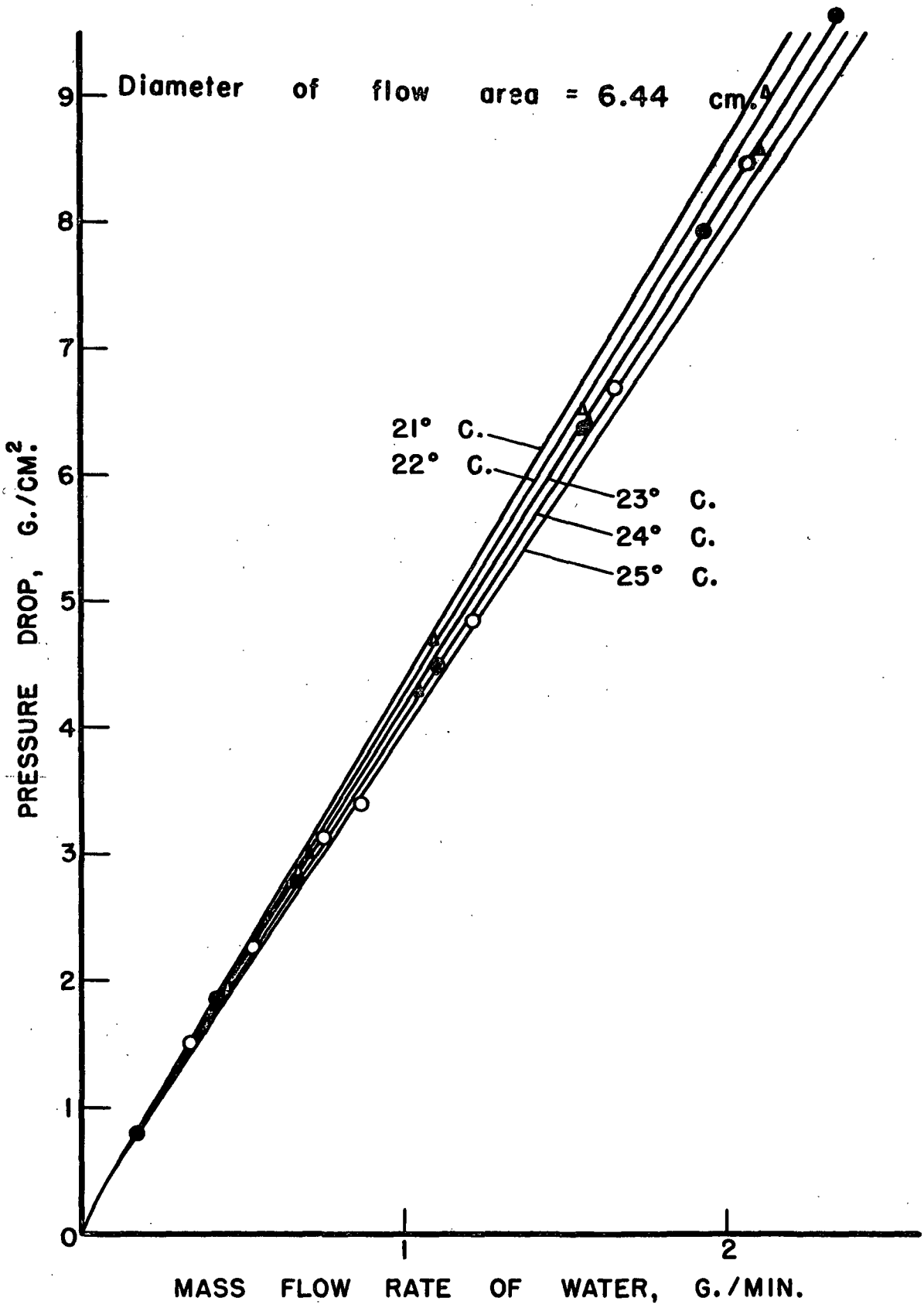

Figure 23. Downstream Fine Grade Porous Plate Calibration

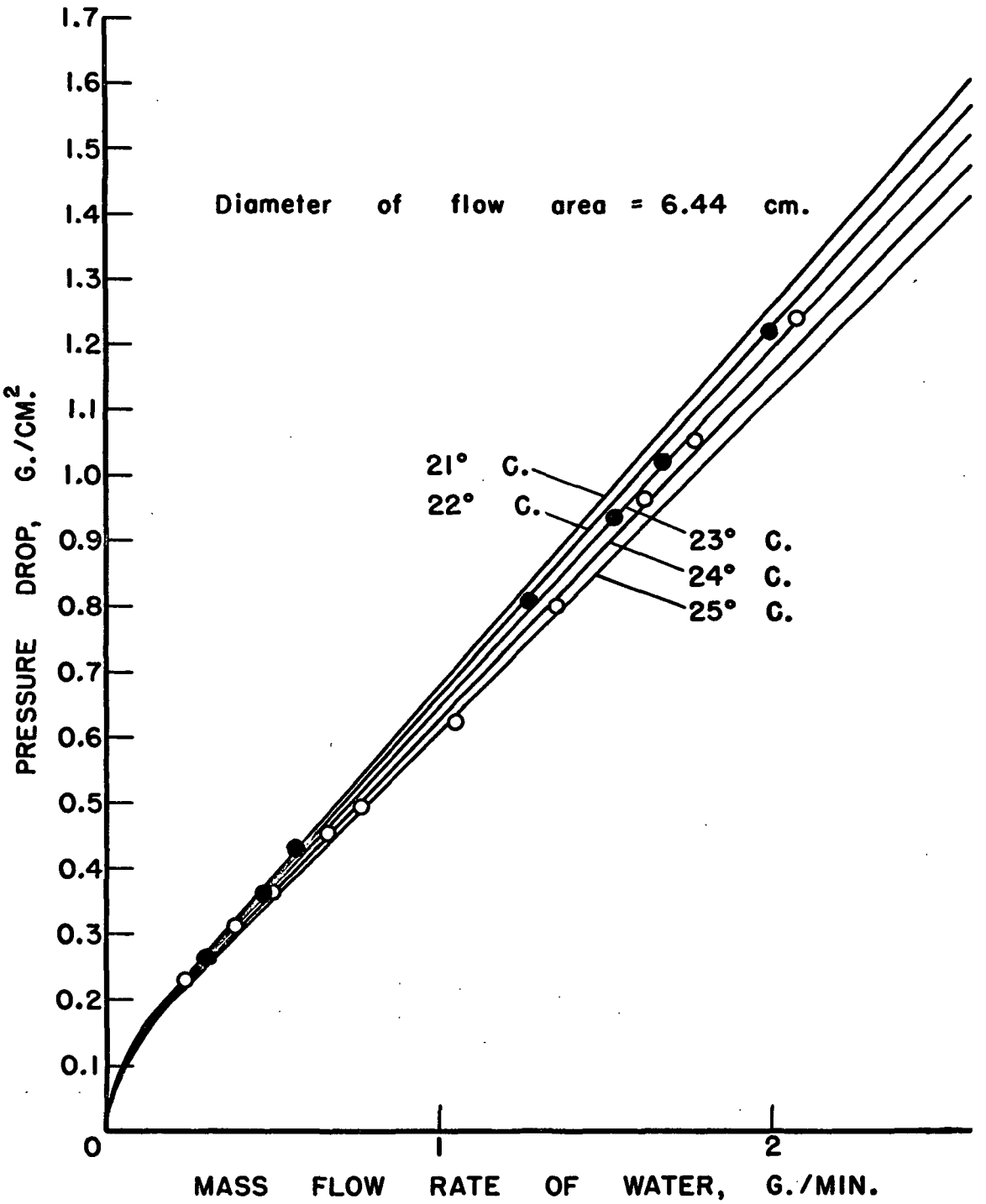

Figure 24. Upstream Medium Grade Porous Plate Calibration

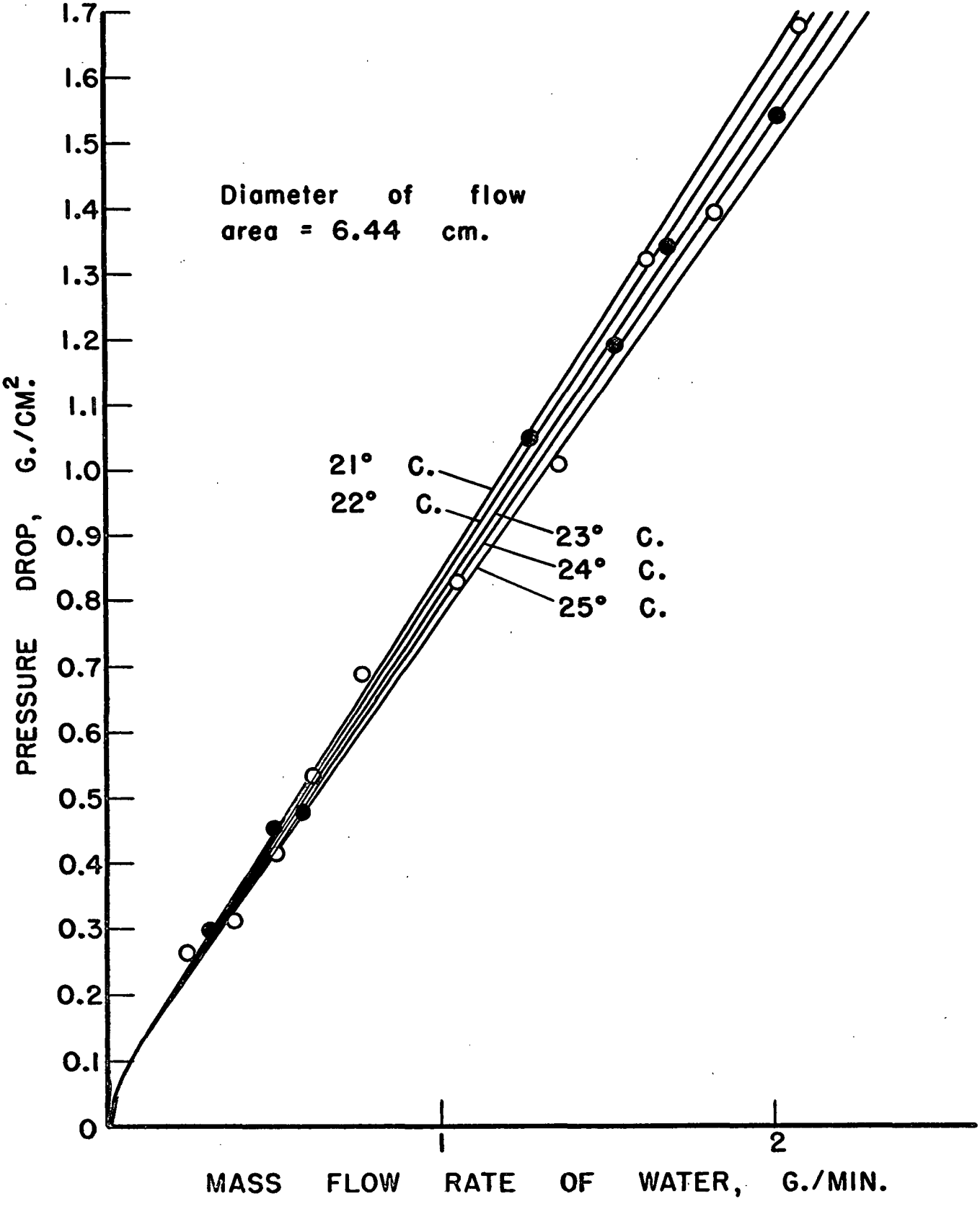

Figure 25. Downstream Medium Grade Porous Plate Calibration

(1) The proper amount of fiber was disintegrated and deaerated.

(2) The porous plates were cleaned and saturated with water.

(3) The rotameter and capillary flowmeters were assembled and filled with water.

(4) The porous plates were then rinsed and filled with deaerated demineralized water and installed in the apparatus. These plates were maintained dripping wet so that good contact could be made between the bed and the plates. All of the flow lines and manometer leads were filled with water and connected, and thermometers were placed in the flow lines.

(5) The fiber bed was formed and transferred to the upstream porous plate by the same technique used in the capillary pressure runs. The gage pegs were positioned, the downstream plate was placed on top of the bed, and the compression device assembled. Two people were required to manipulate this assembly without distorting the bed. The bed was then compressed and the expressed water removed from around the bed with a pipet.

(6) Finally, the entire assembly of bed, plates, and compression device was enclosed in a polyethylene envelope taped together.

To start the run, the predetermined upstream capillary pressure was impressed on the bed by one of two methods: (1) For low capillary pressures, the water supply reservoir, open to the atmosphere, was simply lowered to increase the suction head of water on the bed. The maximum distance this reservoir could be lowered beneath the upstream plate was 140 cm., so the maximum capillary pressure attainable by this method was about 10 cm. Hg.

(2) For capillary pressures greater than 10 cm. Hg, the upstream vacuum system was connected to the supply reservoir and the capillary pressures obtained with the aspirator vacuum. Since this method required constant attendance and fine adjustment, the former method was much superior. After the upstream capillary pressure was applied, the system was allowed to stand until capillary equilibrium was attained. At low capillary pressures, equilibrium was reached in a few minutes, but at the high capillary pressures, several hours were required. At the end of this time, enough vacuum was imposed on the discharge tank to just exceed the upstream capillary pressure. The stopcocks in the flow line and bypass line were then opened to permit flow through the bed. In all the permeability tests, countergravity flow was employed. By holding the upstream capillary pressure constant, the approximate desired flow rate through the bed was produced by manually adjusting the downstream capillary pressure. To increase this capillary pressure, the stopcock between the discharge tank and the low pressure reservoirs was opened; a decrease was obtained by opening the air bleed in the discharge tank. Very fine adjustments could be made with both of these controls. Control of the upstream capillary pressure was effected in the same way. When the system reached steady state, the flow was diverted through the proper capillary flowmeter and the system closely attended to maintain a constant flow rate. Steady state was observed when the differential manometer reading reached a constant value. At low capillary pressures, the time required to reach steady state was on the order of minutes, while at high capillary pressures, several hours were required. When the system reached steady state, the pertinent readings were taken, including

cathetometer readings of the upstream and downstream porous plate levels, differential manometer, and the mercury manometers connected to the plates, a reading of the capillary flowmeter manometer, and readings of the five thermometers in the system. The cathetometer readings were made to the nearest 0.1 mm. This procedure was repeated for successively higher capillary pressures, for the equilibrium saturation of the bed always had to be achieved by desaturation. For this reason, it was important never to allow a higher capillary pressure on the system during a single determination than the final value measured. Usually about eight measurements were made in a single run requiring about 60 hours elapsed time. At the end of each run, the bed was released from compression, inspected for fissures and any distortion; and the diameters of contact between the bed and the plates were measured. It was then transferred to a tared weighing bottle and its wet and dry weights determined gravimetrically. Also, at the end of each run, the water in both the upstream and downstream plates was checked for surface tension. In some runs, as high capillary pressures were applied to the bed, air would come out of solution in the water, and air bubbles would collect in the manometer leads and flow lines. It was expedient, then, to pinch off these lines, disconnect them, and remove the air bubbles and reconnect them filled with freshly deaerated water. The run was then continued as normal.

The practical limit of these permeability measurements was a saturation of about 97%. To fix the permeability curve at the high saturations, then, the permeabilities of beds at 100% saturation were determined with basically the same apparatus developed by Ingmanson (68) in his filtration studies.

The reader is referred to an article by Ingmanson and Whitney (70) for a detailed description of this equipment. The apparatus used for this work was essentially the same as the constant pressure-filtration apparatus described in the article except for an improved pressure-measuring system added later. This system consisted of a strip-recording potentiometer used in conjunction with an electronic-pressure transmitter, of which a comprehensive description is found in the thesis work of Hisey (71). Three separate beds of each size fiber were tested for saturated permeability over a range of porosity values by compressing the beds in the filtration tube of Ingmanson's apparatus and flowing water under steady state conditions through the compressed beds.* Ingmanson's permeable piston was used as the compressing tool, and compression was effected by dead weight loading of the piston. From the steady-state flow rate and pressure drop data, the saturated permeabilities of the beds were calculated by D'Arcy's equation. Using the values of Kozeny constant suggested by Brown (47) for glass fiber beds, the specific surface of the glass fibers were calculated by the Kozeny-Carman equation. With the proper value of specific surface, then, the saturated permeability could be calculated for any porosity which was not too far removed from the experimental porosities. A summary of the acceptable results of these saturated permeability runs is given in Table VII.

For each experimental bed on which relative permeability tests were run, then, its saturated permeability was calculated from the Kozeny-Carman equation using the above average values of specific surface and the Kozeny constant corresponding to its porosity from Brown's data.

* Acknowledgment is made to Bruce Andrews of the Chemical Engineering staff at the Institute who performed these saturated permeability tests.

TABLE VII

SATURATED PERMEABILITY MEASUREMENTS

1.2-mu Fibers

Porosity, ϵ	Permeability, K, $cm.^2$	Specific Surface, S_v, $cm.^2/cc.$
.9528	3625×10^{-11}	30,200
.9541	4074	29,100
.9489	2056	—
	Average =	29,650

3.0-mu Fibers

.9024	7270×10^{-11}	11,390
.9163	9660	11,330
.8996	7060	11,270
.9155	9380	11,410
.9079	7820	11,580
	Average =	11,400

EXPERIMENTAL RESULTS AND DISCUSSION

Before entering into the discussion of the results, it would be helpful to briefly review the objectives and conditions of the experimental program. Two major experimental determinations were made: (1) static capillary pressure curves, from which the pore size distributions could be determined and (2) steady-state relative permeability curves over the range of liquid saturations. These tests were performed on preformed beds of glass fibers which were externally compacted so that they were, in effect, incompressible. The conditions of these experiments were limited to isothermal conditions, flow of the liquid phase only, and only the desorption stage of the liquid at capillary equilibrium. These results, in conjunction with the two-phase flow theory developed, were used to analyze the relative permeability mechanism.

A natural consequence of nonfundamental theory in the analysis of experimental data is the introduction of empirical factors in the derived expressions. The physical significance of these factors is generally vague and poorly defined. Such factors in the Kozeny equation of relative permeability, Equation (42), are k_{oc}, T_c, and C_c. It follows that these factors are the distinguishing features of unlike systems, such as granular and fibrous media. In this analysis of two-phase flow, three aspects of the problem were considered. First, the experimentally measured relative permeability curves of the fiber systems were compared with those of other systems from the literature. Second, the relationship between the relative permeability and the effective pore size distribution, determined from the

capillary pressure curves, was evaluated. This was, in effect, the determination of the empirical factors, which are the factors of proportionality between the relative permeability and the pore size distribution. Since two media of different pore size distribution were tested, a consistency check on this relationship was possible. Third, the empirical factors of the partially saturated fiber systems, calculated from Equation (42), were compared with those suggested in the literature for unsaturated granular systems. It is from a comprehensive knowledge of the variation of these factors in systems of diversified structure that a basic understanding of their physical meaning is achieved.

POROSITY MEASUREMENT

In both the capillary pressure and relative permeability experiments, the principal criterion of accuracy was the reproducibility of separate runs. And the basis for reproducibility was the bed porosity. That is, it was attempted to prepare the experimental beds of each fiber with the same total porosity for every run. It was practically impossible to prepare separate beds having identical porosities for the different runs since there were considerable losses of fiber in the preparation of the beds. The quantity of fiber weighed out initially had to account for these losses. However, after several runs, the proper amount of fiber needed initially to give the desired porosity could be closely estimated. The experimental data, then, for each of the fibers was acquired over a narrow porosity range, varying about 0.3%. It is seen later that the capillary pressure curves are fairly sensitive to this variation in porosity, but the relative permeability curves are not affected by it. The porosities of the beds were

calculated from the total bed volumes and the solid volumes of the fiber in the bed. These values were determined from experimental measurement.

As discussed in the EXPERIMENTAL PROCEDURES section, the bed volume was evaluated from diameter and thickness measurements on the bed. Although diameter measurements were not made on the beds in place in the apparatus during the experimental runs, the excellent reproducibility of the bed dimensions under nearly identical testing conditions permitted the measured values to be applied to the experimental beds. In some cases, however, as the bed was compressed, it became slightly skewed, due to poor alignment of the compression device. This caused a negligible change in the total volume of the bed, as there was no slip between the plates and the bed, and the opposite sides of the bed remained parallel. The flow pattern through these skewed beds was probably changed slightly in the permeability tests; however, the flow path would have been altered only near the outside edges of the bed. Since the beds were thin, the portion of flow which was affected was quite small and the error caused by it was presumably insignificant. This was borne out by the consistency of the permeability results.

The use of gage pegs to determine the bed thickness allowed very precise measurements to be made. Special efforts were applied to keep loose fibers and debris from lodging between the pegs and the plates. Thus, it was possible to distinguish the point contact that the pegs made with the curved plates by shining a light behind the pegs. The accuracy of the bed thickness measurement, then, was of the same order of magnitude as that of the measured length of the pegs, and the pegs were accurate to within at

least ± .005 in. The calculated volume of the bed, therefore, was estimated to be quite accurate and reproducible well within the limits of accuracy of the relative permeability measurement. The correction of the bed volume because of the curvature of the plates has already been discussed. This correction was never more than 1.5% of the total bed volume. Assuming that the measured accuracy of this correction was at least 50%, then the error involved in the calculated total bed volume due to this correction never exceeded 0.8%. The calculated bed volumes for both fiber sizes in both apparatuses are given in Table VI.

The solid volume of the glass fiber was computed from the total weight of fiber in the bed and the solid density of the fiber. The ovendry weight of fiber in the bed was very accurately determined by drying at 105°C. and weighing. The solid density of the fiber was determined by pycnometric means as reported in the experimental procedures section. The technique used and the experimental results obtained are given there. The experimental solid densities determined in this work were subject to a variation of less than 1%. In view of all these factors, then, a conservative estimate of the precision of the bed porosity measurement in general would be about 2%.

STATIC CAPILLARY PRESSURE MEASUREMENT

ACCURACY AND REPRODUCIBILITY

The raw data of a capillary pressure run consisted of cathetometer readings of the level of the center of the bed, or the mean bed height, which remained constant during the run, and the mercury levels in the buret

tube and the reservoir and the wet and dry weights of the bed at the end of the run. The ambient temperature around the bed was also recorded. Of course, there was supplementary data, including the buret tube calibration, the surface tension measurements on the water, and the dimensions of the bed. A typical example of the recorded data of a capillary pressure run is given in Table VIII, omitting the supplementary data. This data is from Run no. 103 on the 3.0-mu fiber using gage pegs of .793 cm. in length. The calculation of this data to yield the capillary pressure vs. saturation results is given in Appendix II. In this calculation, the saturation of the bed was assumed to be uniform across the bed and equal to the average saturation. Of course, this is not strictly true, as a capillary pressure gradient, due to the head of water in the bed, and hence a distribution of saturation does exist in the bed. However, except for very thick beds or very low capillary pressures, this capillary pressure gradient was negligible compared to the total capillary pressure. The measurement of capillary pressure corresponding to this saturation was based on the midpoint of the bed thickness. The resulting values, then, were considered as point values of saturation vs. capillary pressure.

Several experimental precautions were attendant upon the accuracy of these capillary pressure results. As the water in the system had to be accounted for quantitatively, the system had to be sealed against the loss or gain of water or other fluids. Thus, the entry of air into the system could not be tolerated. Before starting a run, it was made certain that the system was purged of air, for a bubble of air in the system initially would expand as the capillary pressure was increased. However, since the

TABLE VIII

RECORDED DATA FOR CAPILLARY PRESSURE RUN NO. 103

Temperature, °C.	(a) Mean Bed Height, cm.	(b) Buret Tube Mercury Level, cm.	(c) Reservoir Mercury Level, cm.
23.3	117.51	74.22	76.66
23.3	117.51	74.01	74.62
23.4	117.51	73.71	72.55
24.0	117.51	72.25	69.52
23.8	117.51	65.88	62.35
23.8	117.51	58.24	54.25
23.8	117.51	53.58	48.91
23.6	117.51	53.66 (Evap.)	48.90
23.8	117.51	50.95	45.15
23.8	117.51	48.98	41.33
23.8	117.51	47.71	35.67
23.9	117.51	47.45	27.47
23.5	117.51	47.55 (Evap.)	27.46
23.5	117.51	47.52	18.69

End of Run

Wet weight of bed at end of run = 5.8516 g.

Dry weight of bed at end of run = 5.5443 g.

Grams water in bed at end of run = .3073 g.

maximum capillary pressure applied to the system was only 36 cm. Hg, a small amount of dissolved air in the water could be tolerated. Apparent evaporation of water from the bed during the run was the only violator of the sealed system. As seen in the data of Table IX, a slight loss of water from the system was noted when the apparatus stood overnight. This loss was estimated from the succeeding measurements as illustrated in Appendix II. Evaporation undoubtedly was occurring at all times during the run and presumably caused a discrepancy between the value of complete saturation determined from extrapolating the capillary pressure curve to zero capillary pressure and that calculated from the dimensions and porosity of the bed. A correction was applied to the capillary pressure curve to allow the extrapolated value of complete saturation to correspond with the calculated value. Since the evaporation was much greater in the early stages of the run, the correction was spread out over about the first half of the determined curve. This correction was never greater than 2% of the total bed saturation and should not have jeopardized the accuracy of the experimental curve.

The capillary pressure curve was quite sensitive to the surface tension of the water, so it was essential that the surface tension of the water in the bed remained constant during the run. This was undoubtedly the case, for the surface tension of the water measured initially in the formation of the bed and that measured at the end of the run in the porous plate were the same and equal to 71.4 dynes/cm. All of the surface tension measurements were made with a Cenco-Du Nouy interfacial tensiometer no. 10403 (72) in the constant humidity room at the Institute at a temperature of approximately 23.0°C. The average tensiometer reading for all the water samples from both

the capillary pressure and relative permeability runs was 76.1. The average temperature of beds in both these runs was taken as 23.5°C. The temperature change from 23.0 to 23.5°C. causes a decrease in the surface tension of water of approximately 0.1 dynes/cm. Applying this change to the average tensiometer reading and multiplying by the tensiometer correction factor of 0.94, the value of 71.4 dynes/cm. for water at 23.5°C. was obtained. The accuracy of this measurement was probably no better than 1%, and since the surface tension of water is not very sensitive to temperature, the deviation in surface tension due to the small fluctuations in temperature of the experimental systems more than likely falls within the expected deviation of the surface tension measurement. Thus, the effect of the temperature on the surface tension was ignored in this work.

The exactness of the buret tube calibration was obviously important in the accuracy of the capillary pressure measurements. The mercury levels in a run could be measured to within .01 cm., corresponding to a volume increment of the buret tube of about .009 cc., according to the calibration value of .876 g. water/cm. Thus, the accuracy of this measurement far exceeded that of other limiting factors in the capillary pressure runs. The precision of the blank runs on the apparatus was at least as good as 10%, as shown in Figure 16. Since this correction never amounted to more than 3% of the total water in the bed, the error in the results due to this correction was never greater than 0.3%.

Two possibilities of experimental error in the moisture content of the bed determined gravimetrically at the end of the run were due to (1) the

pickup of water from the porous plate by the bed as it was released from compaction, and (2) the evaporation of water from the bed when the Plexiglas cover was removed. Since the regime of saturation in the bed was nearly pendular at the end of the run, the rate of water pickup by the bed, if at all, would be extremely low. Further, since the porous plate was sealed off from the rest of the system by the closed stopcock, any water loss from the plate would have to be replaced with air leaking into the plate, and this was not observed. With regard to the possibility of evaporation, the bed was exposed to the open atmosphere not more than 45 seconds. Since the small amount of water in the bed was held in the smallest capillaries and was not readily subject to evaporation, loss of water in this way was almost certainly negligible.

The experimental capillary pressure curves for the 1.2-mu and 3.0-mu fiber beds are shown in Figures 26 and 27, respectively. As expected, a high degree of precision is reflected in these data. The reproducibility of the results was primarily dependent upon the formation of homogeneous beds in the filtration tube, and for this reason, the technique of bed formation was important. Ingmanson (68) reported that homogeneous and reproducible beds of pulp fibers were not obtained when prefilt slurry concentrations greater than .01% were used. In this work, much higher consistencies of the glass fiber, up to .25%, were used. Since the glass fibers were roughly twice as dense as pulp fibers, this maximum consistency was comparable to about .12% pulp fiber concentration. Despite these high concentrations used, the formation of the bed was improved by continuous stirring of the slurry during the filtration. In addition, the compaction

of the bed in the experimental runs undoubtedly reduced the heterogeneities in the bed structure. Apparently, this effect of compaction was quite significant, for the variation in slurry concentration for the different size beds had no perceptible effect on the bed structure, as it is seen from Figures 26 and 27 that the capillary pressure curves were not influenced by the size of the beds. Thus, under the conditions of bed formation employed, the pore size distributions of the different size beds were the same. No capillary pressure runs were made on 1.50-cm. thick beds of the 1.2-mu fibers, but this size bed was not so extreme that it should be different in structure from the less thick beds tested.

COMPARISON OF CAPILLARY PRESSURE CURVES OF DIFFERENT MATERIALS

It is interesting to compare the desorption capillary pressure curves in Figures 26 and 27 with those of several different media from the literature. The range of significant capillary pressures is markedly different in many cases, but all incompressible media appear to exhibit the same general shape of curve, regardless of size or shape of the pore structure. Carman (15) notes this similarity between a microporous plaster-water system and a macroporous sand-water system. He suggests that microporous and macroporous capillary pressure curves are easily compared by plotting the capillary pressure values on a log scale. In Figure 28 are typical examples of capillary pressure curves of various porous systems. For the sake of comparison, values of the capillary pressure were plotted on a log scale.

This widespread similarity of capillary pressure curves for incom-

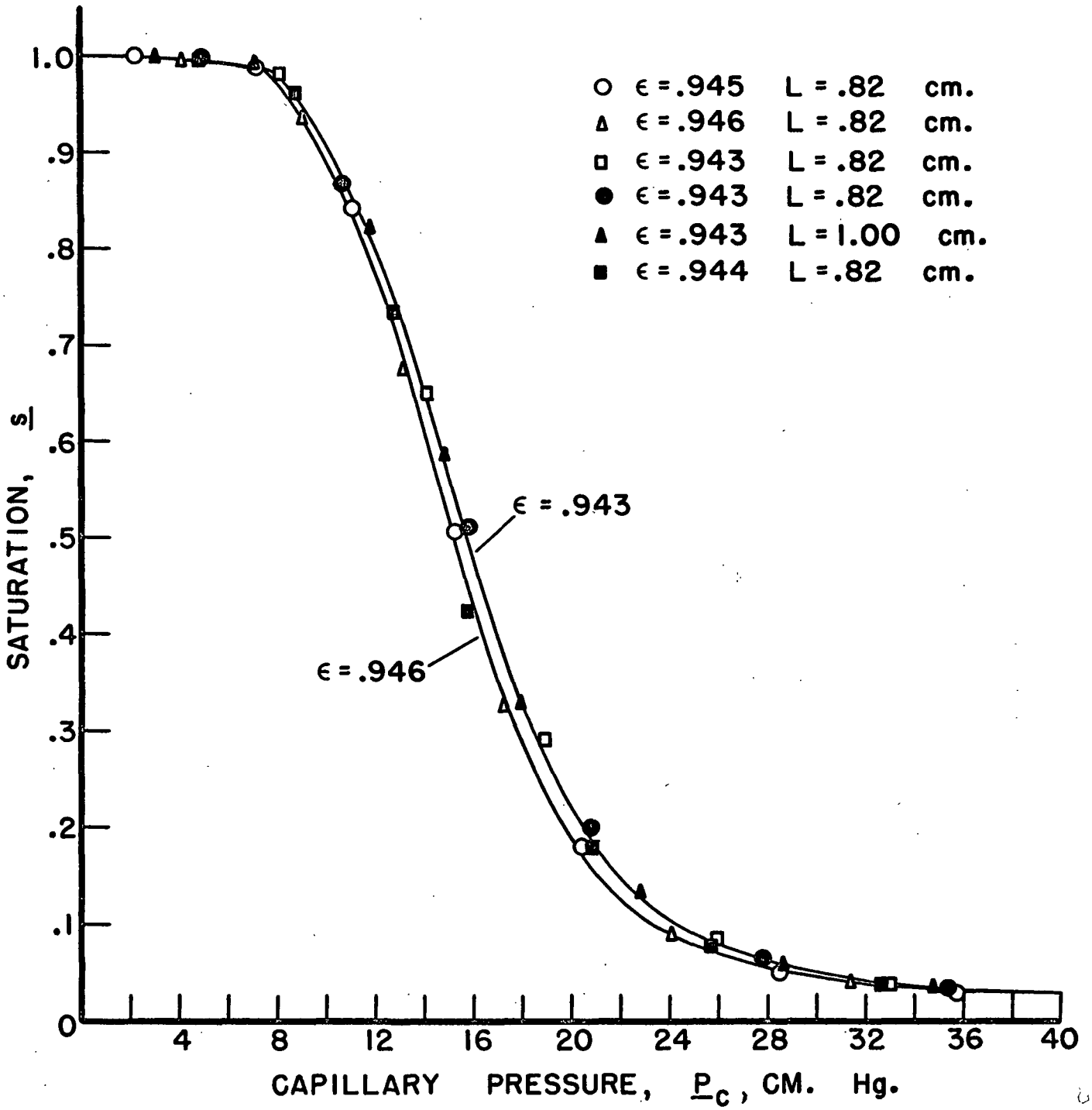

Figure 26. Capillary Pressure Curve of 1.2μ Fibers

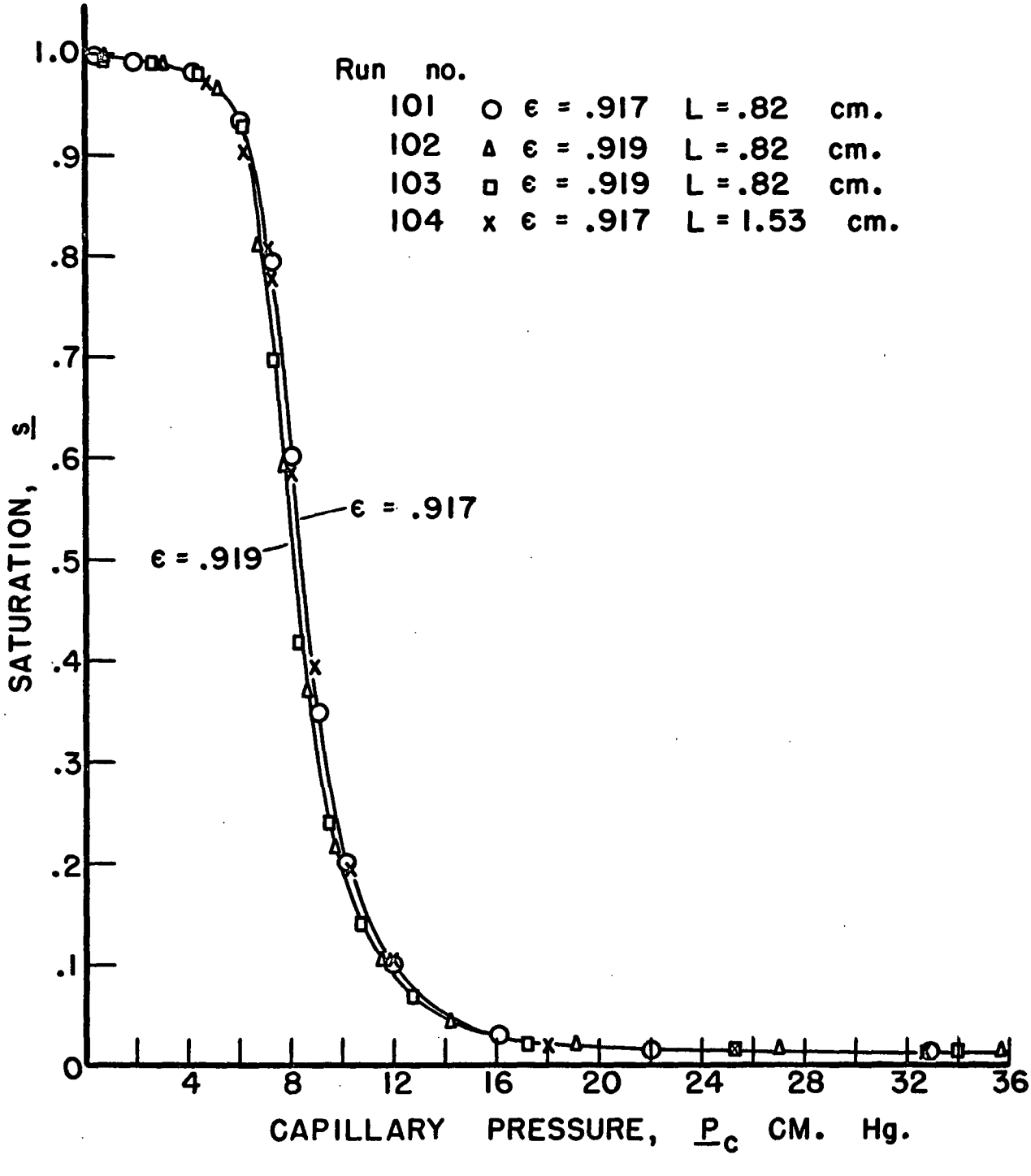

Figure 27. Capillary Pressure Curve of 3.0μ Fibers

pressible porous media suggests a universal correlation between the effective pore size distribution, determined from the capillary pressure curve, and any system variable which is primarily dependent upon the pore size distribution, such as the relative permeability. Actually, the pore size distribution dictates the distribution of liquid, i.e., the configuration of liquid flow channels, at any particular saturation, and the relative permeability depends on this distribution. As discussed later, this suggestion of universal correlation has received substantial experimental support, and a generally applicable relation between the effective pore size distribution and relative permeability is deemed highly probable.

It is manifest in the curves of Figure 28 and Carman (15) points out that the break-off point of the curves becomes less well defined when the pores are not uniform in size. A graphic example of this is the curve for silica flour, Curve 6 in Figure 28. Characteristic of compressible media is the bed of cellulose fibers (Curve 1) which does not have a break-off point at all. This is due to the change in over-all pore size distribution as the bed is desaturated and simultaneously compressed by surface tension, or capillary, forces. In some instances, the experimental capillary pressure curves indicate that saturation was complete at some finite value of the capillary pressure, i.e., the break-off point occurred at $\underline{s} = 1.0$, for example, Curve 7. Wyllie and Spangler (48) devised a visual technique for accurately determining, on the absorption cycle, the displacement, or break-off point, pressure for sandstone cores. They maintained that the rock cores were fully saturated at some relatively large value of the capillary pressure. Although many porous systems may exhibit capillary pressure

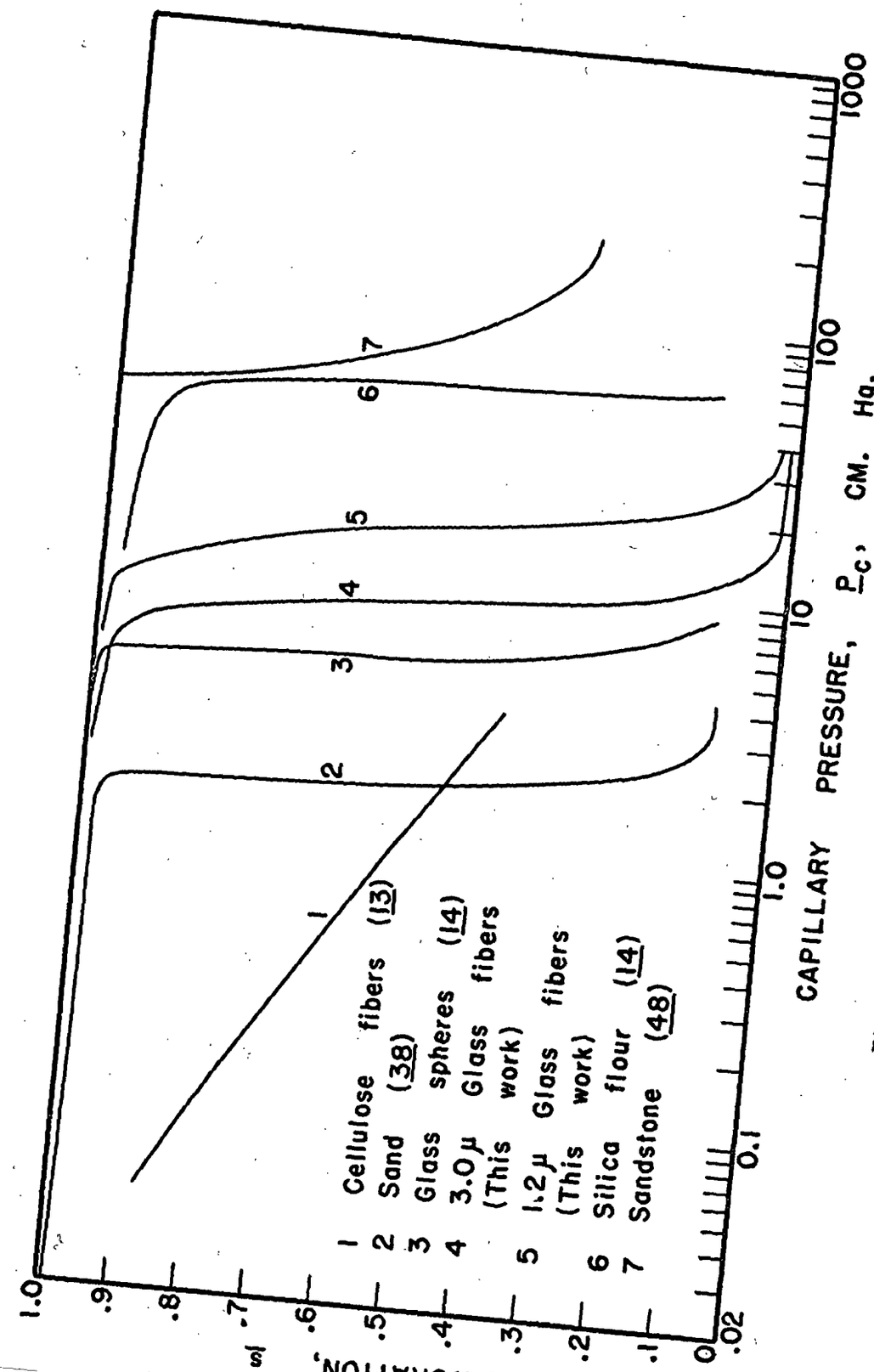

Figure 28. Capillary Pressure Curves of Various Media

relationships that approximate this condition very closely, it is never rigorously true. In the extreme example of single capillary tube or a group of uniformly-sized capillary tubes, the increase in capillary pressure before the break-off point, or entry suction, as it is sometimes called, causes a depression in the liquid interfaces, producing some change in the saturation of the bed. In many real porous systems, this change in saturation before the break-off point is appreciable, e.g., Curves 2 to 6 in Figure 28. It is not implied here that this desaturation before the break-off point in nonuniform pore size media was due entirely to the depression of the liquid menisci. On the contrary, this slight initial desaturation was likely due to the opening up of a few very large pores. This relatively small change preceding the break-off point assumes large significance in the analysis of two-phase flow. As it will be seen later, the capillary pressure measurements enter into the analytical expression of relative permeability in integral form of the pore size distribution, equivalent to the capillary pressure, curve. And the integral of this curve is very sensitive to the large pore sizes, or low capillary pressures. It is important, therefore, to have an accurate measurement of the capillary pressure curve at the low capillary pressures.

SIGNIFICANCE OF PORE SIZE DISTRIBUTIONS CALCULATED FROM CAPILLARY PRESSURE CURVES

To convert a capillary pressure curve to an effective pore size distribution, the values of capillary pressure were simply changed to an effective pore size, $\underline{m}$, equal to $\gamma/\underline{P_c}$. In this conversion, it was assumed that the contact angle between the glass fiber and water was zero. This assumption

was certainly justified in this work, as it has been shown experimentally that the angle of contact between water and glass was zero if the glass was covered by a film of water (73). Cumulative pore size distributions of m vs. s were determined for the beds of 1.2-mm fiber having a porosity of .946 and for the beds of 3.0-mm fiber having a porosity of .919. Graphs of these distributions are shown in Figure 29. As used in this connection, a more meaningful description of the ordinate saturation, s, might be the fractional part of total saturation, or porosity, contributed by pores of a size equal to or smaller than m.

In speaking of the pore size distribution of a real porous medium, it is necessary to qualify the meaning as an "effective" distribution, as several objections are raised against characterizing the pore size distribution by capillary displacement. Thus, Ergun and Owen (74) stated that indirect methods of measuring pore size distribution, such as capillary displacement, were not suitable for pore sizes above 5 microns. Scheidegger (3) suggests that large pores exist in porous media which are only connected to the outside by smaller ones, and these do not empty at the capillary pressures corresponding to this size of pore. In addition, there is the possibility that small amounts of the displaced liquid are isolated in the pendular state in pores that are larger than those corresponding to the residual saturation. This breakdown of the funicular state in portions of the bed before the residual saturation was reached was considered previously and was held to be insignificant.

A realistic analysis of the physical significance of the effective pore

radius in capillary-held liquids has been presented by Carman (15). He contends that one of the most important ways liquid is held in porous systems is in annular rings at the points of particle contact. Such annular rings have principal radii of meniscus curvature in opposite senses. As the annular ring diminishes in size, these radii of curvature decrease at different rates such that the over-all mean hydraulic radius, representing these radii of curvature, also decrease. Thus, if this mean hydraulic radius is interpreted as the radius of a circular capillary, a single annulus corresponds to a group of capillaries varying from zero radius upwards. This illustrates the continuity of pore size in real systems. It is meaningless in such a case to assume that liquid is held in circular capillaries; and the effective pore size, or mean hydraulic radius, is nothing more than an index of the volume of liquid retained, its value depending on the configuration of the pore space. However, in this analysis, the question of a rigorous interpretation of the capillary pore size is relegated to second degree importance. The question of primary import is whether the effective pore size distribution can be usefully incorporated in an analytical expression of two-phase flow.

In the early part of this thesis work, samples of the glass fibers were tested for pore size distribution by the mercury intrusion method. This work was done by The American Instrument Company of Silver Springs, Md. with their recently developed mercury intrusion porosimeter (75). Comparisons of the pore size distributions obtained by this method with those obtained from the capillary pressure curves of this work for the two sizes of glass fiber are shown in Figures 30 and 31. In these curves,

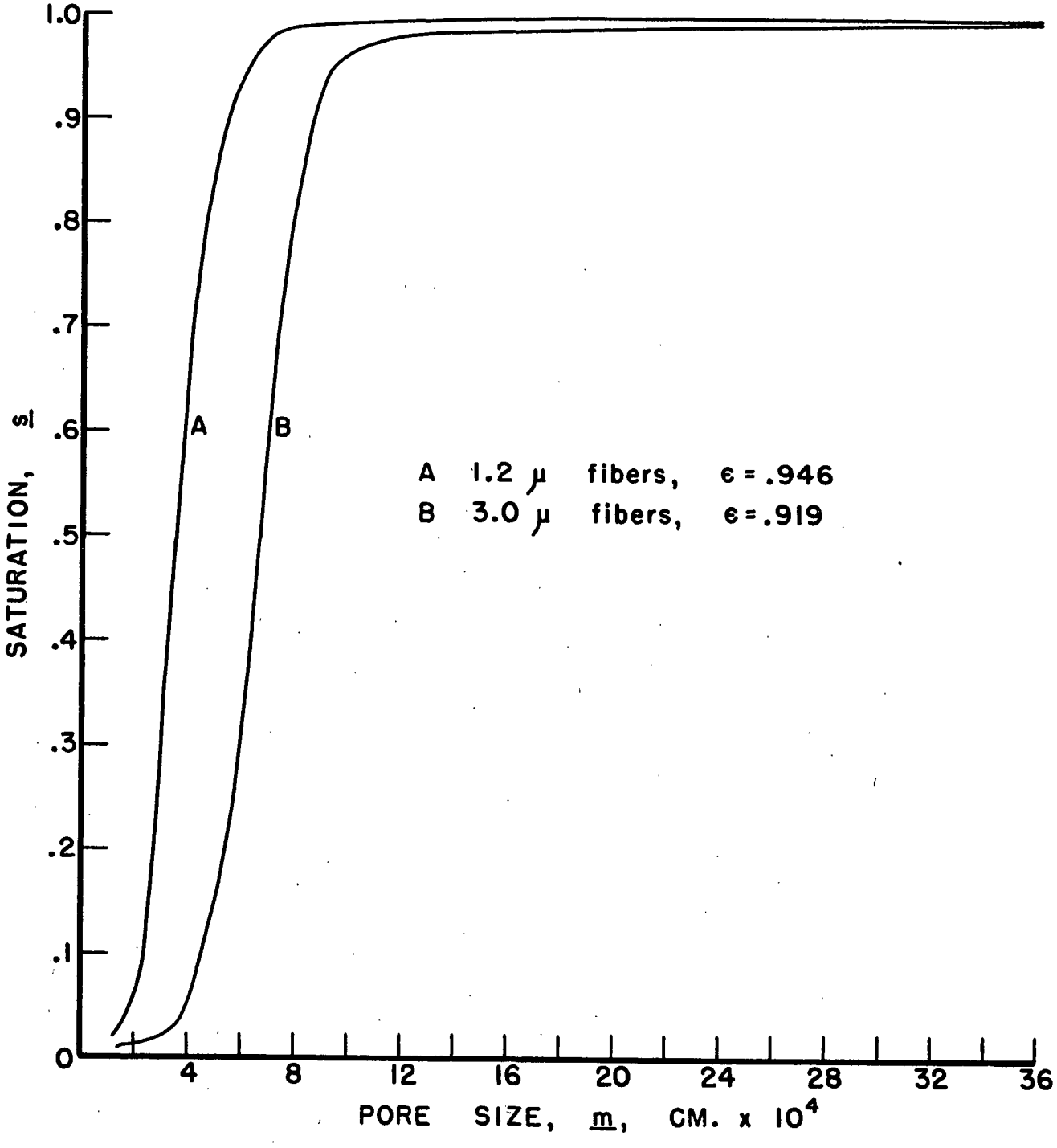

Figure 29. Pore Size Distributions of the Glass Fiber Beds

instead of the pore size, m, the effective pore diameter, $D_p = 4m$, was plotted against the saturation. The mercury intrusion technique employed very small volume beds, approximately 1.0 cc., under very high compression. Under these conditions, it was probable that the beds were not homogeneous, accounting for the irregular curves obtained, and the porosities for the mercury intrusion tests were much lower than those used in the present study. For these reasons, a close agreement of the two curves cannot be expected; however, the curves are markedly similar in shape, and, presumably, these two methods of measuring pore size distribution would give identical curves for the same media.

STEADY STATE RELATIVE PERMEABILITY MEASUREMENT

ACCURACY AND REPRODUCIBILITY

Measurements of the steady state specific permeability were usually made at about eight different saturations during a run, which lasted about 60 hours. Individual measurements required 15 minutes to 4 hours, depending on the saturation of the system. The data of a typical run, no. 6 of the 1.2-mu fiber, is given in Table IX. In order for this data to be complete, of course, it was supplemented with the capillary flowmeter and porous plate calibrations, and measurements of the saturated permeability bed dimensions, density of the differential manometer fluid, and the water surface tension and viscosity. The calculation of this data to yield relative permeability *vs.* saturation results is illustrated in Appendix III. In this calculation, the temperature of the water in the bed was taken as the average of the ambient bed temperature and the water temperatures in the upstream and

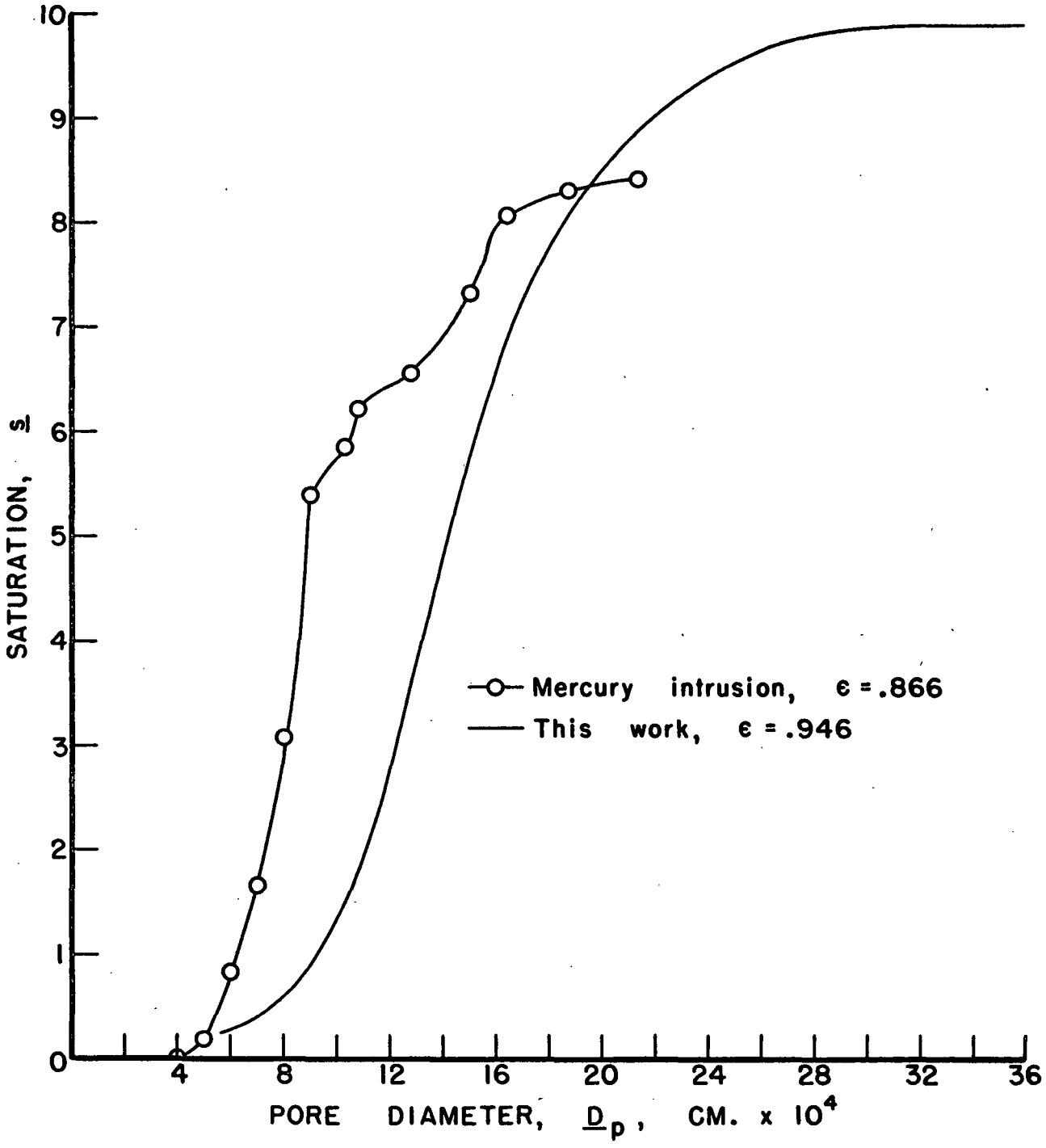

Figure 30. Pore Size Distribution of 1.2-mu Fiber Beds

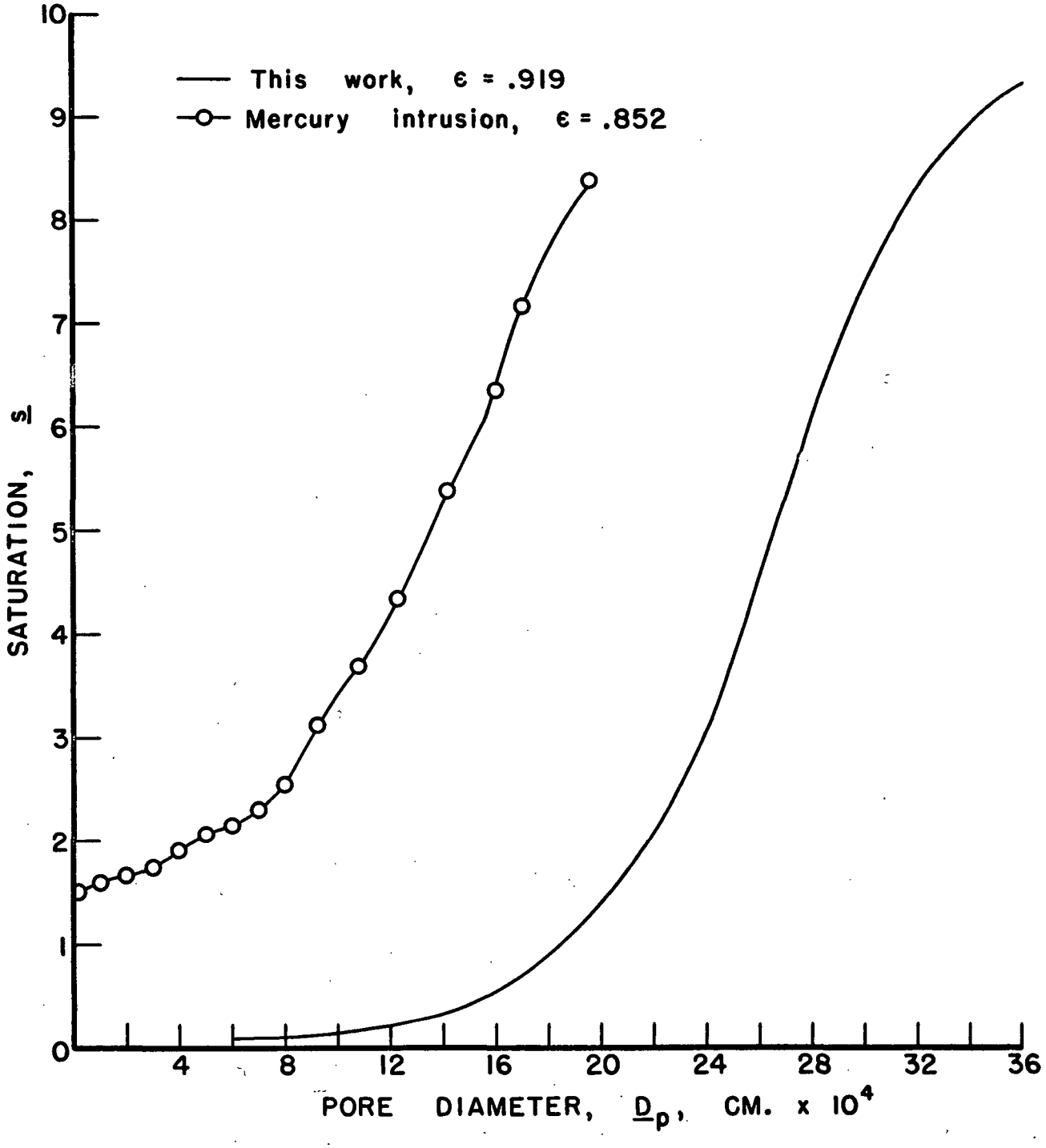

Figure 31. Pore Size Distribution of 3.0-mu Fiber Beds

downstream flow lines. These temperatures seldom differed more than 0.5°C. It was assumed, as in the capillary pressure determinations, that the saturation, and hence the permeability, was uniform over the thickness of the bed. Although this was not rigorously correct, the beds were thin enough and the pressure drops across the beds low enough, generally less than 0.1 cm. Hg except at the very low saturations, to preclude any large experimental error. Thus, the results were obtained in terms of point values of the relative permeability as a function of the average capillary pressure, from which point values of the saturation were determined.

The final step of this permeability calculation consisted of the following two conversions: (1) the experimentally determined specific permeability, K_c, was divided by the saturated permeability, K, to yield the relative permeability, K_r, and (2) the average capillary pressure was converted to point values of saturation by interpolation of the appropriate capillary pressure curve. In the first conversion, values of the saturated permeability were determined experimentally using the apparatus of Ingmanson (68). Since the bed was confined in a cylindrical tube in this apparatus, the question arose as to whether the permeability of this confined bed was equivalent to that of the unconfined bed in the permeability apparatus of this work. Obviously, the dimensions of the bed are much more accurately defined in the apparatus of Ingmanson. However, the measurements of the unconfined compressed bed dimensions were quite precise, so little discrepancy between the two beds was expected on this account. Since the formation tube used to prepare the preformed bed and Ingmanson's filtration tube were about the same size and the conditions of filtration were roughly

TABLE IX

RECORDED DATA FOR RELATIVE PERMEABILITY RUN NO. 6

a	b	c	d	e	f	g	h	i	j	k
					Mercury Manometer Reading					
Upstream Water Temp., °C.	Ambient Bed Temp., °C.	Down-stream Water Temp., °C.	Upstream Porous Plate Level, cm.	Downstream Porous Plate Level, cm.	Upstream Porous Plate, cm.	Downstream Porous Plate, cm.	Differential Manometer Reading, cm.	Ambient Temp. Around Differential Manometer, °C.	Capillary Flowmeter Manometer Reading, ___ cm.	Ambient Capillary Flowmeter Temperature, °C.
25.4	25.0	24.9	121.90	123.40	62.34-63.195	63.825-65.505	49.58-61.57	25.2	H - 58.00-77.30	25.7
25.6	25.2	25.2	121.90	123.40	60.945-64.585	62.54-66.82	51.28-59.935	25.3	I - 40.00-84.15	25.8
25.3	25.2	25.2	121.90	123.40	59.76-65.75	61.385-67.995	51.35-59.86	25.1	I - 41.00-83.20	25.7
24.6	24.7	24.6	121.90	123.40	58.68-66.81	60.30-69.085	51.25-59.92	24.5	I - 44.00-80.30	24.9
24.0	23.6	23.8	121.90	123.40	57.36-68.09	58.92-70.475	49.69-61.41	23.7	I - 45.00-79.40	24.2
24.5	24.3	24.3	121.90	123.40	55.83-69.605	57.065-72.38	42.90-68.09	24.2	I - 49.00-75.39	24.7
25.5	25.3	25.4	121.90	123.40	54.35-71.06	55.385-74.10	38.89-72.13	25.1	I - 58.85-65.50	25.7
24.3	24.0	24.3	121.90	123.40	52.59-72.77	53.36-76.15	33.96-77.11	24.2	L - 56.90-61.25	24.1

End of Run

Upstream diameter of contact at end of run = 6.40 cm.
Downstream diameter of contact at end of run = 6.40 cm.
Wet weight of bed at end of run = 10.9312 g.
Dry weight of bed at end of run = 6.8510 g.

the same, it was unlikely that any differences in formation were introduced; and the compaction of the beds would have further reduced any differences in formation that might have been present. The only other probable source of difference between these beds was the possibility of a significant wall effect in Ingmanson's apparatus on the permeability. In correcting for wall effects, Carman (2) suggested that the permeability be multiplied by the factor, $(1 + 1/2\ S_W/S_o)^2$, where S_W is the surface of the container wall per unit volume of bed covered, and S_o is the surface of the particles per unit volume of the bed. The values of this factor for the saturated permeability runs in Ingmanson's apparatus were calculated as 1.00032 for the 1.2-mu fiber beds, and 1.00056 for the 3.0-mu fiber beds, so the wall effect appears to be negligible. The extension of the relative permeability curve to the saturated value of 1.0 was straightforward.

In converting the average capillary pressures to point values of saturation, it was assumed that the distribution of water under the conditions of flow, i.e., the dynamic distribution, was the same as the static distribution for the same capillary pressure. Theoretically, this was not true since, in the dynamic equilibrium, a gradient of capillary pressure, due to the frictional drag pressure drop, existed over the liquid interfaces. However, when this capillary pressure gradient is sufficiently small, the difference in the static and dynamic liquid distributions is negligible. For example, the over-all capillary pressure gradients in these relative permeability runs generally were not more than 980 dynes/cm.^{2}/cm. If the dimensions of the air-water interfaces are assumed to be of the same order of magnitude as the dimensions of the pores in which the water is held, the

maximum size of the interface spans approximately 50 x 10^{-4} cm. The change in capillary pressure over this interface was, then, roughly 4.90 dynes/cm.^{2} The total capillary pressure that was impressed on the system was never less than 15,000 dynes/cm.^{2} Consequently, the percentage change in capillary pressure over the interface, which is an index of the local difference in the static and dynamic liquid distributions, was never greater than .03%. In general, then, when the capillary pressure difference across a bed is an order of magnitude smaller than the capillary pressure itself, the dynamic equilibrium distribution of liquid in the bed is stable and equivalent to the static distribution. Each phase, then, occupies a specific and well-defined portion of the pore space, and the flow of water takes place in its discrete channels at steady state. Rapoport and Leas (57) term this condition "parallel flow." The point value steady state relative permeability measurements in this work involved the parallel flow, or capillary flow, as it has been termed previously, mechanism. This concept of parallel or capillary flow appears to be an accurate characterization of the two-phase flow system.

The point value steady state relative permeability curves of beds of both size fiber are shown in Figures 32 and 33. As expected, the precision of the results is much better at the low than at the high saturations, primarily because the flow resistance of the porous plates become less significant as the saturation decreases. But the relative permeability measurements were satisfactory up to a saturation of about 0.97. At saturations greater than this, the flow resistance of the plates is predominantly large, on the order of 95% of the total resistance.

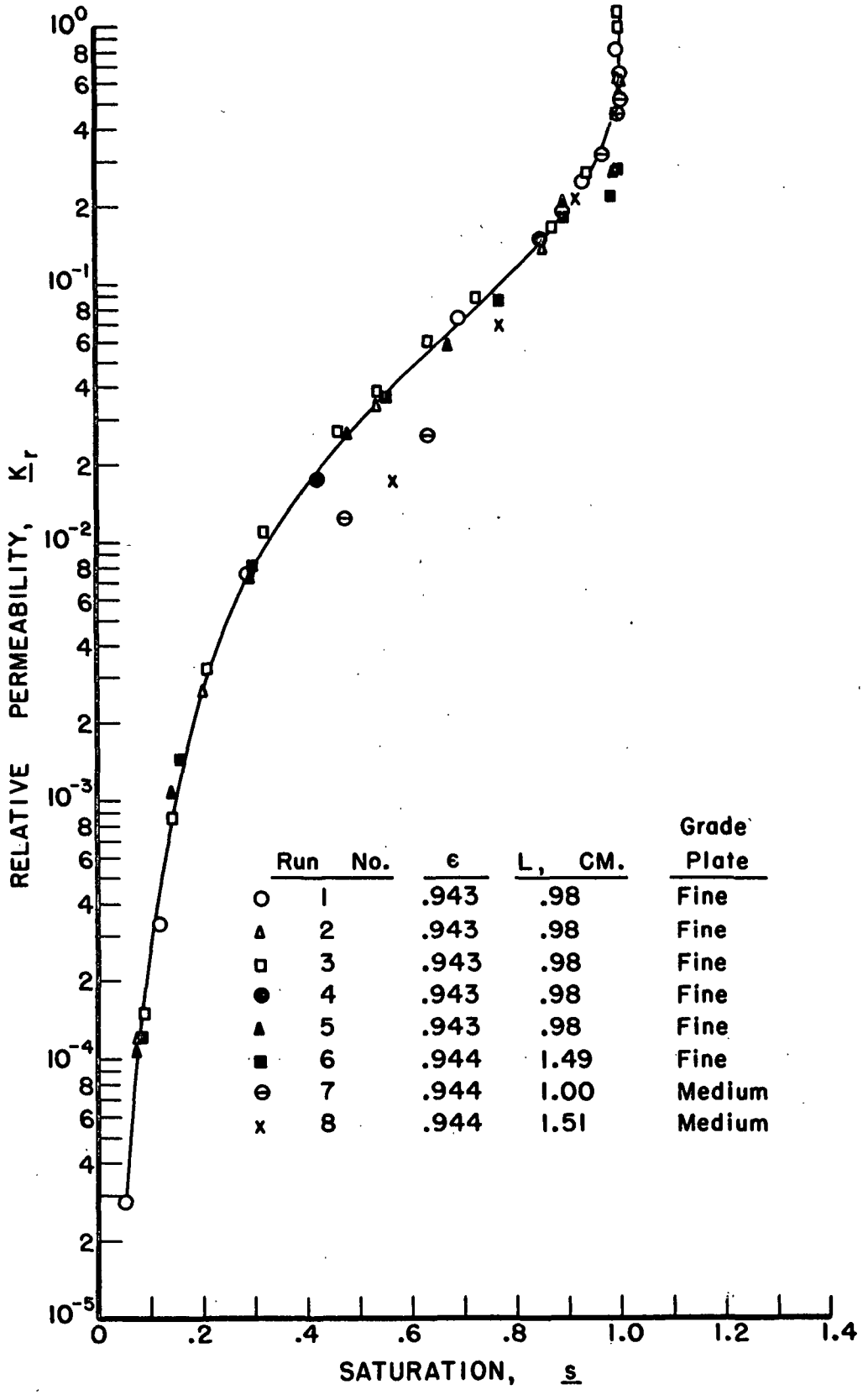

Figure 32. Relative Permeability Curve of 1.2μ Fibers

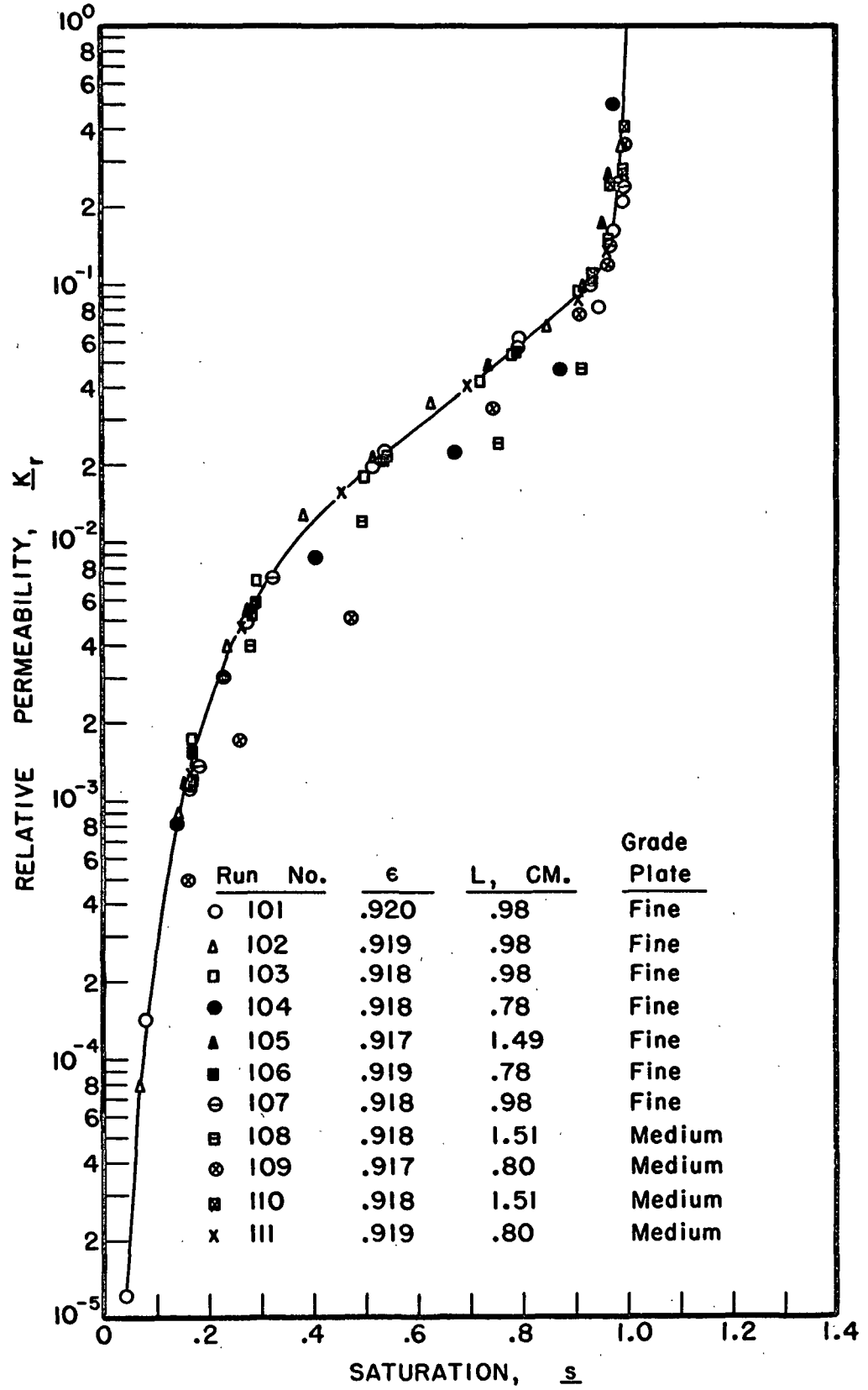

Figure 33. Relative Permeability Curve of 3.0μ Fibers

The consistency of the results using different thickness beds and different porosity-grade plates testified to the accuracy of the relative permeability measurement. Further, the belief that the permeabilities of the porous plates are essentially constant over the range of capillary pressures applied to the system was corroborated by the agreement of the results. Possibly, the permeabilities of the plates were slightly reduced at the high capillary pressures; however, the resistances of the fiber beds at these high capillary pressures (i.e., low saturations) were so great compared to that of the plates that the changes in plate permeability were of little consequence. The exception to this condition is noted in Runs 7 and 8 of the 1.2-mu fiber in Figure 32, in which medium-grade plates were employed. Compared to the fine-grade plates, these medium-grade plates having larger pores, had a more irregular surface and were desaturated at much lower capillary pressures. The limiting value of capillary pressure which these plates could sustain was about 20 cm. Hg. In Runs 7 and 8, as this limiting value was approached, the plates were partially desaturated and the permeability of the plates was probably diminished somewhat. In addition, the liquid contact between the plates and the bed was considerably reduced. This was readily apparent when the bed was removed from the plates at the end of the run, as the desaturated surface areas of the plate appeared white in contrast to the dark areas which still contained water. Consequently, the calculated permeability values were lower than actual as seen from Figure 32. The use of medium-grade plates, therefore, was only effective at the high saturations for the 1.2-mu fiber beds. With the 3.0-mu fiber beds, on the other hand, these plates were useful for the entire range

of saturations, since much lower capillary pressures were required to desaturate these beds. However, plate permeability decay accounted for some discrepancies in the relative permeability measurement of the 3.0-mu fiber beds also, as indicated by Runs 108 and 109 in Figure 33, at least in part. Of course, it was not as significant as for the 1.2-mu fiber beds, since lower capillary pressures were involved. In addition to this plate permeability decay, the calculated permeability values were spuriously reduced by "fissure effects" in the surface of the fiber beds. These effects partially destroyed the liquid contact between the bed and the plates and were easily noticeable as depressions in the surfaces of the bed at the end of the run. Apparently, these fissures arose from irregularities in the bed as a result of poor formation of the bed. Slight indications of fissures were observed in the beds of Runs 7 and 8 for the 1.2-mu fiber, but they were not nearly so pronounced as in the 3.0-mu fiber beds. It appeared that the 3.0-mu fiber beds were more fissure effect-prone than were the 1.2-mu fiber beds, probably because of the coarser nature of the 3.0-mu fibers plus the fact that the 1.2-mu fibers made better contact with the porous plates. In fact, the surface fibers of the 1.2-mu fiber beds were always partially embedded in the plates at the end of a run. It was quite probable that the dewatering of the medium-grade plates initiated the formation of these fissure effects, as the liquid film between the bed and the plates undoubtedly served to bind the bed to the plates. However, it was also possible for the fissures to occur with the fine-grade plates, as illustrated by Run 104 in Figure 33. In this run, the error caused by the fissure effect became less significant at the low saturations until it was

eventually negligible. Permeability decay of the plates resulting from high flow rates was never a serious factor because high flow rates were necessary only at the high saturations, and the time for which these flow rates were employed was always very short.

As in the capillary pressure runs, it was important that the surface tension of the water in the system remained constant during the permeability runs. As discussed previously, the effect of tygon tubing in the apparatus was to markedly reduce the surface tension of the water in the fiber system. However, no appreciable effect of this surface tension change was observed in the permeability measurement on the 1.2-mu fiber beds, as Runs 1-4 were made with tygon tubing. Apparently, the surface tension was not significantly changed until the last part of the run at the low saturations. At these saturations, the capillary pressure curve was quite flat and the saturation was insensitive to the surface tension. After the tygon was replaced with black rubber tubing, the surface tension was found to remain constant in the system at the same value as that in the systems of the capillary pressure runs, viz., 71.4 dynes/cm. The water viscosity was not affected by either of the tubings, and the approximate isothermal conditions kept the viscosity change to a minimum. The changes in viscosity due to the small temperature fluctuations were easily and accurately corrected.

During the permeability measurements, it was sometimes very difficult to determine whether the fall off in permeability was due to the progressive desaturation toward capillary equilibrium or whether there was permeability decay in the beds due to the usual causes of blocking of the channels by

impurities, displacement of fibers, or release of air bubbles. However, this decay of permeability was deemed improbable because pure water and low flow rates were used, and any released air bubbles could easily escape in the two-phase system. In view of the consistent permeability results, then, the permeability decay of the beds was apparently insignificant.

At the end of each permeability run, the wet fiber bed was removed from the apparatus as rapidly as possible in an attempt to get an accurate gravimetric determination of the water content of the bed. In this way, a check on the interpolated values from the capillary pressure curves was obtained. In Table X, these gravimetric and interpolated values of saturation are compared for the runs on both fibers. Run no. 4 of the 1.2-mu fiber was a combination of two separate single point runs in which it was attempted to get independent gravimetric measures of the water content at intermediate saturations. The agreement of these compared values is fairly good. However, complete confidence cannot be placed in the gravimetric values as the water system was not completely sealed with the final capillary pressure at the end of the run. Thus, when the bed was released from compression, it was possible that it picked up some water through the plates.

Special permeability runs on thick beds of both size fibers were made to check the validity of the point value relative permeability curves in Figures 32 and 33. These beds were approximately 5 centimeters thick, and large pressure drops across the bed (5 to 40 g./cm.^{2}) were employed in the permeability measurement. Under these conditions, significant permeability gradients existed across the bed, invalidating the calculation of the overall permeability from average values. Considering an element of these thick

TABLE X

GRAVIMETRIC AND INTERPOLATED VALUES OF SATURATION

Run No.	Gravimetrically Determined Saturation at End of Run	Value of Saturation Interpolated From Capillary Pressure Curve
1	..056	.052
2	.084	.077
3	.091	.087
4	.416-.797	.421-.848
5	.083	.076
6	.090	.086
7	--	.472
8	.534	.564
101	.071	.039
102	.119	.071
103	.190	.169
104	.246	.142
105	.166	.153
106	.183	.170
107	.193	.183
108	.179	.168
109	.158	.160
110	.166	.167
111	.174	.164

beds of differential thickness, dL, having a specific permeability, K_c, the flow rate of water through this element, q, is given by D'Arcy's law:

$$\frac{q}{A} = \frac{K_c}{\mu} \frac{dP_f}{dL} \qquad (22)$$

where dP_f is the differential frictional pressure drop of water flowing across the element. Since the conditions of thin beds and low pressure drops were not used here, Equation (23) does not apply, and it was necessary to use the integral form of Equation (22). Integrating Equation (22) over the entire bed thickness yields

$$\frac{q\mu L}{A} = \int_{P_{f_1}}^{P_{f_2}} K_c \, dP_f, \qquad (48)$$

where P_{f_1} and P_{f_2} are the frictional driving force pressures at the upstream and downstream faces of the bed, respectively. The right hand side of Equation (48) was evaluated from the integral of the point value relative permeability curve and the left hand side was determined experimentally. In evaluating the left hand side of the equation, a procedure similar to that used for the point values of the thin beds, exemplified in Appendix III, was followed. In calculating the right hand side, it was assumed that the distribution of capillary pressure across the bed was linear with the thickness of the bed. The values of capillary pressure at different levels in the bed, then, were corrected for the static gravity head of water in the bed to give a distribution of the frictional drag pressure, P_f, through the bed. The corresponding saturation values were determined from the capillary pressure distribution and these values of saturation were converted

to relative permeability by means of the point value relative permeability curves. These relative permeability values were then changed to specific permeability by multiplying by the saturated permeability. Thus, for each permeability measurement on these thick beds, a distribution of P_f vs. K_c in the bed was determined between the limits of the capillary pressure at each face of the bed. The integral term in Equation (48) was evaluated graphically from a plot of these values. The experimental and calculated results for the special thick bed runs of both size fibers are shown in Table XII. Several experimental difficulties were encountered in these runs as the beds were quite unwieldy and became slightly distorted when they were compressed. Also, extremely long times were required for these systems to reach capillary equilibrium, and the permeability decay may have been significant in these runs. In these special permeability runs, at the high saturations, the frictional pressure drop across the porous plate was abnormally large compared to that across the bed. Because of the high flow rates at these saturations, there was probably significant permeability decay in the plates. For these reasons, the agreement between the calculated and experimental values in Table XI is comparatively poor at the high saturations. At the intermediate and low saturations, however, the values are quite close, particularly in view of the experimental problems encountered. These results confirm the validity of the point value curves and substantiate the contention that capillary flow was the predominant flow mechanism at these saturations. To express this another way, the relative permeability of the medium was independent of the capillary pressure gradient and flow rate and was a function of the medium pore structure and saturation only. Thus, the

applicability of D'Arcy's equation to this system was established and the possible limitations of this equation, turbulence and molecular effects, were shown by implication to be either absent or insignificant. It should

TABLE XI

EXPERIMENTAL AND CALCULATED RESULTS OF THE SPECIAL THICK BED RUNS

1.2-mu Fiber		3.0-mu Fiber	
Experimental	Calculated	Experimental	Calculated
$\frac{g\mu L}{A}$	$\int_{P_{f_1}}^{P_{f_2}} K_c dP_f$	$\frac{g\mu L}{A}$	$\int_{P_{f_1}}^{P_{f_2}} K_c dP_f$
g. x 10^{11}	g. x 10^{11}	g. x 10^{11}	g. x 10^{11}
5091	7845	4448	7375
4812	5049	4438	6110
3031	3946	1927	2126
1610	1930	269.5	252.8
566.0	589.2		
109.4	112.2		
43.34	43.58		

be realized that the relative permeability determined in this work does not necessarily hold for all two fluid-phase systems. Conceivably, the difference in surface tension or angle of contact of different phases could result in significantly different configurations of the liquid and, hence, different permeabilities at equivalent saturations. However, the effects

of these factors in most porous media are probably negligible, as the studies of Wyckoff and Botset (24) and Leverett (28) seem to indicate.

COMPARISON OF RELATIVE PERMEABILITY CURVES OF VARIOUS TWO-PHASE SYSTEMS

A comparison of the relative permeability curves of the glass fiber beds with those of various other media from the literature revealed a marked difference between these systems. The comparison was rather limited since, to this writer's knowledge, only granular type media have been tested for two-phase flow. However, the variations of relative permeability in these media were sufficient to illustrate the qualitative significance of the important variables in two-phase flow. Contrary to Wyckoff and Botset's proposal that all unconsolidated media exhibit the same relative permeability curves, it has been shown that the relative permeability is sensitive to pore structure (23, 30). This was demonstrated experimentally by Brownscombe, et al. (30), on consolidated media. One of Brownscombe's relative permeability graphs is reproduced in Figure 34, and the relative permeability curves of the glass fiber beds from this work are plotted on the same graph. Brownscombe, et al., make the point that as the nonuniformity or "complexity" of the pore structure increases, the permeability curve deviates more from a straight line. Undoubtedly, this complexity of pore structure was considered to be roughly correlated with the geometrical heterogeneity of the solid particles which comprise the medium. This is illustrated by the curves in Figure 34, progressing from the simplest system of a single horizontal capillary tube, in which the flow was simply channel flow (Curve A) (34) through a core of fused alundum particles of uniform

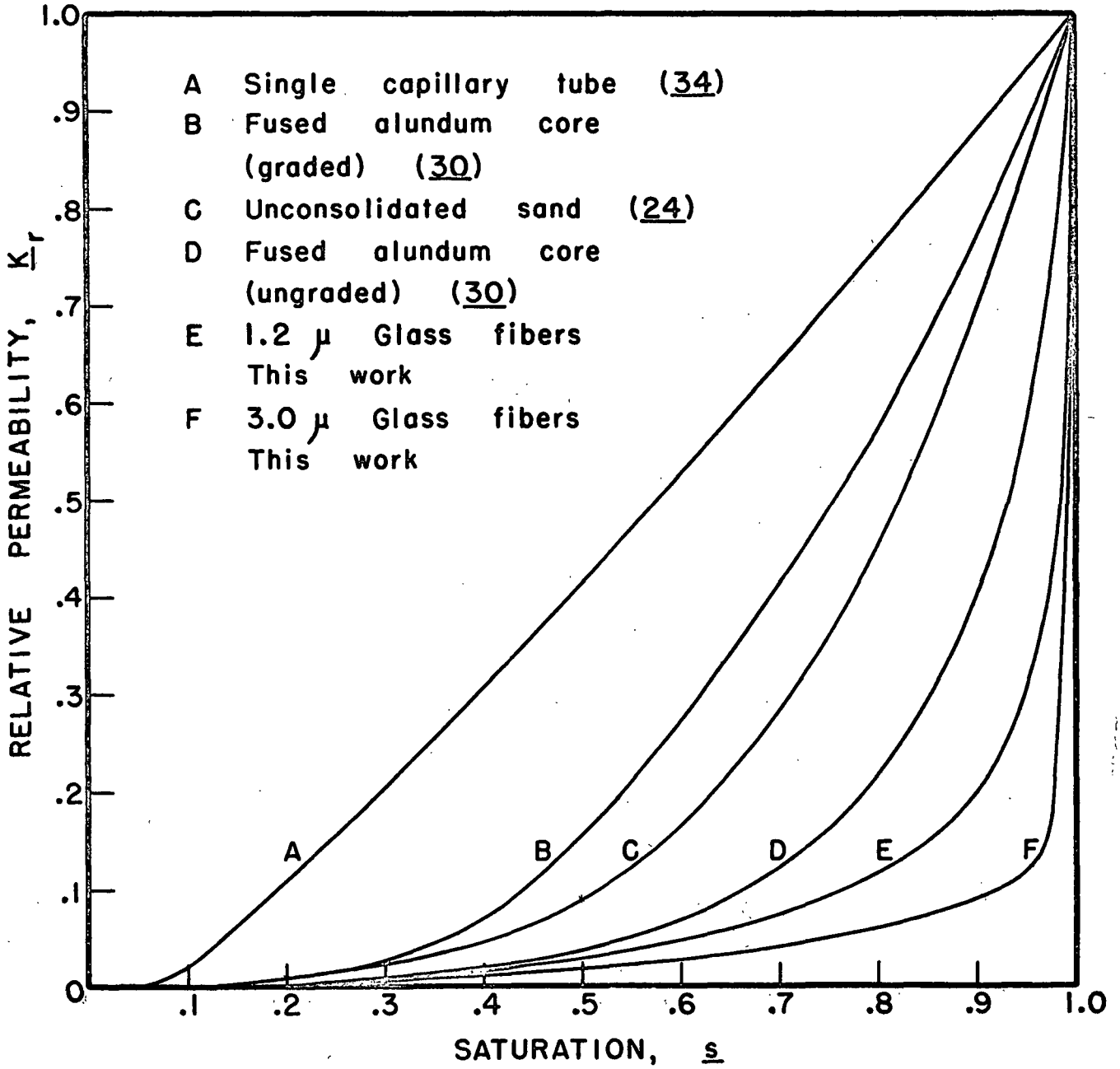

Figure 34. Comparison of Relative Permeability Curves of Different Media

size (Curve B)(30), unconsolidated sands (Curve C)(24), and a fused core of ungraded alundum particles (Curve D)(30). The glass fiber curves, E and F, fall beyond that of the ungraded alundum core, implying that these fiber beds, which are comprised of very regular and uniform particles, paradoxically, have the most complex structure of all. However, the proper analysis and description of this "complexity" is probably involved and complicated. That is, the "complexity" of pore structure manifests itself in more ways than one as far as the relative permeability expression is concerned; and porous media of comparatively uniform particles may give rise to exceedingly complex liquid network configurations at partial saturations. Specifically, the rapid fall off of permeability that accompanies the slight change in saturation of the glass fiber beds at the high saturations was probably due to the change from the regime of total pore saturation to the funicular saturation regime, exemplified in cross section in Figure 35 for the simple case of spherical particles. The pore sizes included in the

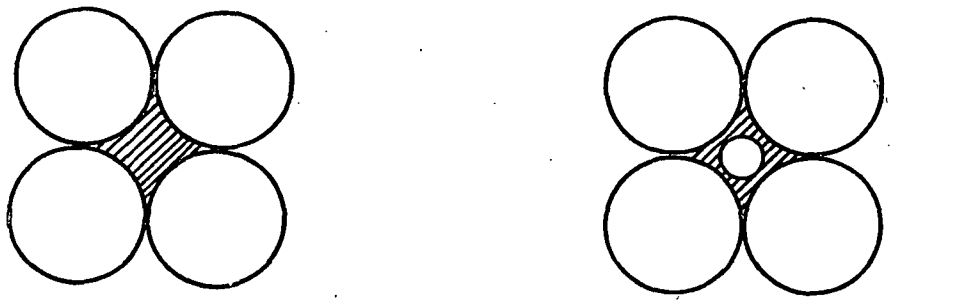

a. Saturation regime b. Funicular regime

Figure 35. Change from Saturation to Funicular Regime of Pore Saturation in Bed of Spherical Particles.

saturation regime are very large, but they do not represent a large volume of

liquid, for the total quantity of water in the pore in the saturation regime, Figure 35a, is distributed over a wide range of pore sizes. Thus, when the saturation regime breaks down to the funicular state, only a relatively small loss of liquid occurs, but the size and shape of the pores which remain filled with liquid undergo a tremendous alteration. This effect is probably exaggerated in naturally high porosity media, such as fiber beds. To illustrate the differences in structure of different porous media with respect to the relationship between pore size and volume of liquid contained in the pores, an analogy can be made between the pores in a medium and the funnels whose cross sections are illustrated in Figure 36. These funnels have the same surface area. When the liquid is drained from these funnels, the curvature of the liquid menisci in both cases follow the same pattern of change, but the volume of liquid which corresponds to any increment of meniscus curvature change is vastly different for the two cases. And the

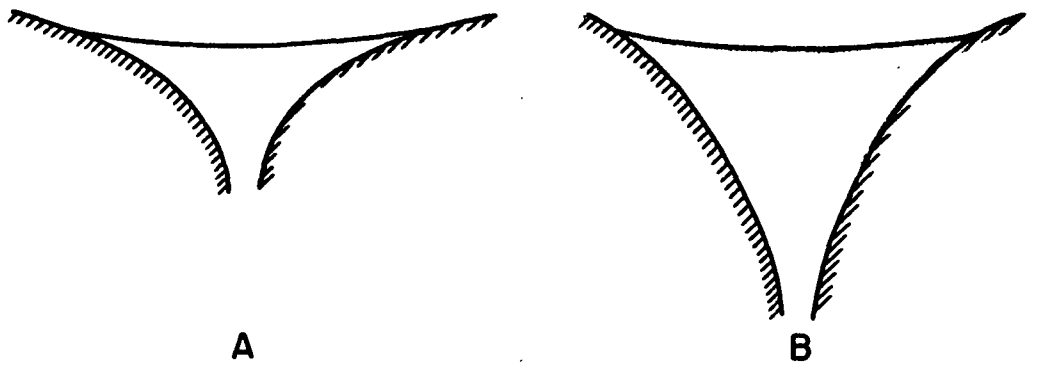

Figure 36. Cross Sections of Differently Shaped Funnels Filled with Liquid

volume corresponding to any particular increment in meniscus curvature can be changed by simply changing the shape of the funnels. This effect of shape

of pores is distinctly different from that of number of pores of a given size, although they cannot be distinguished from the capillary pressure measurements alone for they manifest themselves in the same way in these measurements. However, their effect on permeability is quite different, as a pore corresponding to Figure 36B above would conduct water at a greater rate than a pore corresponding to A, even though both pores had the same "size", i.e., meniscus curvature. Similarly, it is possible for two-phase porous systems to experience large changes in liquid configurations coincident with small changes in liquid volume because of this effect. Thus, the water permeability of the two-phase fiber system was reduced significantly at the slight dewatering occurring at high saturations because of (1) the well-established concept that as pores increase in size, they contribute proportionately more to permeability than to porosity, and (2) the tortuosity of the water channels, which was significantly increased. In some systems, such as granular media, as indicated in the literature, these two factors probably account for practically all of the permeability decrease. However, they only account for part of the reduction in the glass fiber systems and, presumably, in fiber systems in general. A third effect is obviously present in these systems which tends to reduce the liquid permeability even further. This unidentified effect is presumably illustrated by the above analogy and is apparently related to the shape of the pores. In the absence of more fundamental theory, then, this effect was attributed to the shape factors associated with the liquid channel system. This is, essentially, the same argument that was advanced in the section on the development of the Kozeny-Carman equation for two-phase flow, which led to the introduction of the shape factor, C, in the theory. In

short, this argument states that pores of different types of porous media which have the same meniscus curvature of liquid which fills them do not necessarily have the same pore volume to surface ratio. In light of the studies devoted to evaluating the shape factors for various pore shapes and sizes, this seems to be a reasonable explanation.

The variation in pore size has been frequently accounted for in the expression of relative permeability as the integral or summation of the product of the pore size squared and the saturation associated with the pore size from the capillary pressure curve or some equivalent modified form of this product. Thus, the derived equations from several theories of two-phase flow, e.g., Childs and George (23), Wyllie and Spangler (48), Purcell (35), Rapoport and Leas (57), and Gates and Lietz (29) incorporate the pore size distribution in this way and have been moderately successful in practical applications. In this work, the variable pore size term in the derived equation for relative permeability, Equation (42), is $\int_0^{\bar{s}} \bar{m}^2 \, d\bar{s}$. It will be seen later that the difference between the relative permeability curves of the 1.2-mu and 3.0-mu fiber is wholly accounted for by the variation of this term. Thus, the representation of the pore size distribution in this way in the relative permeability expression appears to be generally established. The limitation of this approach is that a knowledge of the distribution of pore sizes corresponding to the residual saturation is not available. However, for most porous systems, the residual saturation represents such a small part of the total pore space that it usually can be ignored. While this relationship may be general for many two-phase systems, it does not necessarily account for the entire variation or "complexity" of

the pore size distribution, as was discussed above. To confirm this, the methods of Childs and George (23) and Wyllie and Spangler (48) for calculating relative permeability curves from the capillary pressure measurements, which were moderately successful in the analysis of two-phase flow in sand beds and consolidated media, were applied to the capillary pressure data of the 3.0-mu fiber beds having a porosity of .919. The empirical constant in Childs and George's equation was chosen so that the calculated and experimental curves agreed at $\underline{s} = 1.0$. In Wyllie and Spangler's calculations, the tortuosity ratio, $\underline{T}/\underline{T}_c$, was assumed to be numerically equivalent to the saturation, $\underline{s}$. These calculated and experimental curves are shown in Figure 37. The calculated curve of Wyllie and Spangler approaches the experimental curve much more closely than that of Childs and George, apparently because of the tortuosity factor introduced by Wyllie and Spangler. However, there is still a large discrepancy between the experimental and Wyllie and Spangler's curves at the intermediate saturations, indicating that there must be other as yet unidentified factors in the general permeability expression of Wyllie and Spangler.

EVALUATION OF THE EMPIRICAL FACTORS FOR THE BEDS OF GLASS FIBERS

If, as it was hypothesized, the empirical factors introduced in the relative permeability equation are the factors that distinguish between different types of porous media, the values of these factors would be the same at any particular saturation in similar media. It follows that these factors should take very nearly equal values for the 1.2-mu and 3.0-mu fiber beds. The composite ratios of the factors, $\underline{k}_o\underline{T}^2\underline{C}^2/\underline{k}_{oc}\underline{T}_c^{\,2}\underline{C}_c^{\,2}$, were evaluated

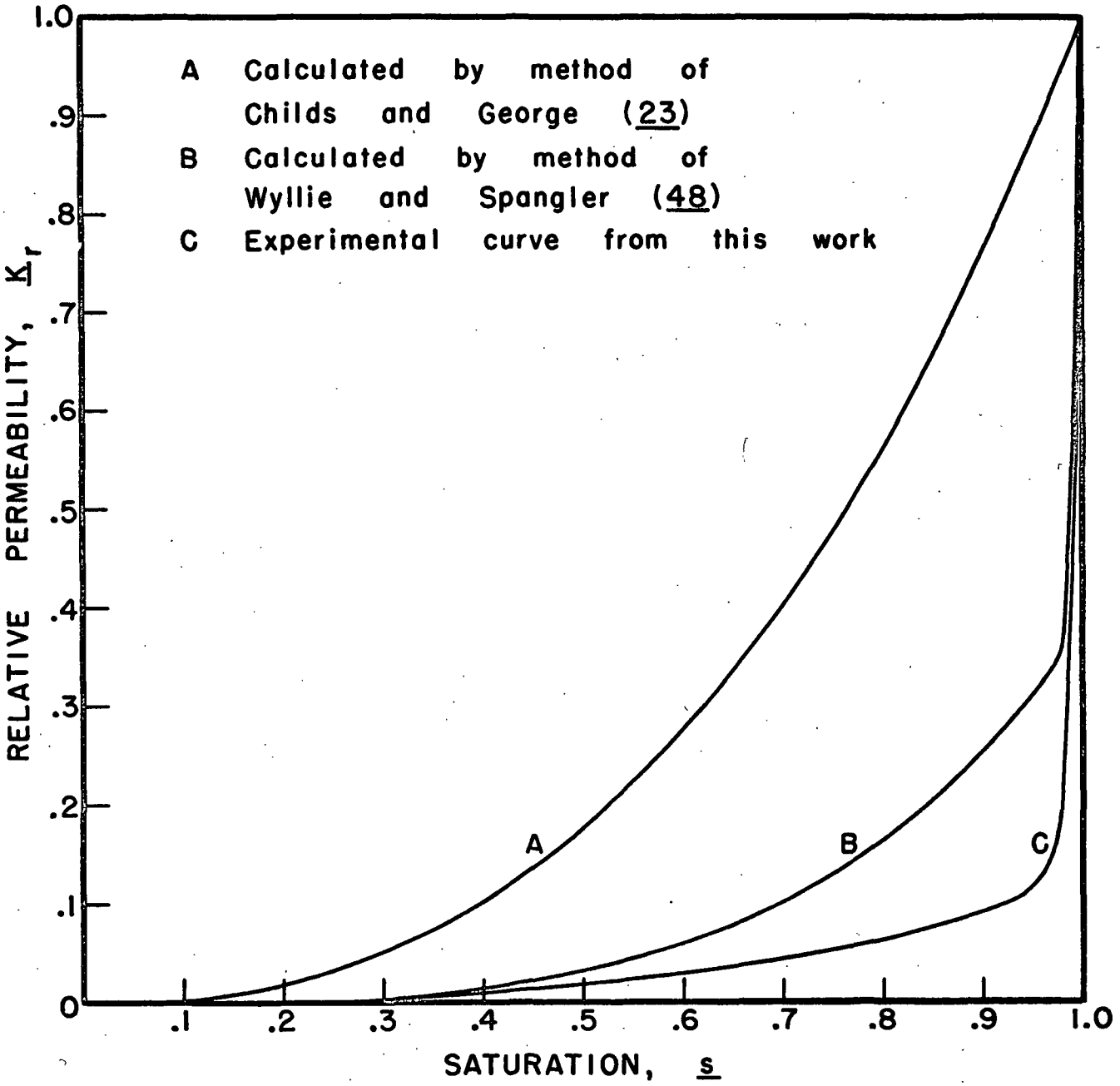

Figure 37. Relative Permeability Curves of 3.0μ Fiber Beds Calculated by Different Methods

as a function of the saturation of these beds from Equation (42). The values of $\underline{K_r}$ and $\int_0^{\underline{s}} \underline{m}^2\ \underline{ds} / \int_0^1 \underline{m}^2\ \underline{ds}$ were evaluated from the experimental relative permeability and pore size distribution, i.e., converted capillary pressure, curves, respectively. In evaluating the integral of the $\underline{m}^2$ vs. $\underline{s}$ curves, it was necessary to fix a limit on the values of $\underline{m}$ at $\underline{s} = 1.0$, for these curves gave the appearance of being asymptotic with the ordinate $\underline{m}^2$ axis. For the 1.2-mu fiber beds, it was assumed that the saturation was complete at a capillary pressure of 2 cm. Hg; for the 3.0-mu fiber beds, the limiting value of $\underline{m}$ was obtained by assuming that the value of the composite empirical factor ratio was .997 at $\underline{s} = .997$. The resulting integral and composite empirical factor ratio values are listed in Table XII, and the composite ratios are plotted in Figure 38.

Within the limits of the experimental measurements and calculations, the two curves in Figure 38 can be considered very nearly the same; so the difference in the relative permeability curves of the two fiber beds is wholly explained by the variations in the integral term of the pore size distribution, $\int_0^{\underline{s}} \underline{m}^2 \underline{ds}$. Thus, this method of analysis is at least internally consistent. The difference, if any, in the absolute values of the factors for the two beds is in the relative magnitude of the values, not their pattern of change with saturation, for the shapes of the ratio curves are the same. It is possible that the magnitude of these factors is fairly sensitive to the total porosity of the bed. These empirical factor ratios appear to be a complex function of the pore structure and saturation of the media, and it is not possible to separate the composite values into their separate components rigorously without additional information.

TABLE XII

CALCULATED INTEGRALS AND COMPOSITE EMPIRICAL FACTORS

	1.2-mu Fiber		3.0-mu Fiber	
$\underline{s}$	$\int_0^{\underline{s}} \underline{m}^2 d\underline{s}$, cm.^{2} x 10^8	$\underline{k}_o\underline{T}^2\underline{C}^2/\underline{k}_{oc}\underline{T}_c^{\,2}\underline{C}_c^{\,2}$	$\int_0^{\underline{s}} \underline{m}^2 d\underline{s}$, cm.^{2} x 10^8	$\underline{k}_o\underline{T}^2\underline{C}^2/\underline{k}_{oc}\underline{T}_c^{\,2}\underline{C}_c^{\,2}$
.1	.288	.0141	1.333	.0240
.2	.938	.0478	3.893	.0705
.3	1.771	.0790	7.170	.107
.4	2.772	.102	10.966	.131
.5	3.939	.126	15.194	.146
.6	5.290	.151	19.826	.166
.7	6.869	.180	24.909	.194
.8	8.771	.224	30.605	.231
.9	11.286	.302	37.198	.283
.94	12.605	.364	40.252	.322
.98	14.261	.499	44.509	.574
.99	14.788	.619	64.209	.737
1.00	16.785	1.00	118.320	1.00

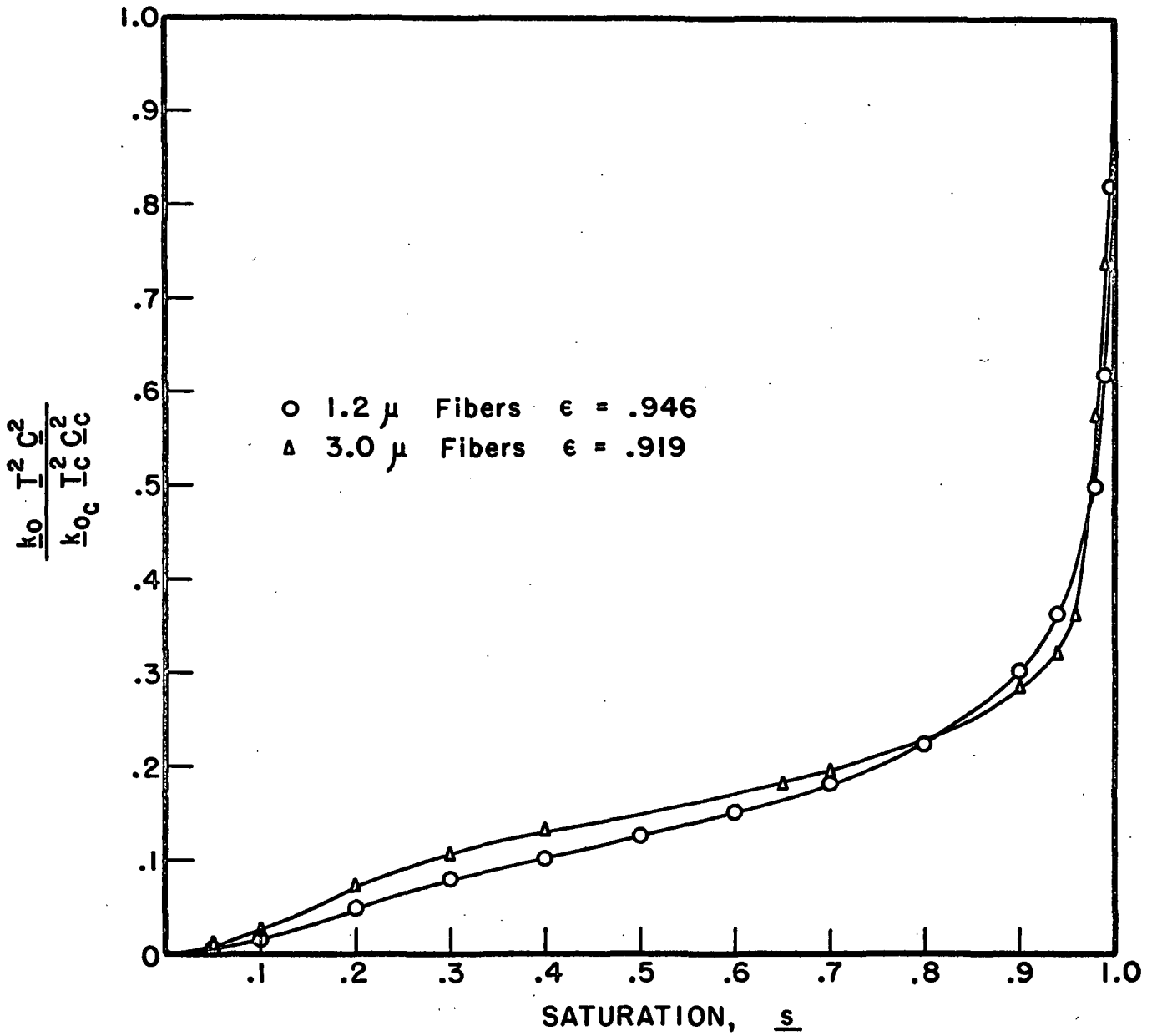

Figure 38. Calculated Empirical Constants of the Glass Fiber Beds

ANALYSIS OF THE EMPIRICAL FACTORS

Qualitatively, the rapid fall off in relative permeability of the glass fiber beds as the saturation decreased has been attributed to three effects: (1) the decrease in size of pores which remained filled with water, (2) the increase in tortuosity of the liquid-filled channels, and (3) the variation in shape factors associated with the liquid channel network. The quantitative significance of the first effect has been demonstrated, but the other two effects have not been quantitatively defined for fibrous systems and to do so requires either (1) a basic understanding of the physical meaning of these factors or (2) specific knowledge of the variation of these factors, empirically, with saturation in fiber systems. At the present time, neither of these requirements can be met, at least not rigorously. However, a reasonable but speculative solution to this problem suggests itself when the experimental data is analyzed by Wyllie and Spangler's method (48). As discussed in the historical review, Wyllie and Spangler proposed that the tortuosity ratio of a partially saturated system, $\underline{T}_c/\underline{T}$, is defined by Equation (10) from electrical resistivity measurements:

$$\underline{I} = \frac{\underline{F}_c}{\underline{F}} = \frac{\underline{T}_c}{\underline{T}} \frac{1}{\underline{s}}. \qquad (10)$$

They also suggested that the resistivity index, $\underline{I}$, conforms, for many porous media, to the equation,

$$\underline{I} = \underline{s}^{-\underline{n}}, \qquad (11)$$

where $\underline{n} \simeq 2.0$ for unconsolidated media. They tested their theory against the experimental data for consolidated systems from Gates and Lietz (29) by calculating a resistivity index from the relative permeability and capillary

pressure data using Equation (21). They obtained a mild confirmation of their theory, as the calculated values of log I were approximately linear with log s, having slopes of nearly the same value as determined by electrical resistivity measurement. They maintained that the electrical and hydraulic tortuosities were equivalent.

The same analysis was performed on the experimental data of the glass fiber systems from this work. From Equation (42), assuming $k_o C^2 / k_{oc} C_c^2 = 1$, the tortuosity ratio, T_c/T, was calculated as it varied with saturation. Dividing this ratio by the saturation value, the resistivity index was obtained according to Equation (10). These calculations were carried out for the 1.2-mu fiber beds of .946 porosity and for the 3.0-mu fiber beds of .919 porosity. The results of these calculations are plotted in Figures 39 and 40. These calculated resistivity index curves for the two different fibers deviated from linearity in the same way. It is interesting to note that the resistivity index curves calculated from Gates and Lietz's data for consolidated systems by Wyllie and Spangler (48) were similar in shape to these curves as shown in Figure 41. But they do not have such extreme slopes at the high saturations. Even Wyllie and Spangler admit that the slopes of the curves from Gates and Lietz's data were not independent of saturation in all cases. In attempting to explain the deviation of these curves from linearity, they suggested that true capillary equilibrium possibly was not attained. This is hardly plausible, however, since nonequilibrium conditions were very unlikely to occur at high saturations, and the nonequilibrium experimental data would fall above the capillary equilibrium line, not below it. Of course, the possibility remains that the

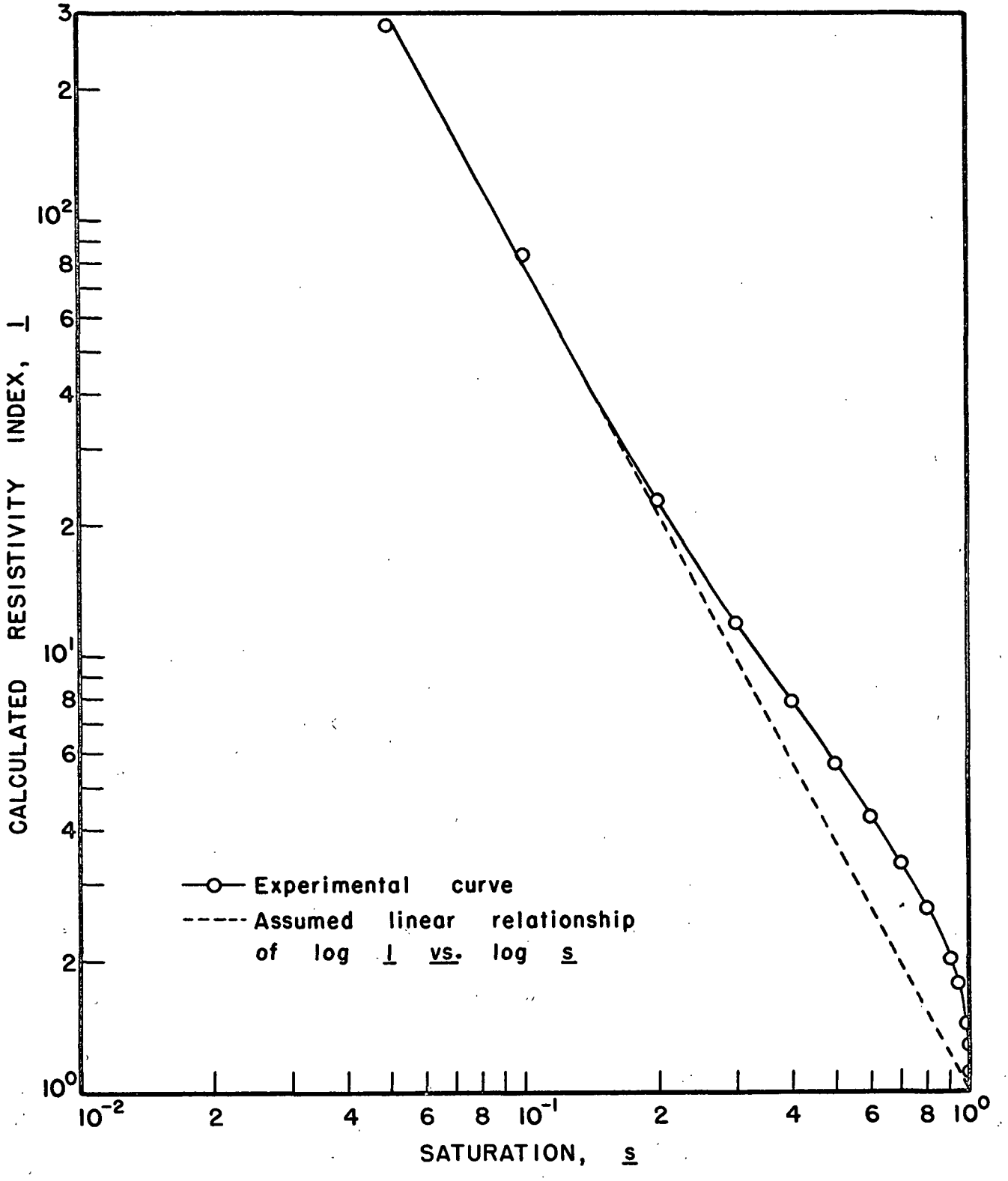

Figure 39. Resistivity Index Calculated From Experimental Data of 1.2μ Fibers

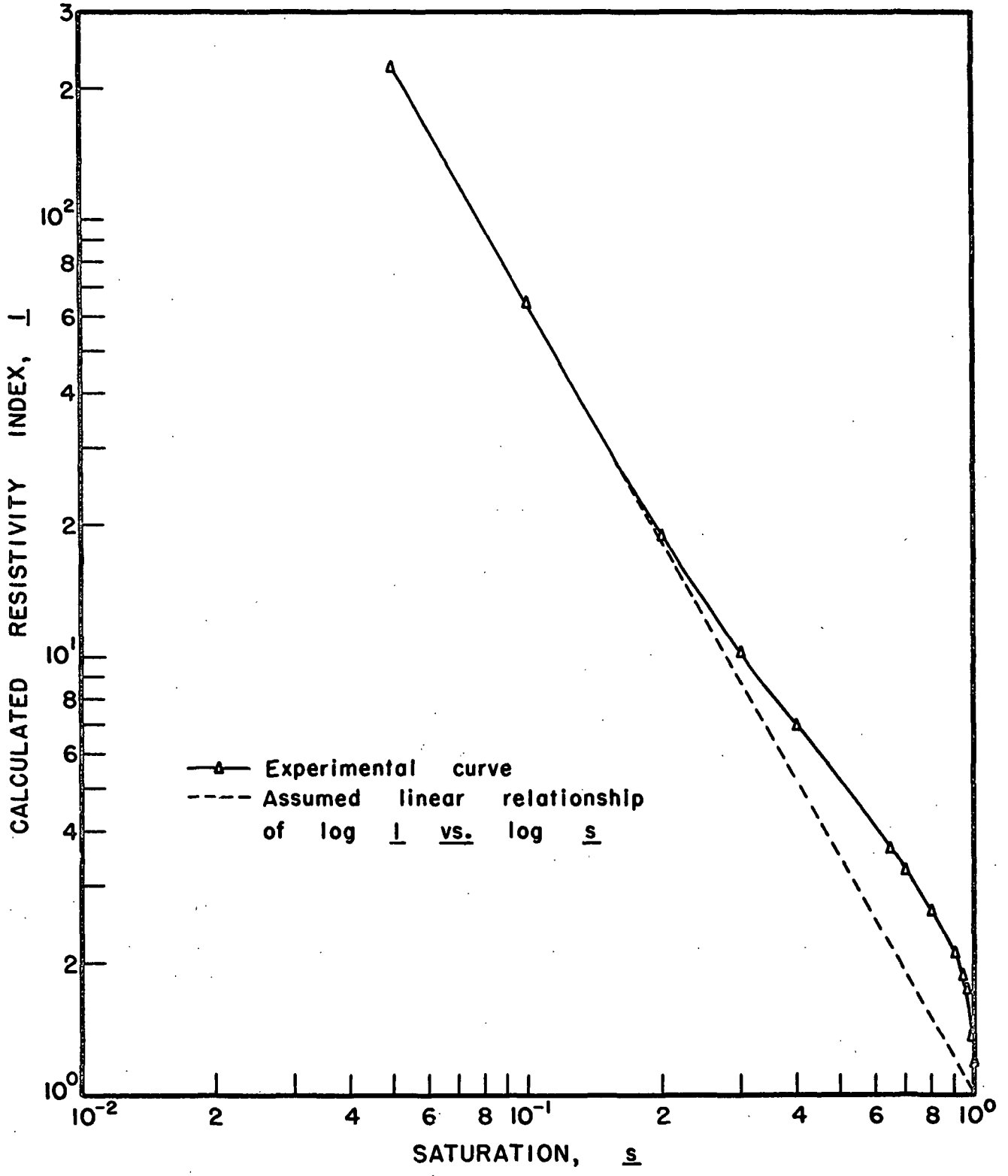

Figure 40. Resistivity Index Calculated From Experimental Data of 3.0μ Fibers

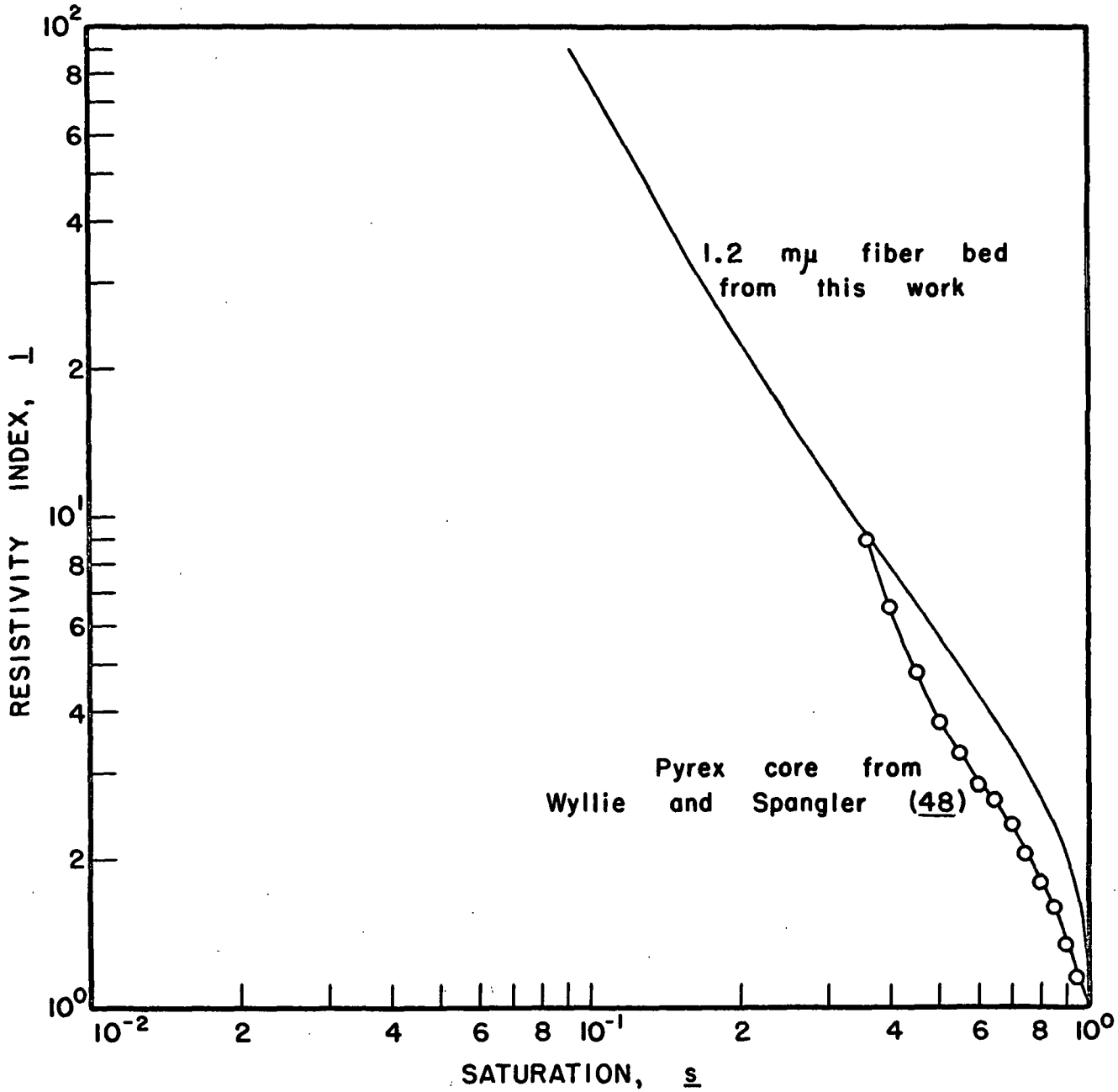

Figure 41. Comparison of the Calculated Resistivity Index Curves for a Pyrex Core and a Glass Fiber Bed

electrical and hydraulic tortuosities are not equivalent. In any case, there should be little doubt that the variation of the calculated log $\underline{I}$ - log $\underline{s}$ curves for the glass fiber beds from linearity was a true effect.

Both of the calculated curves in Figures 39 and 40 approach and become integral with a straight line passing through the point $\underline{s} = 1.0$, $\underline{I} = 1.0$ at the low saturations. The slopes of these lines, (the broken lines in Figures 39 and 40) are -1.90 for the 1.2-mu fiber and -1.80 for the 3.0-mu fiber, not much different from the value of -2.0 proposed by Wyllie and Spangler for unconsolidated media. This similarity suggests that these broken lines may be a reasonable approximation of the actual log $\underline{I}$ *vs.* log $\underline{s}$ relationship in the fiber beds. On the basis of Wyllie and Spangler's observations, therefore, it was assumed that the resistivity index, which is a measure of the tortuosity ratio, varied with the saturation in the fiber beds in accordance with the broken lines in Figures 39 and 40. Evaluating the tortuosity ratio, $\underline{T_c}/\underline{T}$, from this assumed linear variation of the resistivity index, the values of the quantity, $\underline{k_o C^2}/\underline{k_{oc} C_c^2}$ were calculated by means of Equation (42). These values are tabulated in Table XIII. This analysis continues to exhibit a high degree of internal consistency as the shape factor ratios shown in this table are very nearly the same for the two different size fibers.

At this stage of the analysis, the separation of the composite term, $\underline{k_o C^2}/\underline{k_{oc} C_c^2}$, into its separate components is open to criticism, particularly since the values of this term in Table XIII were based on the dubious assumption of linearity of the logarithmic resistivity index-saturation plot.

TABLE XIII

CALCULATED VALUES OF THE COMPOSITE SHAPE FACTORS RATIO

Saturation, $\underline{s}$	1.2-mu Fiber, $\epsilon = .946$ $\underline{k_o C^2}/\underline{k_{oc} C_c^2}$	3.0-mu Fiber, $\epsilon = .919$ $\underline{k_o C^2}/\underline{k_{oc} C_c^2}$
.05	1.049	1.00
.1	.906	.952
.2	.892	.938
.3	.725	.738
.4	.544	.567
.5	.450	.437
.6	.389	.374
.7	.346	.343
.8	.335	.333
.9	.364	.343
.94	.407	.354
.98	.513	.597
.99	.631	.752
1.00	1.00	1.00

However, in the absence of a rigorous approach, this speculative method appeared to be the most promising. As seen from Table XIII, the composite shape factor term passed through a minimum at $\underline{s} = 0.8$. Qualitatively, since it was highly improbable that either of these factors would reverse their direction of variation, both $\underline{k}_o/\underline{k}_{o_c}$ and $\underline{C}^2/\underline{C}_c^2$ probably started to vary simultaneously from their initial value of 1.0 at $\underline{s} = 1.0$ when the saturation began to decrease, but in opposite directions and at different rates. Thus, the change of one of these factors was initially predominant, but as the desaturation progressed, the other factor became more and more important and eventually overshadowed the first. Finally, they both reached constant values such that $\underline{k}_o\underline{C}^2/\underline{k}_{o_c}\underline{C}_c^2$ equalled unity. Possibly, in granular media, where the log $\underline{I}$ vs. log $\underline{s}$ plot yields a straight line over the entire range of saturations, these factors vary in such a way as to exactly compensate each other. As discussed earlier, the experimental data of Gates and Lietz yielded a log $\underline{I}$ — log $\underline{s}$ curve which was S-shaped. This nonlinearity could be accounted for by the nonexact compensation of the two variable shape factor ratios. In the glass fiber beds, this nonexact compensation was simply more pronounced.

A rough speculative estimate of the quantitative variation of the individual ratios, $\underline{k}_o/\underline{k}_{o_c}$ and $\underline{C}^2/\underline{C}_c^2$, was obtained by means of Equations (43) and (44). These are independent equations of the same liquid-solid contact surface area, involving the $\underline{k}_o$ factor in one and the $\underline{C}$ factor in the other. Hence, any combination of $\underline{k}_o/\underline{k}_{o_c}$ and $\underline{C}^2/\underline{C}_c^2$ that satisfies the composite value in Table XIII must also yield the same surface areas calculated from Equations (43) and (44). It must not be supposed, however, that

these equations provide for a unique solution of the shape factors; for the composite term, $\underline{k}_o\underline{C}^2/\underline{k}_o\,\underline{C}_c\,\underline{C}_c^{\,2}$ was derived from a combination of Equations (43) and (44). Consequently, any combination of shape factor values which yielded the same surface area values from Equations (43) and (44) would necessarily yield the composite value given in Table XIII, within the limits of experimental error, of course. In short, there were three unknowns and only two equations. To solve for these factors, uniquely, it was necessary to know some other limiting condition.

A semiquantitative solution to this problem was effected by assuming a distribution of the liquid-solid contact surface areas with saturation and calculating the shape factor values from Equation (43) and (44). The use of Equation (44) involved the graphical integration of the $1/\underline{m}$ vs. $\underline{s}$ curve. As this curve gave the appearance of being asymptotic to the $1/\underline{m}$ axis, it was impossible to accurately integrate this curve between saturations of zero and .028 for the 1.2-mu fiber beds and zero and .015 for the 3.0-mu fiber beds. Therefore, values of the integrals of these portions of the curves were arbitrarily assumed. The values of these integrations are given in Table XIV. Further, an independent value of $\underline{S}_o$ was required for this solution. Thus, for the 1.2-mu fiber beds, the value of $\underline{S}_o$ was taken as that determined from microscopic measurements, viz., 1580 $cm.^2/cc.$, whereas for the 3.0-mu fiber beds, the average value determined from saturated permeability measurements was used, 920 $cm.^2/cc.$ Obviously, the liquid-solid contact area must decrease as the saturation decreases, so, as a crude approximation, the surface area term, $\underline{S}_c$, was assumed to be linearly proportional to the saturation, i.e., $\underline{S}_c/\underline{S}_o = \underline{s}$. Of course, more realistic

TABLE XIV

GRAPHICAL INTEGRATION VALUES OF THE $1/\underline{m}$ vs. $\underline{s}$ CURVES

Saturation, $\underline{s}$	1.2-mu Fiber $\int_0^{\underline{s}} 1/\underline{m}\ d\underline{s}$ cm.$^{-1}$	3.0-mu Fiber $\int_0^{\underline{s}} 1/\underline{m}\ d\underline{s}$ cm.$^{-1}$
.05	412.4	2064
.10	650.4	3238
.20	1045	5216
.30	1393	6969
.40	1710	8592
.50	2003	10127
.60	2276	11598
.70	2528	13003
.80	2757	14335
.90	2958	15572
.94	3027	16029
.98	3090	16423
.99	3103	16489
1.00	3110	16514

distributions could have been assumed, but they would have been considerably more complex. The object of this analysis was not to speculate on the exact values of the shape factors, but rather to determine the direction in which they varied and the order of magnitude of their variation. For this purpose, the assumed linear distribution was adequate. Under these conditions, then, the calculated values of the shape factor ratios are listed in Table XV.

The composite products of these calculated ratios are not in close numerical agreement with those in Table XIII; however, they do reach a minimum at the same saturation and follow the same variation pattern with the saturation. Further, the variations of both factors are the same for the two fiber sizes. The ratio, $\underline{k}_o/\underline{k}_{o_{\underline{c}}}$, falls off very rapidly as the saturation drops below 100% and reaches a constant value which it maintains at about $\underline{s} = 0.8$. The ratio, $\underline{C}^2/\underline{C}_{\underline{c}}^2$, experiences a moderate and regular increase as the saturation decreases over the major part of the saturation range. The direction of change of these shape factor ratios is just opposite to that expected from related investigations. Studies by Carman (2) and Emersleben (40) indicated that the $\underline{k}_o$ shape factors would take small values for pores having angular, slitlike cross sections. Hence, in partially saturated media, the $\underline{k}_{o_{\underline{c}}}$ term would be expected to decrease and the ratio, $\underline{k}_o/\underline{k}_{o_{\underline{c}}}$, to increase. The $\underline{C}_{\underline{c}}$ term, on the other hand, is analogous to the ratio of surface to volume shape factors used to characterize solid particles. Herdan (64) demonstrated that this ratio increased as the heterogeneity and angularity of the particles increased. By analogy, the value of $\underline{C}_{\underline{c}}$, which applies to the liquid-filled pore space would be expected to increase as the saturation decreased and the ratio, $\underline{C}^2/\underline{C}_{\underline{c}}^2$, to decrease.

TABLE XV

CALCULATED SHAPE FACTOR RATIOS

Saturation, $\underline{s}$	1.2-mu Fiber			3.0-mu Fiber		
	$\underline{k_o}/\underline{k_{o_c}}$	$\underline{C}^2/\underline{C_c}^2$	$\underline{k_o C}^2/\underline{k_{o_c} C_c}^2$	$\underline{k_o}/\underline{k_{o_c}}$	$\underline{C}^2/\underline{C_c}^2$	$\underline{k_o C}^2/\underline{k_{o_c} C_c}^2$
.10	.155	4.41	.684	.108	3.84	.415
.20	.250	2.86	.715	.153	2.50	.303
.30	.256	2.22	.568	.150	1.99	.299
.40	.226	1.90	.429	.130	1.69	.220
.50	.211	1.66	.350	.113	1.51	.171
.60	.202	1.49	.301	.105	1.37	.144
.70	.202	1.35	.273	.104	1.25	.130
.80	.219	1.23	.269	.108	1.19	.129
.90	.271	1.12	.304	.120	1.10	.132
.94	.328	1.08	.354	.129	1.06	.137
.99	.506	1.02	.577	.411	1.02	.419
1.00	1.00	1.00	1.00	1.00	1.00	1.00

Little can be said to reconcile this nonconformity of the shape factor variations, but since the directions of change of both factors were consistent with each other, it possibly is a true effect.

A slight refinement of the above analysis is afforded by the following procedure. Combining Equations (42), (43), and (44), it is easily shown that:

$$\frac{\int_0^{\underline{s}} \underline{ds/m}}{\int_0^1 \underline{ds/m}} = \underline{s}^{3/2} \sqrt{\frac{\int_0^1 \underline{m}^2 \underline{ds}}{\int_0^{\underline{s}} \underline{m}^2 \underline{ds}}}. \qquad (49)$$

This equation provides a means to more or less accurately evaluate the integrals of the $\underline{m}^2$ vs. $\underline{s}$ and $1/\underline{m}$ vs. $\underline{s}$ curves. By a trial and error technique, the optimum integral values of the steep indeterminate portions of the curves were obtained such that Equation (49) was satisfied at all saturations with the same numerical value of $\int_0^1 \underline{m}^2 \underline{ds}$. The cause of disagreement between the calculated values of the composite term, $\underline{k}_o \underline{c}^2 / \underline{k}_{o_{\underline{c}}} \underline{c}_{\underline{c}}^2$, in Table XV and those in Table XIII was probably the inaccuracy of the graphical integrations involved. With the revised integrals, this disagreement should be significantly reduced. Thus, carrying through the analysis in the same way as before, using the revised integral values, slightly different resistivity index-saturation logarithmic curves were obtained. These revised curves led to very small changes in the magnitude of the previously calculated composite shape factor ratios, but their basic pattern of variation was unchanged. Assuming a linear distribution of the frictional drag surface area with the saturation as before, the individual

variations of $\underline{k_o}/\underline{k_{o_c}}$ and $\underline{C}^2/\underline{C_c}^2$ were calculated as shown in Table XVI. Comparing these revised values with those in Table XV, it was apparent that the revision had little effect on the shape factor variations. The same conclusions hold for these shape factor ratios as for those listed in Table XV.

TABLE XVI

REVISED INDIVIDUAL SHAPE FACTOR RATIOS

Saturation, $\underline{s}$	1.2-mu Fiber			3.0-mu Fiber		
	$\underline{k_o}/\underline{k_{o_c}}$	$\underline{C}^2/\underline{C_c}^2$	$\underline{k_o C}^2/\underline{k_{o_c} C_c}^2$	$\underline{k_o}/\underline{k_{o_c}}$	$\underline{C}^2/\underline{C_c}^2$	$\underline{k_o C}^2/\underline{k_{o_c} C_c}^2$
.10	.201	4.58	.921	.270	3.28	.886
.20	.296	2.89	.855	.276	2.31	.638
.30	.280	2.25	.630	.231	1.88	.434
.40	.248	1.90	.471	.186	1.04	.305
.50	.228	1.66	.378	.147	1.46	.215
.60	.214	1.49	.319	.127	1.35	.171
.70	.213	1.35	.288	.118	1.25	.148
.80	.228	1.23	.280	.116	1.17	.136
.90	.277	1.12	.310	.121	1.10	.133
.94	.325	1.06	.345	.131	1.06	.139
.98	.450	1.02	.459	.229	1.02	.234
1.00	1.00	1.00	1.00	1.00	1.00	1.00

MECHANISM OF LIQUID FLOW IN PARTIALLY SATURATED POROUS MEDIA

On the basis of this and other investigations of two-phase systems, a mechanism of liquid flow in such systems is postulated, and a semiempirical expression of liquid relative permeability is proposed. This mechanism is limited, rigorously, to the comparatively simple systems of isothermal, incompressible, homogeneous, macroporous media having hydraulically smooth surfaces, a liquid wetting phase, and a gaseous nonwetting phase. The partially saturated glass fiber beds in this work are examples of such systems.

In these two-phase systems, the wetting phase distributes itself uniformly in the smallest pores, or capillaries, of the medium in conformance with the laws of surface tension and capillarity. At static capillary equilibrium, the menisci of the capillary-held liquid have the same curvature at all points in the system. The radius of curvature, of course, is dependent upon the capillary pressure, surface tension, and contact angle of the liquid according to the familiar capillary equation, $\underline{r} = (2\gamma \cos \theta)/\underline{P_c}$. Thus, a void space in a porous medium, initially saturated with the liquid wetting phase, passes through three successive states of saturation as the medium is progressively desaturated:

(1) In the <u>saturation</u> regime, the space is completely filled with liquid.

(2) In the <u>funicular</u> regime, gas has permeated the void space, displacing part of the liquid. The remaining liquid forms a continuous network of channels in the smallest pore spaces. The

distribution of the liquid and gas phases is fixed at capillary equilibrium for each particular saturation.

(3) In the pendular regime, the volume of liquid in the void space has been reduced to such an extent that the continuity of the liquid channels has been destroyed, and the liquid is retained in small isolated pockets. This regime is also referred to as the residual saturation.

In real porous systems, these three regimes overlap to some extent, so at some saturations more than one of them may be in effect. A rigorous separation of the saturation into components, then, corresponding to each regime is unlikely. However, in the theory of relative permeability, it is an apparently good approximation to assume that the breakdown of the funicular to the pendular state occurs simultaneously in all the liquid channels. That is, none of the liquid is removed from the flow system before the residual or pendular saturations. Furthermore, it is assumed that no pore spaces are sealed off and the entire liquid saturation is available for flow. In the glass fiber beds, the pendular regime occurred at a saturation of about 2%. In sand beds, it occurs at about 10% saturation, and in sandstone, at saturations greater than 30%. Characteristic of real porous systems is a hysteresis effect, manifest in the different liquid distributions at the same capillary equilibrium saturation, depending on whether it was reached by desorption or absorption. In this analysis, only the desorption phase is considered.

At saturations greater than residual, the flow of liquid occurs

predominantly as channel flow through the interconnected liquid-filled capillary system. At the residual saturation, of course, the discontinuity of the liquid channels precludes any liquid flow. Under the condition of streamline flow, the frictional drag exerted on the flowing liquid at the surface of the solid medium comprises the total resistance to flow. In the absence of a condensed film at the liquid-gas interfaces, the frictional drag at these surfaces is negligible. For this reason, the state of motion of the gaseous phase has no appreciable effect on the permeability to the liquid phase. The fluid pressure gradients in the flowing liquid tend to distort the distribution of liquid from a static capillary equilibrium to a dynamic equilibrium. However, under normal operating conditions, this distortion is negligible and the dynamic and static equilibrium distributions are, for most practical purposes, equivalent. This flow of liquid in stable, well-defined capillary channels is termed parallel, or capillary, flow, and the specific permeability of the porous medium for this type of flow is defined by D'Arcy's law. Molecular effects, such as diffusion, slippage, adsorption, etc., which impose limitations on D'Arcy's law, are either absent or of little consequence in most capillary flow systems.

In these two-phase systems, as D'Arcy's law implies, the liquid relative permeability is independent of the liquid flow rate and pressure gradient. It is readily seen, then, that the permeability is characterized by the configuration of the liquid flow channels, and this configuration is obviously sensitive to the basic pore structure of the medium and the saturation. Exactly what is implied by the term, pore structure, is not completely known now; however, it must include total porosity, pore size

distribution, and those variables which govern the shape of the pores. Among these variables are possibly particle shape and orientation and uniformity of the particle sizes. That the permeability is a function only of the pore structure and saturation of the medium is stated with some reservation, for it is possible that the surface tension may have some effect on the liquid distribution and, hence, the liquid permeability. However, if there is an effect due to this fluid property, it is probably small and can be safely ignored.

In attempting a quantitative description of the relative permeability, the geometrical complexity of the two-phase systems inhibits a fundamental and rigorous evaluation of the channel configuration on a microscopic plane. In lieu of a microscopic analysis, then, a less fundamental but practical analysis of the relative permeability has been developed by considering the macroscopic structure. Direct measurement of the relative permeability of various systems revealed several facts about two-phase flow which are almost intuitively evident: The presence of a second phase greatly decreases the permeability to the first phase and also the permeability to the mixture; the permeability is quite sensitive to the total porosity and pore size distribution; uniform particle shapes and sizes do not necessarily produce a simple uniform pore structure; and the differences in relative permeability of different systems are not always wholly explained by the differences in porosity and pore size distribution. The liquid permeability of the two-phase systems was evaluated by D'Arcy's equation experimentally, and a general expression of the liquid relative permeability was derived from the Kozeny-Carman equation modified for two-phase systems.

It is an inherent limitation of this analysis that the pore space is characterized and not the solid medium. A more fundamental treatment would relate the relative permeability to the fundamental properties of the solid medium. For this reason it is important to know the relationship between the properties of the solid medium and the pore space. Thus, the variation in relative permeability as the saturation decreased was attributed to three principal effects of the pore structure and saturation combination:

1. Pore size distribution. It is a well-known concept that as pores increase in size, they contribute proportionately more to permeability than to porosity. But this effect is not necessarily the same for all pores of the same effective size and may be exaggerated or attenuated, depending on the surface-volume shape factors associated with the pores. Thus, in the initial stages of desaturation of a porous medium, a small loss in saturation results in a considerable decrease in permeability. The explanation probably lies in the change from the regime of complete saturation to the funicular regime accompanying this saturation loss. In the Kozeny-Carman equation, a pore size, m, is introduced as the mean hydraulic radius, which is equivalent to the ratio of volume to surface of the pores. An independent evaluation of this mean hydraulic radius is presumably obtained from static capillary pressure measurements, or effective pore size distribution measurements. However, the capillary pressure is actually a measurement of the radius of curvature of liquid menisci in the system. In relating the volume to surface ratio of the pores in the Kozeny-Carman equation to the capillary pressure mean hydraulic radius (or radius of menisci curvature), then, it was necessary to introduce a factor of proportionality, C_c, between them. This

factor is a function of the pore shape and is discussed below. The final form which the variable mean hydraulic radius takes in the relative permeability expression is the integral of the radius squared times the cumulative saturation corresponding to the radius from the capillary pressure curve, viz., $\underline{m^2 ds}$. As this or some ramification of this form of the pore size distribution has been successfully applied in the expression of relative permeability for many different types of porous media, it probably holds for porous systems in general.

2. Tortuosity. The qualitative physical significance of the tortuosity is easily grasped; and as a porous medium is desaturated, it is obvious that the average tortuosity of the liquid channels increases. However, the geometrical complexity of the liquid network, dividing, rejoining, and passing through continuously varying sizes of pores renders a rigorous quantitative description of the tortuosity virtually impossible. From empirical studies, it has been suggested that the tortuosity varies reciprocally with the saturation for unconsolidated media and as some negative power of the saturation for consolidated media. This has been supported with some modest experimental evidence. Whether there is a general direct relationship between the tortuosity and the saturation has yet to be proved conclusively, but in the absence of a better theory, this relation appears to be approximately correct and, hence, is practically useful.

3. Shape factors. Two shape factors are alluded to here. One has already been mentioned as the proportionality factor between the capillary pressure mean hydraulic radius and the ratio, volume to surface of the pore.

By surface of the pore is meant the surface of the liquid-solid contact at which frictional drag is exerted on the flowing liquid. As the liquid is held in extremely complicated configurations, the calculated radii of the pores in which the liquid is contained do not have the same simple physical significance as the radius of a cylinder. It is necessary, therefore, to introduce an empirical factor which will convert the hypothetical pore radius, i.e., the radius of meniscus curvature, to the physically real volume to surface ratio of the liquid which corresponds to this radius. This factor is designated as C_c at saturation s and is, presumably, a function of the over-all saturation just as the tortuosity is. It is reasonable to expect this factor to be characteristic of the different particle shapes and orientations, and should take similar values for similar shaped pore spaces. The other factor is the Kozeny shape factor which has little physical meaning associated with it. Both of these shape factors apply to the geometrically complex liquid channel system and it appears that they can be evaluated only by extensive empirical investigations. Very little information is available concerning the variation of these factors with saturation; however, in this investigation of glass fiber beds, a speculative analysis revealed that they both apparently start to vary in opposite directions and at different rates immediately as the saturation is reduced below unity. The Kozeny shape factor, k_{o_c}, increased, and the C_c factor decreased as the saturation was lowered. It is these shape factors which distinguish between geometrically unlike systems such as granular and fibrous media.

Thus, the final expression of liquid relative permeability is

$$\underline{K_r} = \frac{\underline{k_o T^2 C^2} \int_o^{\underline{s}} \underline{m^2 ds}}{\underline{k_{o_c} T_c^2 C_c^2} \int_o^1 \underline{m^2 ds}} .$$

The above analysis of the relative permeability mechanism is postulated for thick beds only. In thin beds having the same gross characteristics, the statistical arrangement of pore sizes might be so limited that the bed does not behave as a homogeneous medium. Consequently, the over-all distribution of wetting and nonwetting phases may be significantly affected, and, hence, the permeability will be altered.

Although the Kozeny method produces a useful working theory of two-phase flow, it is severely limited in its capacity to analyze the fundamental mechanism of this process, and the basic theoretical advances which are possible by this method have seemingly been exhausted. It follows, therefore, that a new and more fundamental theory is needed for an increased understanding of the basic two-phase flow mechanism.

SUMMARY AND CONCLUSIONS

An investigation of two-phase flow in fibrous media was carried out under the following idealized conditions:

1. The experimental systems were comprised of incompressible beds of glass fibers as the porous medium, pure demineralized water as the liquid wetting phase, and air as the gaseous nonwetting phase. Incompressible, as used here, refers to beds which had been externally compacted to such an extent that they were not further compacted by the action of the flowing liquid drag resistance or the surface tension effect.

2. Approximate isothermal conditions were maintained experimentally.

3. The permeability of the fiber beds to the liquid wetting phase only was studied; the air phase was always stationary in the system.

Apparatus and techniques were developed to measure (1) the static equilibrium saturation, i.e., the fractional volume of the void space which is filled with water, of the fibrous beds as it varied with the capillary pressure applied to the system and (2) the steady state liquid permeability of the beds as a function of the saturation. The former measurement was made directly by the familiar capillary displacement method, while the latter consisted of measuring the liquid flow rate and pressure drop across the bed and calculating the permeability from these data by D'Arcy's equation. In using D'Arcy's equation, it was assumed that the mechanism of water movement was that of capillary flow(i.e., the water flowed in discrete

channels of its own). Each of these tests were run on beds of two different size glass fibers, having diameters of about 1.2 microns and 3.0 microns, with slightly different total porosities and considerably different pore size distributions.

Using thin beds and assuming a uniform saturation in the beds, point values of (1) capillary pressure vs. saturation and (2) liquid relative permeability vs. saturation were obtained. The static capillary pressure curves exhibited a high degree of precision, and from these curves, effective pore size distributions were obtained by converting the capillary pressure, P_c, to a mean hydraulic radius, m, of the pores by the capillary equation, $m = \gamma/P_c$. It was shown by using different thickness beds that the pore structure was not influenced by the size of the bed. The relative permeability, which is the percentage of the total liquid permeability at complete saturation, was found to fall off very rapidly as the saturation was reduced below unity. Below a saturation of .95, the precision of the permeability measurements was quite good, and the sensitivity of the apparatus allowed accurate measurements at saturations as low as .05. At this value of saturation, the permeability was less than 1/10,000 of its original value. Accurate measurements of the permeability at complete saturation were obtained with the filtration apparatus developed and used by Ingmanson (68).

The validity of the relative permeability point value curves was established by making special permeability runs on thick beds in which there was a significant variation of the saturation and, hence, the permeability across

the bed. The over-all permeabilities of these thick beds, calculated from the integral of the point value curves, were in good agreement with the experimentally measured permeabilities. Thus, the relative permeability was established as independent of the flow rate and pressure drop, and capillary flow was substantiated as the permeability mechanism.

Compared to relative permeability curves of various granular media from the literature, the relative permeability of the glass fiber beds deviated from linearity with the saturation to a much greater extent than those of the granular systems. Although several investigators in the field have demonstrated that different pore size distributions may result in dissimilar relative permeability curves, the extreme difference of the glass fiber curves suggested that more factors than the pore size distribution alone were involved. In support of this suggestion, the relative permeability of a glass fiber bed was calculated from the capillary pressure data according to supposedly general theories proposed in the literature. Although these theories were fairly successful in characterizing two-phase flow in granular media, they were far from adequate for the glass fiber systems.

On the basis of a capillary flow mechanism and streamline flow, a general theoretical expression of the liquid relative permeability, $\underline{K}_r$, was developed from the Kozeny-Carman equation modified for two-phase systems. In this theory, the change of permeability with saturation was attributed to three major effects:

(1) the change in effective pore size of the liquid-filled pore space,

(2) the change in tortuosity of the liquid channel network,

and (3) the change in shape factors associated with the liquid channel system.

The derived equation is

$$\underline{K_r} = \frac{\underline{k_o}\ \underline{T}^2\ \underline{O}^2 \int_0^{\underline{s}} \underline{m}^2 \underline{ds}}{\underline{k_{o_c}}\ \underline{T_c}^2\ \underline{C_c}^2 \int_0^1 \underline{m}^2\ \underline{ds}}$$

where $\underline{k_o}$ is the Kozeny shape factor, $\underline{T}$, the Kozeny-Carman tortuosity, and $\underline{C}$, a shape factor of proportionality between the effective size of a pore space and its volume to surface ratio. The values of these factors at partial saturation $\underline{s}$ are designated by the subscript $\underline{c}$. The integral term was evaluated graphically from the effective pore size distribution curve.

In several previously developed theories of two-phase flow, which were tested on granular systems, the expression of relative permeability included the variable pore size distribution in the same way as in the above equation, i.e., as the integral or sum of the product of the pore size squared and the saturation. This relationship is suggested as universal for two-phase flow systems. In support of this concept, it was shown that the differences in relative permeability of the two different size glass fiber beds were wholly explained by the variation in this integral term. That is, the composite value of the empirical factors, $\underline{k_o T^2 C^2}/\underline{k_{o_c} T_c^2 C_c^2}$, which is the proportionality factor between the relative permeability and the integral term, was essentially the same for both fiber beds over the entire saturation range. Thus, the distinctions between different types of media are manifest in the values of this empirical factor, and this factor takes equivalent values for the same types of media.

It was not possible to rigorously evaluate the individual variations of the empirical factors with changes in saturation without additional information. However, a speculative analysis revealed that the shape factors, $\underline{k_{o_c}}$ and $\underline{C_c}$ started to change immediately as the saturation was reduced below 1.0. Assuming that the tortuosity ratio, $\underline{T/T_c}$, was numerically equal to the value of the saturation, $\underline{k_{o_c}}$ was found to increase and $\underline{C_c}$ to decrease as the saturation decreased. By contrast, these factors are apparently constant or else cancel out at all saturations in granular systems. A knowledge of these shape factors enables the distribution of the surface area of liquid-solid contact, which is presumed to be the same as the frictional drag surface of the flowing liquid, to be determined over the saturation range.

SIGNIFICANCE OF RESULTS AND SUGGESTIONS FOR FUTURE RESEARCH

There are many areas of science and industry in which two-phase flow in fibrous media plays an important role, such as chromatographic research, textile finishing, and the manufacture of paper. This study may contribute to all of these areas, but the contribution will be chiefly one of long range understanding, not one of immediate practical benefits. The systems of glass fibers and the conditions of incompressibility and capillary equilibrium were too idealized for commercial application. In this sense, the study was fundamental and introductory. In conjunction with previous studies, it emphasized the complexity of the two-phase flow mechanism and stressed the logic of making small discrete advances of some depth rather than attempting shallow empirical generalizations.

In some aspects, support was given by the results of this work to the most advanced theories of two-phase flow developed by other investigators in the field. Conversely, the generality of other aspects of these theories were disqualified. Thus, an expected contribution of this study was to build confidence in certain proposed generalities in previously developed theory and to clarify the specific areas of two-phase flow which are little understood and require additional investigation. In addition, this was an initial study of two-phase flow in fibrous media, and it indicated that the same general approaches to the problem, used in the study of other types of media, are applicable to fiber systems also. Thus, the significance of the results of this study is that it serves as a guide for further work in the field; its specific contributions would be manifest in the future research suggested below.

CONTINUED STUDY OF IDEAL SYSTEMS

Obviously, this study of glass fiber systems was far from complete, and many fundamental questions of the relative permeability mechanism in these simplified media remain unanswered. Specifically, the proper values and physical significance of the empirical factors need to be resolved. Presumably, an independent evaluation of the tortuosity of the liquid channels at partial saturation could be attained from electrical resistivity measurements. As suggested by Wyllie and Spangler (48), the electrical resistivity measurements should be made simultaneously with the relative permeability measurements. The configuration of the liquid channels at partial saturation determines the values of the shape factors, but it seems that the complexity of the configuration defies any fundamental description. However, a useful characterization of this configuration is afforded by the volume to surface ratio of the liquid channels. The volume of the liquid can be easily evaluated, but it remains for an accurate method of measuring the surface to be developed. Specifically, a means to measure the surface of liquid-solid contact as a function of saturation independently would be of value. Since this study was limited to only two fiber systems of not too greatly differing pore structure, it would be interesting to make additional investigations of similar media having more extreme pore structure to confirm the general theory presented.

Investigations of the effect of surface tension on the relative permeability have been cursory and incomplete, and it should be worthwhile to establish the quantitative significance of the surface tension in two-phase systems. Surface tension can be varied by using (1) different pure liquids or (2) different concentrations of a liquid solution.

In view of the prevalence of thin beds in commercial operations, the practical application of two-phase flow theory will eventually necessitate a study of "thin" systems. As mentioned before, the mechanism of two-phase flow in thick beds may not hold for thin beds. Consequently, an investigation of thin beds, in which beds of progressively decreasing thickness are tested is recommended.

Finally, the inherent limitations of the Kozeny approach naturally restricts its usefulness in elucidating the mechanism of flow in porous media. More fundamental approaches are required. Thus, new methods of analysis of the two-phase flow problem should be investigated. Possibly Emersleben's drag theory (40) or Scheidegger's statistical approach (43) offer an improved approach to this problem.

ANALYSES OF PRACTICAL SYSTEMS

Two-phase flow is an integral part of many practical operations such as drying, pressing, and suction dewatering of fibrous media, and an understanding of this flow mechanism is essential to a complete understanding of the over-all operation. Investigations of these operations have often been limited by the lack of knowledge of the two-phase flow mechanism. Dreshfield (8), for example, in his study of hot surface drying of cellulose beds, emphasizes the need for a working quantitative concept of two-phase flow, as it is a basic part of the drying mechanism. Thus, a real necessity exists for an understanding of the two-phase flow mechanism in many practical systems. It would be premature to attempt a rigorous fundamental study of two-phase flow in such systems as paper and pulp, for the flow

mechanism in these systems is complicated by the factors of compressibility, swelling, and surface effects. However, a practical empirical investigation of these systems is not beyond reason. These systems have been successfully characterized for single-phase flow, and it is not unreasonable to suppose that the complicating factors in two-phase systems could be handled empirically, at least approximately. The effect of compressibility on the total porosity and pore size distribution could probably be determined separately in static studies. The swelling and surface effects undoubtedly would manifest themselves in the values of the empirical factors and naturally would introduce additional uncertainty in the expression for relative permeability. Nevertheless, the results of such studies may permit real advances to be made in the knowledge of the over-all operations.

STUDY OF NONCAPILLARY EQUILIBRIUM CONDITIONS

In practically all commercial operations involving two-phase flow, the prevailing condition is generally one of noncapillary equilibrium or unsteady state. This was graphically demonstrated in the hot surface drying study by Dreshfield (8), and it is obviously the case in the dewatering of a paper sheet on a Fourdrinier machine as it passes over the suction boxes and couch roll and through the wet presses. There must be marked differences between the dewatering mechanism of a medium under equilibrium and nonequilibrium conditions, as demonstrated by the efficiency of the suction box stage on a paper machine. The period of time for which the wet sheet remains over the suction boxes is of the order of magnitude of fractions of seconds. Yet, in this time, a considerable quantity of water is removed. It is impossible to explain this water removal on the basis of the capillary

equilibrium permeability curve, for these curves experience an extremely rapid fall off when the water content is only slightly reduced below complete saturation. A real understanding of two-phase flow for practical application, therefore, will eventually be based on investigations of nonequilibrium conditions. The results of a study in which the different stages of dewatering on a paper machine are simulated by a dynamic pilot scale apparatus would have extensive practical application. This type of study was made empirically by Nordman (9), but a more fundamental approach with ideal systems is warranted.

LITERATURE CITED

1. Muskat, M. The flow of homogeneous fluids through porous media. New York, McGraw-Hill, 1937. 763 p.

2. Carman, P. C. Flow of gases through porous media. New York, Academic, 1956. 182 p.

3. Scheidegger, A. E. The physics of flow through porous media. New York, Macmillan, 1957. 236 p.

4. Palmer, W. B., J. Textile Inst. 44, no.8/9:T391-400(Aug.-Sept., 1953).

5. Preston, J. M., and Chen, J. C., J. Soc. Dyers and Colourists 64, no.2: 60-4(Feb., 1948); Preston, J. M., and Bennett, A. J., J. Soc. Dyers and Colourists 67, no. 3:101-3(Mar., 1951); Preston, J. M., and Nimkar, M. V., J. Textile Inst. 43, no.8:T402-22(Aug., 1952).

6. Simmonds, F. A., Paper Trade J. 97, no. 10:40-2(Sept. 7, 1933).

7. Fujita, H., J. Phys. Chem. 56, no. 5:625-9(May, 1952).

8. Dreshfield, Arthur C. A study of transverse moisture distribution and movement during hot-surface drying of paper. Doctor's Dissertation. Appleton, Wis., The Institute of Paper Chemistry, 1956. 175 p.

9. Nordman, L., Tappi 37, no. 11:553-60(Nov., 1954).

10. Buchanan, E. T., Paper Ind. 30, no. 5:296-8(May, 1948).

11. Campbell, W. B., Pulp Paper Mag. Can. 48, no. 3:103-9, 122(Conv., 1947).

12. Nissan, A. H., Tappi 37, no. 12:597-608(Dec., 1954).

13. Christensen, G. N., and Barkas, W. W., Trans. Faraday Soc. 51, no. 1:130-45(Jan., 1955).

14. Pearse, J. F., Oliver, T. R., and Newitt, D. M., Trans. Inst. Chem. Engr. (London) 27:1-18(1949).

15. Carman, P. G., J. Phys. Chem. 57, no. 1:56-64(Jan., 1953).

16. Chatenever, A., Oil Gas J. 51, no. 3:174(1952); Wilson, D. A., Calhoun, J. C., and Chatenever, A., Oil Gas J. 51, no. 3:175(1952).

17. Emmett, P. H. Catalysis. Vol. 1. p. 24. New York, Reinhold, 1955.

18. Carman, P. C., Soil Sci. 52:1-14(1941).

19. Schultze, K., Kolloid Z. 36:65(1925); 37:10(1925).

20. Marshall, W. R., Jr., and Friedman, S. J. Drying. In Chemical Engineer's Handbook. 3d ed. p. 801ff. New York, McGraw-Hill, 1950.

21. Ceaglske, N. H., and Hougen, O. A., Ind. Eng. Chem. 29, no. 7:805 (July, 1957).

22. Hougen, O. A., McCauley, H. J., and Marshall, W. R., Jr., Trans. Am. Inst. Chem. Engrs. 36:183(1940).

23. Childs, E. C., and George N. C., Discussions Faraday Soc. 3:78(1948); Proc. Roy. Soc.(London) A201:392(1950); Trans. 4th Inter. Congr. Soil Sci. 1:60(1950).

24. Wyckoff, R. D., and Botset, H. G., Physics 7, no. 9:325-45(Sept., 1936).

25. Hassler, G. L., Rice, R. R., and Leeman, E. H., Trans. AIME 118:116(1936).

26. Reid, L. S., and Huntington, R. L., AIME T. P.:873(1938).

27. Botset, H. G., Trans. AIME 136:91(1940).

28. Leverett, M. C., Trans. AIME 132:149(1939).

29. Gates, J. I., and Lietz, W. T., A. P. I. Drilling and Production Practice.:285(1950).

30. Brownscombe, E. R., Slobod, R. L., and Caudle, B. H., Oil Gas J. 48, no. 41:98(1950).

31. Brownell, L. E., and Katz, D. L., Chem. Engr. Progr. 43, no. 11:601; no. 12:703(Nov., Dec., 1947).

32. Baver, L. D. Soil Physics. 2d ed. New York, John Wiley and Sons, 1948. 398 p.; Soil Sci. Soc. Amer. Proc. 3:52(1938).

33. Smith, R. M., Browning, D. R., and Pohlman, G. G., Soil Sci. 57:197 (1944).

34. Martinelli, R. C., Putnam, J. A., and Lockhart, R. W., Trans. Am. Inst. Chem. Engrs. 42:681(1946).

35. Purcell, W. R., Trans. AIME 186:39(1949).

36. Fatt, I., and Dykstra, H., Trans. AIME 192:249(1951).

37. Richards, L. A., Physics 1:318(1931).

38. Ceaglske, N. H., and Kiesling, F. C., Trans. Am. Inst. Chem. Engr. 36:211(1940).

39. Miller, E. E., and Miller, R. D., J. Appl. Phys. 27, no. 4:324(April, 1956); Soil Sci. Soc. Amer. 19:267(July, 1955).

40. Emersleben, O., Physik Z. 26:601(1925).

41. Iberall, A. S., J. Research Natl. Bur. Standards 45:398(1950).

42. Taub, A. H., Proc. Midw. Conf. Fluid Dynamics, 121(May, 1950).

43. Scheidegger, A. E., J. Appl. Phys. 25:994(1954).

44. Carman, P. C., Discussions Faraday Soc. 3:72(1948).

45. Sullivan, R. R., and Hertel, K. L. The permeability method for determining specific surface of fibers and powders. In Kraemer's Advances in colloid science. Vol. 1. p. 37ff. New York, Interscience, 1942.

46. Wyllie, M. R. J., and Gregory, A. R., Ind Eng. Chem. 47, no. 7:1379 (July, 1955).

47. Brown, Joseph C. Determination of the exposed surface of the pulp fibers from air permeability measurements, using a modified Kozeny equation. Doctor's Dissertation. Appleton, Wis., The Institute of Paper Chemistry, 1949, 146 p.

48. Wyllie, M. R. J., and Spangler, M. B., Bull. Am. Assoc. Petrol. Geologists 36, no. 2:359-403(Feb., 1952).

49. Lord, E. J., Textile Inst. 46, no. 3:T191(1955).

50. Coulson, J. M., Trans. Inst. Chem. Engrs.(London) 27:237(1949).

51. Carman, P. C., Trans. Inst. Chem. Engrs.(London) 15:150(1937).

52. Wyllie, M. R. J., and Rose, W. D., Nature 165:972(1950); Trans. AIME 189:105(1950).

53. Sullivan, R. R., J. Appl. Phys. 13:725(1942).

54. Thornton, O. F., Trans. AIME 186:328(1949).

55. Cornell, D., and Katz, D. L., Ind. Eng. Chem. 45:2145(1953).

56. Rose. W. D., and Bruce, W. A., Trans. AIME 186:127(1949).

57. Rapoport, L. A., and Leas, W. J., Trans. AIME 192:83(1951).

58. Rose, W. D., Trans. AIME 186:111(1949).

59. Rose, W. D., and Wyllie, M. R. J., Trans. AIME 186:329(1949).

60. Payne, D., Nature 172:261(1953).

61. Swanson, John W. The Institute of Paper Chemistry. Personal communication, 1957.

62. Pierce, C., J. Phys. Chem. 57:149(1953).

63. Barrett, E. P., Joyner, L. G., and Halenda, P. P., J. Am. Chem. Soc. 73:373(1951).

64. Herdan, G. Small particle statistics. p. 50. Houston, Elsevier, 1953.

65. Barkas, W. W., and Hallan, R., Brit. Paper and Board Makers Assoc., Proc. Tech. Sect. 34:289(1955); Christensen, G. N., and Barkas, W. W., Nature 171:165(Jan., 1953).

66. Grace, H. P., AIChE J. 2, no. 3:307-36(Sept., 1956).

67. Chicago Apparatus Company. Catalog 55. p. 420. Chicago, The Company, 1954.

68. Ingmanson, William L. An investigation of the mechanism of water removal from pulp slurries. Doctor's Dissertation. Appleton, Wis., The Institute of Paper Chemistry, 1951. 119 p.; Tappi 35, no. 10:439-48(Oct., 1952).

69. Knight, M. A., J. Am. Ceram. Soc. 28, no. 11:297-302(Nov. 1, 1945).

70. Ingmanson, W. L., and Whitney, R. P., Tappi 37, no. 11:523-34(Nov., 1954).

71. Hisey, Robert W. An investigation of the mechanism of the dewatering of compressible beds. Doctor's Dissertation. Appleton, Wis., The Institute of Paper Chemistry, 1955. 83 p.

72. Central Scientific Co. Bulletin 101. The ring method for surface tension and interfacial tension measurement. New York, The Company.

73. International Critical Tables. Vol. 4. p. 434. New York, McGraw-Hill, 1926.

74. Ergun, S., and Owen, J., Anal. Chem. 25, no. 8:1222-6(Aug., 1953).

75. Dosik, Stanley. American Instrument Co., Silver Spring, Md. Personal communication, 1956.

76. Hudson, Ralph G. The engineer's manual. 2d ed. p. 16, 19. New York, John Wiley and Sons, 1947.

APPENDIX I

CALCULATION OF BED DIMENSIONS

A schematic cross-sectional view of the compressed bed of 1.2-mm fiber in the capillary pressure apparatus is shown in Figure 42. The plate is assumed to be spherical and the bed cylindrical. The length of the pegs was .793 cm. From Hudson's Engineering Manual (76), the length of a chord

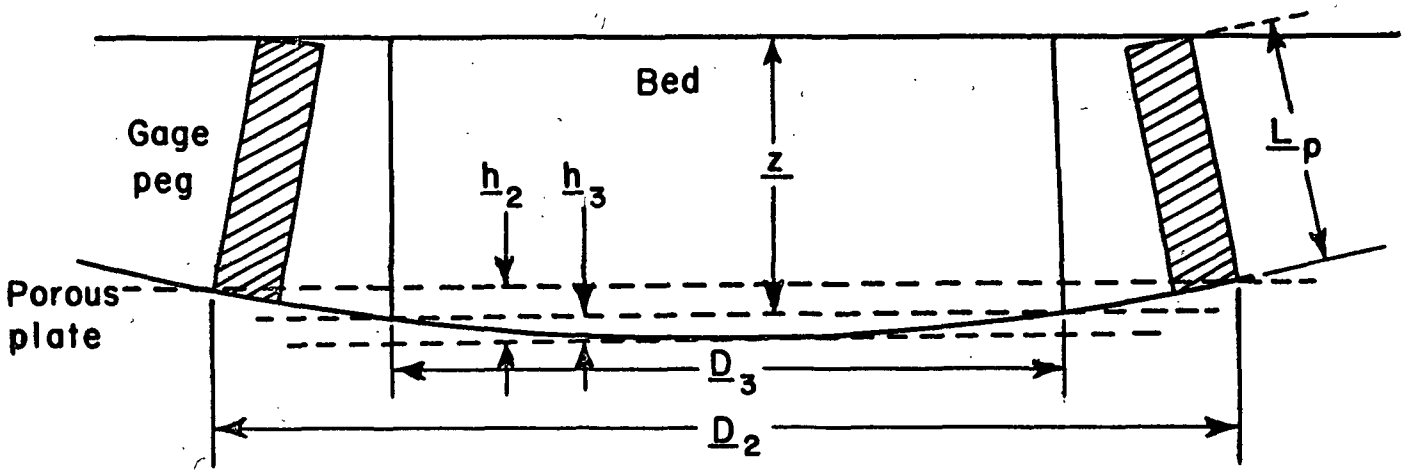

Figure 42. Cross-Sectional Diagram of the Compressed Bed.

of a circle, D, is related to the displacement of the chord from the subtended arc, h, according to the equation,

$$\frac{D + 4h^2}{8h} = \text{constant, or } \frac{D_1^2 + 4h_1^2}{8h_1} = \frac{D_2^2 + 4h_2^2}{8h_2}. \qquad (50)$$

For the porous plates of this work, Equation (50) can be simplified for

practical purposes to

$$\frac{D_1^2}{8h_1} = \frac{D_2^2}{8h_2}, \tag{51}$$

since the radius of curvature of the plates is so large compared to the diameter of the plates. Experimentally, D_1 and h_1 were determined by means of the steel bar as 7.45 cm. and .0368 cm., respectively. As indicated in Figure 42, the distances D_2 and D_3 were 8.20 cm. and 6.44 cm., respectively.

From Equation (51), h_2 and h_3 were calculated as .0407 cm. and .0251 cm., respectively. The volume of a spherical segment of one base from Hudson (76) is given by

$$V_s = \pi \frac{h}{6} \left(\frac{3D^2}{4} + h^2\right). \tag{52}$$

From this equation, the volume of the spherical segment of the porous plate having a diameter equal to that of the bed was calculated as .409 $cm.^3$ The volume of the bed, then, was equal to

$$V_b = \pi \frac{D_3^2 z}{4} + V_s. \tag{53}$$

The curvature of the plate was so slight that for practical purposes, the quantity, $z - h_2 + h_3$, is equivalent to the length of the pegs, L_p. Substituting numerical values into Equation (53), the volume of the bed was calculated to be 26.81 $cm.^3$ The average thickness of the bed was calculated as the ratio of the bed volume to the cross-sectional area. In this case, the average bed thickness was .82 cm.

APPENDIX II

CALCULATION OF CAPILLARY PRESSURE DATA

This calculation was for capillary pressure run no. 103 of the 3.0-mu fiber beds. The recorded data was presented in Table IX in the Results and Discussion section. Supplementary data for this run included:

Bed diameter	= 6.40 cm.
Bed volume	= 26.44 $cm.^3$
Buret tube calibration	= .876 g./cm.

The porosity of the bed was calculated from the volume of the bed, the total weight of dry fibers in the bed, and the solid density of the fiber as .919. The calculated results of this run are tabulated in Table XVII. The columns of figures in this table are in inverse order compared to the recorded data in Table VIII, i.e., the bottom line of data in Table VIII corresponds to the top line of results in Table XVII. Column (1) in Table XVII is the capillary pressure acting on the bed which is due to the head of water above the mercury in the buret tube. It was obtained from the data in Table VIII as the reading of column (a) minus that of column (b), this quantity being divided by the density of mercury at 23.5°C., the average temperature of the beds in this run. Similarly, column (2) refers to the difference in mercury levels, column (b) minus column (c). Column (3), the total capillary pressure acting on the system is the sum of columns (1) and (2). Column (4) is the difference between consecutive values of the mercury level in column (b) (subtracting the lower from the upper) except where evaporation had occurred at equilibrium when the system was left

TABLE XVII

CALCULATION OF CAPILLARY PRESSURE RUN NO. 103

(1) Capillary Pressure Due Water, cm. Hg	(2) Capillary Pressure Due Mercury, cm. Hg	(3) Total Capillary Pressure, $\underline{P}_c$, cm. Hg	(4) Mercury Level Change in Buret Tube, cm.	(5) Water Expressed From Plate Plus Bed, g.	(6) Water Expressed From Plate Only, g.	(7) Water to Be Added to That in Bed, g.	(8) Corrected Water Addition to Bed Because of Evaporation, g.	(9) Total Water in Bed, g.	(10) Fractional Water Content of Bed, g. Water/g. Fiber	(11) Saturation of Bed, $\underline{s}$
5.16	28.83	33.99	0	0	0	0	0	.307	.0554	.0127
5.16	20.09	25.25	.03	.026	.019	.007	.007	.314	.0567	.0130
5.16	19.98	25.14	0	0	0	0	0	.314	.0567	.0130
5.14	12.04	17.18	.26	.228	.017	.211	.214	.528	.0953	.0218
5.05	7.65	12.70	1.27	1.113	.005	1.108	1.123	1.651	.298	.0681
4.91	5.80	10.71	1.97	1.726	.003	1.723	1.746	3.397	.613	.140
4.71	4.76	9.47	2.71	2.374	.002	2.372	2.404	5.801	1.047	.239
4.71	4.67	9.38	.184	.161	0	.161	.163	5.964	1.076	.246
4.37	3.99	8.36	4.66	4.082	.002	4.080	4.135	10.099	1.822	.417
3.81	3.53	7.34	7.64	6.693	.002	6.691	6.782	16.881	3.045	.697
3.34	2.73	6.07	6.37	5.580	.003	5.577	5.653	22.534	4.065	.930
3.23	1.16	4.39	1.46	1.279	.006	1.273	1.290	23.824	4.298	.980
3.21	-0.61	2.60	.30	.263	.011	.252	.255	24.079	4.344	.990
3.19	-2.44	0.75	.21	.184	.029	.155	.157	24.236	4.372	.997

standing for a long time. In such cases, the mercury level rose rather than fell in the buret tube, as in the second value from the bottom in column (b). To obtain an approximate value for the change in mercury level corresponding to the accompanying increase in capillary pressure had the evaporation not occurred, the change in level was assumed to be proportional to that per cm. Hg change in total capillary pressure immediately preceding it in Table XVII. Thus, the mercury level change corresponding to the evaporation which occurred as mentioned above was (25.25 - 25.14)(.03/33.99 - 25.25) = <.001. For practical purposes, this is a negligible change and appears as zero in column (4), the third value from the top. Column (5) was obtained by multiplying column (4) by the buret tube calibration value. The values in column (6) were obtained from the blank calibration curve of the porous plate in Figure 16. Column (7) was simply the difference between columns (5) and (6). As mentioned in the experimental procedure, evaporation occurred throughout the run which could not be accounted for quantitatively. The discrepancy caused by this evaporation was evident in the disagreement between the value of total water in the bed at complete saturation calculated from the volume and porosity of the bed and that determined from the accumulated changes in the capillary pressure run. To correct for this evaporation, the difference between these values of water content was distributed over the range of measurements as corrected values of water to be added to the bed such that the corrected total water content from the capillary pressure measurements agreed with the calculated value. The individual corrections were assumed to be proportional to the values in column (7). This correction was about 1%, and the corrected values of water

addition are shown in column (8). The first value in column (9) was determined experimentally at the end of the run, and the succeeding values were obtained by adding, cumulatively, the values in column (8). Column (10) was obtained by dividing the values in column (9) by the weight of dry fibers in the bed. The last column was calculated by multiplying the values of fractional water content in column (10) by the factor, $(1/\rho_{\underline{L}})(\underline{W}/\underline{V}_{\underline{b}})(1/\epsilon)$, where $\rho_{\underline{L}}$ is the density of liquid water, $\underline{W}$ is the weight of dry fiber in the bed, $\underline{V}_{\underline{b}}$ is the volume of the bed, and ϵ is the bed porosity. The capillary pressure curve was obtained by plotting the values of column (3) against those of column (11).

APPENDIX III

CALCULATION OF PERMEABILITY DATA

This calculation was made on the data of run no. 6, presented in Table IX. Only a single set of measurements, underscored in Table IX, was analyzed here, since the same calculations were made for each set. The supplementary data included:

Bed diameter	= 6.44 cm.
Bed volume	= 48.37 $cm.^3$
Average bed thickness	= 1.49 cm.

The calculated results of this analysis are presented in Table XVIII. The porosity was calculated to be .944. The flow rate was evaluated as .618 g./min. from the intermediate capillary flowmeter calibration chart in Figure 19 in conjunction with the recorded manometer reading in column (j) and the ambient temperature in column (h). This flow rate was equivalent to .0103 $cm.^3/sec.$ at a water temperature of 24.6°C. which is the average of the temperatures in columns (a), (b), and (c). The capillary pressure at the upstream face of the bed due to the water head was determined from the difference of the highest mercury level in the upstream mercury manometer, column (f), and the level of the upstream porous plate, column (d). The capillary pressure attributed to the mercury head was determined from column (f).

TABLE XVIII

CALCULATION OF PERMEABILITY RUN NO. 6

Value No.	Description	Numerical Value
1	Mass flow rate of water	.618
2	Water temperature, °C.	24.6
3	Volumetric flow rate of water, q, cc./sec.	.0103
4	Capillary pressure at upstream face of bed due to water head, cm. Hg	4.06
5	Capillary pressure at upstream face of bed due to mercury head, cm. Hg	8.13
6	Frictional pressure drop across upstream plate, g./cm.^{2}	2.06
7	Frictional pressure drop across upstream plate, cm. Hg	.15
8	Capillary correction for upstream and downstream mercury manometers, cm. Hg	.07
9	Total capillary pressure at the upstream face of the bed, cm. Hg	12.27
10	Capillary pressure at downstream face of bed due to water head, cm. Hg	4.00
11	Capillary pressure at downstream face of bed due to mercury head, cm. Hg	8.79
12	Frictional pressure drop across the downstream plate, g./cm.^{2}	2.46
13	Frictional pressure drop across the downstream plate, cm. Hg	.18
14	Total capillary pressure at downstream face of bed, cm. Hg	12.54
15	Average capillary pressure in bed, cm. Hg	12.41
16	Difference in densities of differential manometer fluid and water, g./cc.	.741
17	Differential manometer reading, difference in cm.	8.67
18	Frictional pressure drop across both plates and bed, g./cm.^{2}	6.43

TABLE XVIII (Continued)

CALCULATION OF PERMEABILITY RUN NO. 6

Value No.	Description	Numerical Value
19	Sum of the frictional pressure drops across both plates, $g./cm.^2$	4.52
20	Frictional drop across the bed alone, ΔP_f, $g./cm.^2$	1.91
21	Viscosity of the flowing water, μ, $g.-sec./cm.^2$	9.20×10^{-6}
22	Specific permeability of bed, K_c, $cm.^2$	226.8×10^{-11}
23	Specific permeability of bed at $s = 1.0$, $cm.^2$	2586×10^{-11}
24	Relative permeability of bed, K_r	.0877
25	Saturation of bed, s	.765

The frictional pressure drop across the upstream plate was interpolated from the calibration chart in Figure 22, using the flow rate of value 1, corrected for the measured diameter of contact between the plate and the bed. This pressure drop was converted to cm. Hg for evaluating the capillary pressure in the system. The capillary correction for the mercury manometers was calculated from the difference between the interfacial tensions of mercury and water and mercury and air and the dimensions of the manometer tube. Thus, the total capillary pressure at the upstream face of bed was calculated as the combination of the values, 4 + 5 + 7 - 8. Similarly, values 10 and 11 were determined from columns (e) and (g) and value no. 12 was interpolated from the calibration chart in Figure 23 and corrected for the measured diameter of contact. The total capillary pressure at the downstream face of the bed was calculated as the combination of values, 10 + 11 - 13 - 8. The mean capillary pressure in the bed was taken as the arithmetic average of values 9 and 14. The frictional pressure drop across the bed and plates was measured directly by the differential manometer and was equal to the product of values 16 and 17, since no capillary effect existed in the differential manometer. The frictional pressure drop across the bed alone, then, was simply the frictional pressure drop across the bed plus plates, value no. 18, minus the sum of those across the plates alone, value nos. 6 and 12. The water viscosity was evaluated for its temperature, value no. 2. The specific permeability was calculated by D'Arcy's law from value no. 3, 20, and 21 and the measured average bed thickness, $\underline{L}$, and cross-sectional area, $\underline{A}$. Thus,

$$\underline{K_c} = \frac{q\mu\underline{L}}{\underline{A}\Delta\underline{P_f}} \cdot \qquad (54)$$

The specific permeability at complete saturation was determined from the saturated permeability results in Table VII for a porosity of .944. The relative permeability was then calculated as the ratio of value 22 to value 23. The degree of saturation was interpolated from the capillary pressure curve of Figure 26 using the average capillary pressure in the bed, value no. 15. Thus, a single point on the relative permeability curve was obtained by plotting value no. 24 against value no. 25.